

INTERNAL FRICTION IN HYDROGEN CHARGED  
ALUMINUM ALLOYS

To the memory of my father

INTERNAL FRICTION IN HYDROGEN CHARGED  
ALUMINUM ALLOYS

by

MARC LEGER, B.Sc., M.Sc.

A Thesis

Submitted to the School of Graduate Studies

in Partial Fulfilment of the Requirements

for the D egree

Doctor of Philosophy

McMaster University

August 1976

DOCTOR OF PHILOSOPHY (1976)  
(Materials Science)

McMASTER UNIVERSITY  
Hamilton, Ontario

TITLE: Internal Friction in Hydrogen Charged Aluminum Alloys

AUTHOR: Marc Léger, B.Sc. (McGill University)  
M.Sc. (McGill University)

SUPERVISOR: Dr. G. R. Piercy

NUMBER OF PAGES: xi, 154

## ABSTRACT

Measurements of the internal friction of several aluminum alloys were made over the temperature range from 80 to 300 K using the two component resonator technique. The technique was improved, by using a metallic bond between the two components, so that measurements in the  $Q^{-1} \approx 10^{-6}$  range could be made at three frequencies. Preliminary experiments using quartz crystals as specimens were performed in order to check the properties of the metallic joint. A method of checking the bond, by measuring the resonator properties at about half the fundamental frequency of the quartz transducer alone, was developed.

Comparisons of the internal friction spectra of hydrogen charged samples with spectra of vacuum annealed samples were used, in conjunction with a simple model of the distribution of hydrogen, to determine upper limits on the binding energy between hydrogen and substitutional solutes in the aluminum matrix.

## ACKNOWLEDGEMENTS

I would like to express my appreciation to Dr. G.R. Piercy, for his guidance, encouragement and patience throughout the course of the work. The opportunity of observing his approach to problem solving has been enlightening. I would like to thank other members of the department and the Institute for Materials Research and also Dr. Z. Popović for helpful discussions. The advice and assistance of the technical staff were greatly appreciated.

My wife, Martha, already knows how much I have appreciated her support and encouragement throughout the several years of this work. She was also responsible for typing the manuscript. She swears it is the last one.

A Quebec government post graduate scholarship for myself and National Research Council grants to Dr. Piercy are gratefully acknowledged.

## TABLE OF CONTENTS

	Page
DESCRIPTIVE NOTE	ii
ABSTRACT	iii
ACKNOWLEDGEMENTS	iv
TABLE OF CONTENTS	v
LIST OF FIGURES	viii
LIST OF TABLES	xi
CHAPTER	
1 INTRODUCTION	1
2 POINT DEFECTS AND INTERNAL FRICTION	6
2.1 Thermodynamics of Point Defects and Hydrogen Solubility	7
2.2 The electrostatic Properties of Point Defects in Metals	13
2.3 The Elastic Properties of Point Defects	17
2.4 Defect Interaction	23
2.5 Internal Friction	26
3 EXPERIMENTAL APPARATUS	41
3.1 Introduction	41
3.2 (a) The Composite Resonator	42
(b) Electrical Properties of the Composite Resonator	45
3.3 The Alternating Current Bridge	48
3.4 Environment	55

CHAPTER		Page
4	EXPERIMENTAL TECHNIQUE	58
	4.1 Sample Preparation	58
	a) Pure aluminum samples	58
	i) Single crystal preparation	58
	ii) Polycrystalline sample preparation	61
	b) Aluminum alloy samples	61
	c) Heat treatment and hydrogen charging	62
	d) Gas analysis	62
	3) End preparation	62
	4.2 Quartz Crystal Preparation	64
	a) The joint between quartz transducer and the sample	67
	b) Checks of the joint and suspension	71
	4.3 Measurement Technique	72
5	RESULTS	77
	5.1 Treatment of the Data	77
	5.2 Results of Preliminary Experiments	79
	a) The suspension	79
	b) The joint between quartz and sample	81
	c) Criteria for validity of measured peaks	84
	5.3 Pure Aluminum Results	87
	5.4 Aluminum Copper Results	90
	5.5 Aluminum Magnesium Alloys	95
	5.6 Commercial Alloys	99

CHAPTER		Page
6	DISCUSSION	105
	6.1 General Discussion	105
	6.2 Peak Temperature	108
	6.3 Sensitivity of the Measurements	110
	a) The aluminum copper alloys	111
	b) The aluminum magnesium alloys	112
	c) The commercial alloys	112
	6.4 The strain anisotropy ( $\lambda_1 - \lambda_2$ ) for the hydrogen-substitutional pair	113
	6.5 Hydrogen-Substitutional Solute Binding Energy	117
	6.6 The 7075 Alloy Results	121
	6.7 Hydrogen Distribution in Aluminum	122
	a) Grain boundaries	122
	b) Dislocations	123
	c) Vacancies	123
7	SUMMARY AND CONCLUSIONS	125
	APPENDIX A	
	Internal Friction in Hydrogen Charged and Deformed Aluminum	128
	APPENDIX B	
	Hydrogen Analysis	137
	APPENDIX C	
	Internal Friction Due to Temperature Dependence of the Elastic Compliance	148
	REFERENCES	151

## LIST OF FIGURES

	Page
2.1 Octahedral interstitial sites about a substitutional atom in a f.c.c. lattice.	11
2.2 Screened electrostatic potential about a proton in aluminum.	18
3.1 Typical 35 kHz composite resonator.	43
3.2 Stress distribution in a resonator at resonance.	43
3.3 Electrical equivalent circuit of the composite resonator.	46
3.4 Admittance diagram for the composite resonator.	47
3.5 Admittance diagram for the composite resonator with additional parallel capacitance.	47
3.6 Schematic of bridge circuit.	49
3.7 Interior of the decade resistance box.	54
3.8 Schematic of the cryostat.	56
4.1 A powder mould.	60
4.2 Section of the alloy preparation apparatus.	60
4.3 Sample holder for polishing.	63
4.4 Initial step in making of the suspension.	63
4.5 Damping in quartz crystals showing effect of colloidal silver.	66
4.6 Damping in quartz crystals showing effect of faulty suspension.	66
4.7 The temperature-controlled trough and ultrasonic soldering unit.	69

	Page
5.1 Quartz transducer damping measured by step heating.	80
5.2 Quartz transducer damping measured during continuous cooling.	80
5.3 Internal friction of quartz sample - matched to transducer.	82
5.4 Damping of composite oscillator made of unevenly matched quartz crystals.	82
5.5 Total damping of unevenly matched quartz resonators measured by continuous cooling.	85
5.6 Quartz specimen internal friction determined from 5.5a.	85
5.7 Internal friction of Al <100> single crystal.	88
5.8 Internal friction of polycrystalline Al following room temperature deformation.	88
5.9 Internal friction of an <u>Al</u> Cu polycrystalline sample - vacuum annealed.	91
5.10 Internal friction of same sample - hydrogen annealed and quenched.	91
5.11 Internal friction of the <u>Al</u> Cu single crystal.	94
5.12 Internal friction of the <u>Al</u> 0.16 at.% Mg polycrystalline sample - annealed in helium.	94
5.13 Internal friction of the <u>Al</u> 0.16 at.% Mg polycrystalline sample - hydrogen charged.	98
5.14 Internal friction of <u>Al</u> 0.54 at.% Mg polycrystalline sample.	98
5.15 Internal friction of 7075-T6 aluminum.	101
5.16 Internal friction of 7075 aluminum after hydrogen anneal at 560°C.	101
5.17 Internal friction of 6061 aluminum.	103

## APPENDIX A

1. Normalized internal friction of a vacuum annealed aluminum polycrystal deformed at room temperature. 131
2. Normalized internal friction of a hydrogen charged aluminum polycrystal deformed at room temperature. 131
3. Normalized internal friction of a hydrogen charged aluminum polycrystal after room temperature deformation. 133

## APPENDIX B

1. Schematic of the high vacuum system. 138
2. Sample holder for gas analysis. 139
3. Gas analysis measurements for the aluminum sample. 143
4. Gas analysis measurements for the aluminum-magnesium alloy. 143
5. Measurements used for calibration of the response of the analytical ion gauge and pumping speed. 145

LIST OF TABLES

	Page
3.1 Transformer Characteristics	51
5.1 Solute Content of Commercial Alloys in Weight Per Cent	100
6.5.1 Summary of results	120

## CHAPTER 1

### INTRODUCTION

The study of the interaction of hydrogen and metals has both practical and theoretical significance. Hydrogen has been recognized as a problem in iron base alloys for more than 100 years (Troiano, 1974) because it is directly associated with catastrophic embrittlement of such alloys. Embrittlement due to hydrogen is not limited to iron base alloys and has recently been postulated for some nonferrous materials including aluminum (Speidel, 1974). Another type of problem associated with hydrogen-metal interactions is hydride formation and resulting cracking of zirconium alloy pressure tubes used in nuclear reactors. Although many of the properties associated with hydrogen in metal systems are of a harmful nature, there are exceptions. For example, hydrogen purification can be accomplished with Pd Ag alloy membranes--a direct consequence of high diffusivity and solubility of hydrogen in these alloys.

The practical problems associated with hydrogen in aluminum and its alloys have primarily been problems of porosity, blistering and void formation. These are a consequence of the fact that molten aluminum dissolves twenty times as much hydrogen as the solid metal at the melting point. The hydrogen is thought to be introduced into the melt by reactions between molten aluminum and water vapour in the atmosphere or moist

refractories. The excess hydrogen which is not removed by degassing before casting shows up later as porosity in the casting, or voids and blisters formed during hot working or annealing treatments. These problems can usually be controlled by proper degassing techniques. The solubility of hydrogen in molten aluminum alloys has been shown to be dependent upon the alloying elements present (Opie and Grant, 1950; Baukloh and Oesterlen, 1938). This indicates that there may be interaction between hydrogen and the alloying elements. In solid alloys, there is a large range of variation in the observed effects of alloying additions.

Observations of interactions between hydrogen and substitutional solutes in aluminum are of interest from a theoretical viewpoint because they are calculable with the techniques presently available and would be a good test of these theoretical techniques. Aluminum is one of the simple metals in the sense that it has a simple electronic structure which is well described by nearly free electron theory. Pseudopotential theory applied to vacancy properties yields reasonable results (Popović, 1974). Substitutional solutes, such as Mg, Si and Cu can also be well represented using pseudopotential theory. Since hydrogen dissolves in aluminum (and other metals) in atomic form, interstitial hydrogen is simply a proton screened by conduction band electrons. Although the model is simple, only non-linear electron screening theory produces reasonable values for the heat of solution of hydrogen in aluminum (Popović, 1974). This results from the fact that since there are no core electrons in the hydrogen ion, the potential which must be screened is very strong and simple perturbation techniques cannot be expected to produce a good representation.

Since there was an indication of interaction effects between hydrogen and substitutional solutes in the molten alloys and since aluminum is an "ideal" system for comparisons with theoretical models, experiments were undertaken to detect pairing of hydrogen with substitutional solutes in the solid alloys which would result from interactions between hydrogen and substitutional solutes. There are many techniques which have been used to detect point defect interactions in metals. These include Mössbauer effect measurements (Sørensen and Cotterill, 1974), resistivity measurements of quenched samples (Murty and Vasu, 1972), simultaneous length and lattice parameter measurements at high temperature (Beaman et al, 1965) and internal friction measurements. The internal friction technique was chosen for this work because it has been shown to be a powerful technique for examining point defect behaviour.

There are many defect parameters which can be obtained from internal friction peaks. If measurements are done at several frequencies, then the activation energy for reorientation of the defect can be obtained from the change in temperature of the peak maximum with changing frequency. The defect symmetry can be determined with studies using single crystal specimens. If the concentration of defects is known, then the strain field of the defect can be calculated. The concentration of defect pairs may be temperature dependent as a result of a binding energy between the point defects which form the pair. The binding energy can be found, [as has been done by Mosher et al. (1970) for the case of Zr - N pairs in Nb and by Sagues and Gibala (1974) for complexes in Ta-Re-O] from the changes in peak size with measurement frequency. All the parameters mentioned above should also be obtainable from theoretical calculations.

The second chapter presents a brief review of point defect theory including thermodynamics of defect distribution, elastic and electrostatic properties and the theory of internal friction due to point defects. Special attention is given to the substitutional-interstitial pair.

Since the expected peak height from preliminary calculations was in the  $Q^{-1} \approx 10^{-6}$  range, the composite resonator technique of internal friction measurement was chosen. The experimental apparatus is described in the third chapter and the techniques which were used to reduce the background damping to a very low level are described carefully in the fourth chapter.

The fifth chapter presents the experimental measurements with extensive preliminary measurements of quartz specimen damping included to illustrate the capabilities and limitations of the technique.

The results are discussed in the next chapter in terms of the implications on the binding energy between hydrogen and substitutional defects and on the distribution of hydrogen in the lattice.

Some internal friction measurements were performed on hydrogen charged samples of pure aluminum which were deformed before measurement. These were carried out in order to detect possible dislocation-hydrogen interactions in aluminum. The results are reported in the first appendix.

The second appendix reports gas analysis experiments performed in order to verify that the hydrogen charging procedure used for the internal friction experiments did achieve the desired result.

The final appendix is concerned with the effect of changing temperature on internal friction measurements. The calculation indicates that, for low frequency measurements, rapid temperature changes may

produce spurious internal friction results.

## CHAPTER 2

### POINT DEFECTS AND INTERNAL FRICTION

This chapter is a review of the theoretical background essential to the understanding of internal friction due to hydrogen in aluminum alloys. The first section deals with some of the thermodynamic aspects of point defects in general and relates the macroscopic effects to microscopic phenomena. In particular, a simple expression for the number of substitutional-interstitial pairs is derived which depends upon the binding free energy ( $\Delta G_b$ ) of the pair. The origin of this binding energy is in the electrostatic and elastic interactions which take place between point defects in metals. The second section, therefore, deals with the electrostatic properties of point defects and the third section with the elastic properties.

Since it is the elastic strain distribution of point defects which is responsible for the observation of their contribution to internal friction, expressions for this strain distribution are presented. The very close relationship between the electrostatic and the elastic properties of the defects is discussed. The fourth section gives expressions for the interaction of point defects due to the electrostatic and elastic properties. Finally, the last section describes expressions for the internal friction due to these point defects.

## 2.1 Thermodynamics of Point Defects and Hydrogen Solubility

There are two main types of point defects in metals: intrinsic and extrinsic defects. Intrinsic defects are those defects which, because they are in thermal equilibrium with the lattice, are present in all metals at temperatures above absolute zero. They include vacancies (missing atoms), interstitials (atoms at positions other than regular lattice sites) and various combinations of these. Extrinsic defects are impurity atoms which may either replace host atoms on regular lattice sites (substitutionals) or remain in the interstices in the atomic array (interstitials). The concentrations of intrinsic defects and the solubilities of slightly soluble solutes can be determined from simple thermodynamic arguments for dilute solutions.

The thermodynamic behaviour (characterized by the Gibbs free energy) of a homogeneous phase containing low levels of impurities has been summarized by Flynn (1972). He shows that the chemical potential of a species  $\alpha$  is given by

$$\mu_{\alpha} = \Delta G_{\alpha} + RT \ln c_{\alpha} \quad (2.1.1)$$

where  $R$  is the gas constant,  $T$  the temperature and  $c_{\alpha}$  the occupied fraction of sites available to species  $\alpha$ .  $\Delta G_{\alpha}$  is the excess free energy per mole of species  $\alpha$  and is given by

$$\Delta G_{\alpha} = \Delta H_{\alpha} - T\Delta S_{\alpha} \quad (2.1.2)$$

where  $\Delta H_\alpha$  is the enthalpy change of the phase per mole of species  $\alpha$  added to the phase at constant temperature and pressure and  $\Delta S_\alpha$  is the entropy change caused by the addition which is in excess of the contribution due to the configurational entropy. If two phases containing the same species  $\alpha$  are in thermodynamic equilibrium at constant temperature and pressure, then the chemical potential of the species must be uniform throughout the two phases.

In the case of non-dilute solutions,  $\Delta H_\alpha$  and  $\Delta S_\alpha$  will also depend upon the concentration of the species  $\alpha$  because of interactions between atoms. If there is more than one species dissolved in the phase then the chemical potential of a given species will depend upon the concentration of all the other species. Again this is a result of microscopic interactions (both electrostatic and elastic) between the different species in the phase.

Hydrogen dissolves in all metals to some extent with a solubility which depends upon both temperature and pressure (Sokol'skaya, 1961). The steps in the chemical reactions which lead to dissolution in the metal lattice are not well understood but the thermodynamics of the dissolution can be described quite adequately. For metals such as aluminum, in which hydrogen dissolves as single atoms, the solubility,  $S$ , is given by Sieverts' law

$$S = S_0 p^{1/2} \exp \left[ - \frac{\Delta H_S}{kT} \right] \quad (2.1.3)$$

where  $\Delta H_S$  is the heat of solution,  $p$  is the pressure,  $k$  is Boltzmann's

constant and  $S_0$  a constant related to the vibrational entropy of hydrogen in the lattice. The heat of solution is the difference in enthalpy between a hydrogen atom dissolved in the metal and a hydrogen atom in a hydrogen molecule. The heat of solution for hydrogen in aluminum is positive, indicating that the hydrogen atoms of gas molecules must be supplied with energy in order to dissolve in the metallic lattice.

If hydrogen can occupy various sites in the metal, then the total hydrogen content will not be given by the simple relationship described above. In order to find the total hydrogen content, the energies of hydrogen atoms at sites other than the normal octahedral site in the perfect lattice must be known. These could be defect sites such as near other point defects, dislocations, grain boundaries and second phase particles. When the metal is in equilibrium with the gas, the chemical potential must be uniform within the sample. This means that in the perfect lattice the concentration is uniform.

In order to determine the concentration of hydrogen at defect sites, kinetic arguments can also be used since the rate at which hydrogen atoms arrive at a defect site must be equal to the rate at which they leave when equilibrium is established. The case of hydrogen atoms interacting with substitutional impurities in a face centred cubic lattice is of particular interest for this thesis. It will be assumed that the hydrogen atoms occupy octahedral interstices and only those interstices nearest to the impurity atom are different in energy from the normal interstices. The rate of arrival of hydrogen to these near-neighbour sites can be calculated as follows. Each interstitial site in the lattice has twelve adjacent

interstitial sites. Each substitutional impurity atom has six neighbouring interstitial sites. The number of normal interstitial sites which are adjacent to the interstitial sites next to the impurity is 32 (refer to Figure 2.1). Of these normal interstitial sites, 24 have only one adjacent interstitial site next to the impurity while the other eight have three. If the jump rate of hydrogen between a normal interstitial site and one next to the impurity is  $w_n$  then the rate at which hydrogen arrives at all six sites next to the impurity is given by

$$\begin{aligned} \dot{n}_i &= (1 - p_i) [(1) (24) (p_n) w_n + (3) (8) (p_n) w_n] \\ &= 48 (1 - p_i) (p_n) w_n \end{aligned} \quad (2.1.4)$$

where  $\dot{n}_i$  is the number of hydrogen atoms in interstitial sites next to the impurity and  $p_i$  and  $p_n$  are the probabilities of occupation of interstitial sites next to the impurity and in the normal lattice respectively. At equilibrium this flow of hydrogen to the impurity is balanced by an equal outward flow. Since each of the sites nearest the impurity has eight of twelve adjacent interstitial sites which are not next to the impurity, the rate at which hydrogen leaves these six near neighbour sites is given by

$$\dot{n}_i = -(6) (8) p_i (1 - p_n) w_i \quad (2.1.5)$$

where  $w_i$  is the jump rate of an interstitial between a site next to the impurity and a normal site.

FIGURE 2.1

Octahedral interstitial sites next to a substitutional impurity in  
an f.c.c. lattice

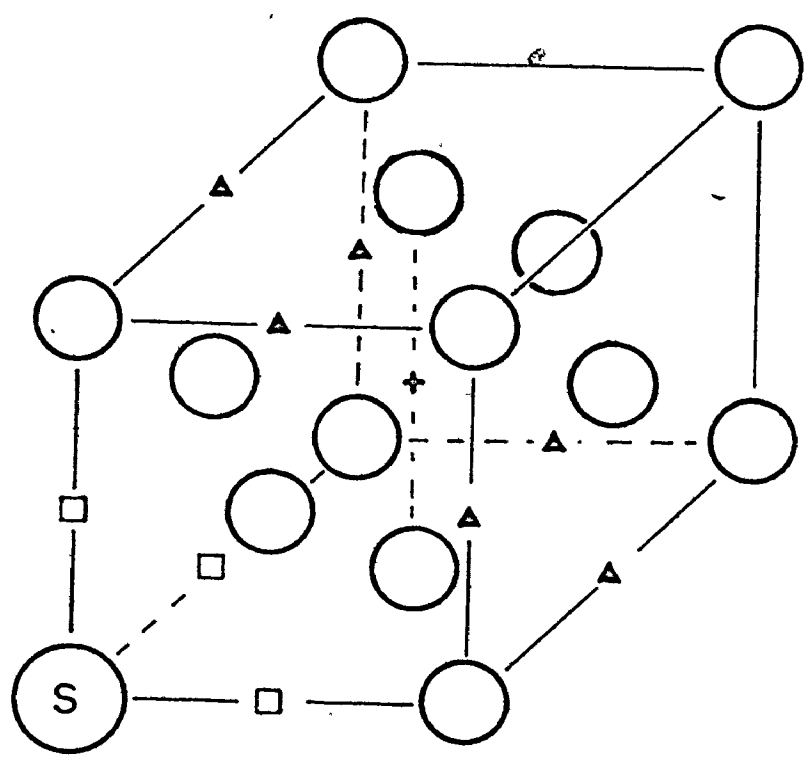
S - substitutional

□ - nearest interstitial site

▲ - site with one adjacent site next to substitutional

+ - " " three " sites " " "





Since the two rates of equations (2.1.4) and (2.1.5) are equal in magnitude and of opposite sign, the following relationship is obtained

$$\frac{p_i}{1 - p_i} \frac{1 - p_n}{p_n} = \frac{w_n}{w_i} \quad (2.1.6)$$

which reduces in the case  $p_i$  and  $p_n \ll 1$  to

$$\frac{p_i}{p_n} \approx \frac{w_n}{w_i} \quad (2.1.7)$$

The ratio on the right hand side is determined using rate theory to be

$$\frac{w_n}{w_i} = \exp + \frac{\Delta G_b}{kT} \quad (2.1.8)$$

where  $\Delta G_b$  is the change in free energy between the normal lattice site and the site next to the impurity (also known as the binding free energy).

The additional quantity of dissolved hydrogen due to the presence of such impurity defects can now be evaluated. If the atomic fraction of impurities is  $c_i$ , then the fraction of interstitial sites next to impurities is  $6c_i$ . If the normal hydrogen atomic fraction for a given pressure of hydrogen gas outside the metal is  $c_H$ , then the atomic fraction at impurity sites is  $c_0$  given by

$$c_0 = 6 c_i p_i = 6 c_i c_H \exp + \frac{\Delta G_b}{kT} \quad (2.1.9)$$

The total hydrogen content will be

$$c_H + c_O = c_H \left[ (1 - 6c_i) + 6c_i \exp \frac{\Delta G_b}{kT} \right] \quad (2.1.10)$$

The approach just outlined can be applied to find the concentration of hydrogen at other types of interstitial sites e.g. near dislocations. Each different type of interstitial site will have a concentration determined by an expression similar to that in equation 2.1.9 and corresponding changes would be made to find the total hydrogen content given by equation 2.1.10.

## 2.2 The Electrostatic Properties of Point Defects in Metals

The presence of a point defect in a metal not only disturbs the distribution of neighbouring atoms but also disturbs the electron distribution. Most theories of metals begin by assuming that each atom can be represented by a "bare ion", which includes the filled shell electrons, which is then screened by the conduction or valence electrons which are free to move in the lattice. It can be expected that the presence of a defect which has a different charge from the normal ionic charge will cause electrons to be either attracted or repelled. The result is that a local screening charge develops which ensures that at large distances there will be no electric field due to the defect. The theory of electron screening is now quite sophisticated and what follows is merely a brief summary. It is important to keep in mind that the results of this theory which are of interest in this work are the interaction energies between point defects.

An excellent presentation of electron screening theory as applied to hydrogen and vacancies in simple metals was made by Popović (1974) who applied it to the problem of solubility of hydrogen in aluminum and magnesium.

It is the electrostatic potential energy of a unit positive charge around a point defect in a metal which is of interest. The effective electrostatic potential of the defect at a distance  $r$  from the defect is given by

$$V_{\text{eff}}(r) = V(r) + V_{\text{ind}}(r) \quad (2.2.1)$$

where  $V(r)$  is the potential of the inserted ion (e.g. a substitutional ion or an interstitial hydrogen ion) and  $V_{\text{ind}}(r)$  is the potential due to the change in the electron density around the defect site. The induced potential  $V_{\text{ind}}$  must satisfy Poisson's equation

$$\nabla^2 V_{\text{ind}}(r) = -4\pi e \Delta n(r) \quad (2.2.2)$$

where  $\Delta n(r)$  is the change in electron density due to the defect.

Using first order perturbation theory on plane wave electron states, where the perturbation is  $V_{\text{eff}}(r)$  so that the result will be self consistent, the effective potential (now in Fourier transformed form,  $V(q)$ ) is given by

$$V_{\text{eff}}(q) = \frac{V(q)}{\epsilon(q)} \quad (2.2.3)$$

where  $\epsilon(q)$  is the dielectric function.  $\epsilon(q)$  describes the behaviour of the electron gas in wavevector space and should include the effects of electron exchange and correlation (Singwi et al, 1970). It turns out that this behaviour of the electron gas results in the so called Friedel oscillations of effective potential in real space which for a point charge have the form

$$V_{\text{eff}}(r) = - \frac{\alpha_F}{2\pi k_F^2} \frac{\cos(2k_F r + \phi_F)}{r^3} \quad (2.2.4)$$

at large distances from the defect instead of the  $1/r$  dependence which would be obtained in vacuum.  $k_F$  is the Fermi wavevector,  $\alpha_F$  and  $\phi_F$  are constants.

The screening of any potential can therefore be calculated in principle. The problem then is to find a potential for an impurity atom. In some cases this can be done using pseudopotential theory, which provides a weak potential that can be handled with the perturbation treatment described above. The theory and application of pseudopotentials are very well presented in three articles by Cohen, Heine and Weaire (1970). Essentially, a pseudopotential replaces the true nuclear and core electron potentials, but gives the same scattering to valence electrons of the conduction band. Pseudopotentials can be calculated from first principles using several methods, but these often do not reproduce the metallic properties very well. Empirical pseudopotentials fitted to experimentally determined properties (such as lattice parameters and elastic moduli) give

much better results. In particular the model potential of Abarenkov and Heine (1965) has been particularly successful. The potential is described by the following equation.

$$\begin{aligned} V(r) &= -\frac{Z}{r}, \quad r > R_M \\ &= -\frac{ZD}{R_M}, \quad r < R_M \end{aligned} \quad (2.2.5)$$

with two adjustable parameters;  $R_M$ , the core radius, and  $D$  which fixes the depth of the spherical potential well for  $r < R_M$ .  $Z$  is just the valence of the metallic ion. This is a local pseudopotential because its interaction with the valence electron gas does not depend upon the electron energy.

In order to find the effective potential with electron screening, we must use the Fourier transform of the model potential given by the following equation.

$$V(q) = -\frac{4\pi Z}{\Omega_0 q^2} \left[ D \frac{\sin(q R_M)}{q R_M} + (1 - D) \cos q R_M \right] \quad (2.2.6)$$

which is then inserted into equation (2.2.3). The resultant effective potential may be written in either real space or  $q$ -space.

The approach used to describe the screening of an interstitial hydrogen ion (proton) in a metal is different because this potential cannot be represented by a weak pseudopotential (Popović, 1974). Popović has

determined the effective potential and the screening charge density around protons in aluminum and magnesium using a nonlinear screening technique that includes the effects of electron exchange and correlation. The results for the effective potential in aluminum are shown in Figure 2.2, and include comparisons with the linear theory. The Friedel oscillations are clearly visible.

### 2.3 The Elastic Properties of Point Defects

The observation of internal friction in metals containing point defects depends upon the interaction of the applied stress with the strain fields of the defects. The methods used for calculating the strain fields of simple defects will be shown in this section.

There are several approaches to the problem of calculating defect strain fields. One approach which has been used is that of Eshelby (1956) who assumed that the matrix and defect have linear elastic properties which can be represented by an isotropic continuum. Eshelby has shown that the solutions of the elastic equation depend critically upon the conditions at the boundary of the continuum. Hardy (1968) has calculated the displacement field of a point defect in a discrete lattice and has related the elastic strength of point defects to the interatomic forces. March and Rousseau (1971) have related the forces on atoms near the defect to the displaced charge surrounding the defect as developed in the previous section.

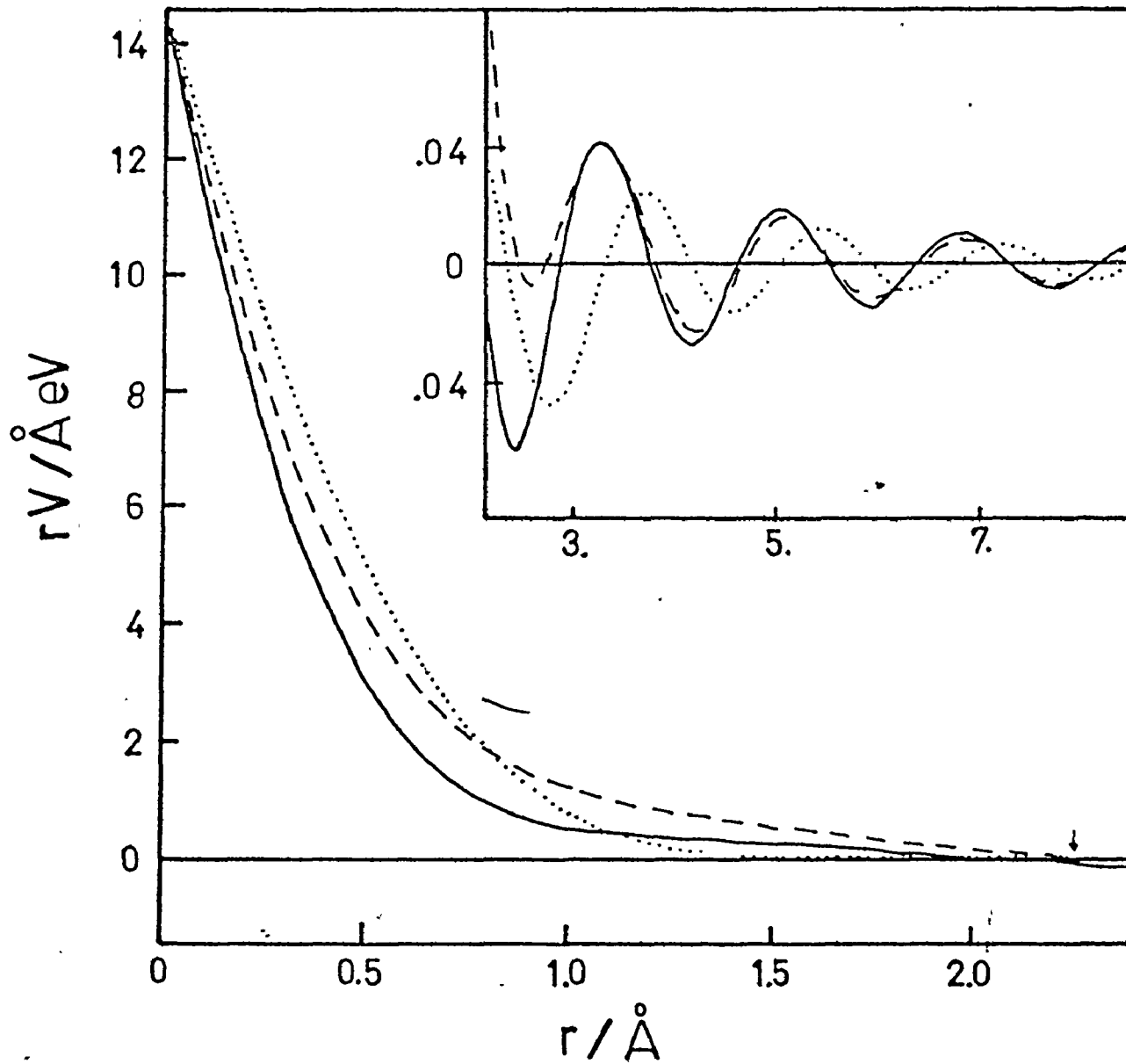
Consider first the isotropic continuum approach to point defect strain fields. The most simple defect is just a centre of dilatation. The

FIGURE 2.2

The screened electrostatic potential (times  $r$ ) around a proton  
in aluminum (Popović, 1974)

———— nonlinear theory with exchange and correlation corrections  
----- nonlinear Hartree theory  
..... linear theory

The arrow indicates the position of the centre of the nearest aluminum  
atom in the unrelaxed case.



point defect is assumed to be formed by removing at some origin a sphere of matrix material with volume equal to one atomic volume. In the case of a substitutional atom, this sphere is replaced by another sphere with volume equal to the atomic volume of the substitutional material and with the same elastic constants as the substitutional material. Since this second sphere, in general, will not be the same size as the hole created by removing the first sphere, the matrix and the substituted sphere must be strained in order that hole and sphere surfaces may be joined. This results in a radial displacement  $u(r_0)$  of the hole surface at the initial radius  $r_0$ . Flynn (1972) shows that the resulting displacement field in the matrix material which satisfies the elastic equation is given by

$$\underline{u}(\underline{r}) = \frac{(A + B)}{r^3} \underline{r} \quad (2.3.1)$$

where  $\underline{r}$  is the position vector. In an infinite crystal, B must be zero. In a finite crystal, however, the boundary condition at the outer surface (vanishing normal stresses) can only be satisfied with B nonzero. If the displacement of the hole surface is  $nr_0$ , then the constants A and B can be calculated and the solution for  $\underline{u}(\underline{r})$  is

$$\underline{u}(\underline{r}) = nr_0^3 \left[ \frac{\underline{r}}{r^3} + \frac{4\mu \underline{r}}{(3\lambda + 2\mu) R^3} \right] \quad (2.3.2)$$

where  $\mu$  and  $\lambda$  are the usual Lamé constants of isotropic elasticity. R is the radius of the outer surface of the material. For an infinite crystal

( $R \rightarrow \infty$ ) the displacement field is pure shear because the dilatation

$$\nabla \cdot \underline{u}(\underline{r}) = 0.$$

Non-spherical defects are usually approached in a somewhat different manner. Any defect which is in mechanical equilibrium with the lattice must exert zero net force on the lattice. It follows that the forces which the defects do exert can be represented by double forces without moment.

These forces can be represented by the following equation (Hardy, 1968)

$$-F_i(\underline{x}) = \sum_j G_{ij} \frac{\partial}{\partial x_j} \delta(\underline{x}) \quad (2.3.3)$$

where  $i$  and  $j$  are Cartesian coordinate indices and  $G_{ij} = G_{ji}$ .  $\delta(\underline{x})$  is the Dirac delta function. Hence the forces are nonzero only at the origin, the site of the point defect. The elastic equation which must be solved is (Brudnoy, 1974)

$$\sum_{j,k,\ell} C_{ij,k\ell} \frac{\partial^2 u_k(\underline{x})}{\partial x_j \partial x_\ell} = F_i(\underline{x}) \quad (2.3.4)$$

where  $C_{ij,k\ell}$  is the elastic modulus tensor and  $u_k$  is a component of  $\underline{u}$ . This equation can be simplified in the case of isotropic elasticity where all the  $C_{ij,k\ell}$  can be written in terms of the two Lamé constants and in the cubic case where there are only three independent  $C_{ij,k\ell}$ .

Huntington and Johnson (1962) have solved an equivalent equation for the case which corresponds to having only  $G_{11}$  non-zero. This represents

a defect having uniaxial symmetry. If the defect is at the centre of a sphere of radius  $R$  which has a free surface, then the displacement of the surface due to the defect can be shown to be

$$\underline{u} = \frac{G_{11}}{4\pi R^3} \left[ \frac{5\lambda}{2\mu(19\lambda + 14\mu)} (3R_1 \hat{x}_1 - \underline{R}) + \frac{35(\lambda + \mu)(3 \cos^2\theta - 1)\underline{R}}{2\mu(19\lambda + 14\mu)} \right] \quad (2.3.5)$$

where  $\underline{R}$  is a vector normal to the surface with components  $R_1$ ,  $R_2$  and  $R_3$ .  $\hat{x}_1$  is a unit vector in the  $x_1$  direction which is also the direction along which the forces act.  $\theta$  is the angle between the  $x_1$  direction and the vector  $\underline{R}$ .

Hardy (1968) has determined the  $G$  tensor from the interatomic force constants. The change in the energy of a monatomic lattice upon introducing a defect at the origin is

$$\Delta U = \sum_{\ell} \psi(|\underline{R}^{\ell} + \underline{u}^{\ell}|) + \frac{1}{2} \sum_{\ell\ell'} \sum_{ij} u_i^{\ell} A_{ij}^{\ell\ell'} u_j^{\ell'} + \text{higher order terms} \quad (2.3.6)$$

where  $\psi(|\underline{r}|)$  is the interaction between the defect and an atom of the host lattice a distance  $r$  away. The  $A$ 's are generalized spring constants.  $\underline{R}^{\ell}$  is the position vector of the  $\ell^{\text{th}}$  perfect lattice site. If the lattice is in equilibrium then  $\frac{\partial(\Delta U)}{\partial u_i^{\ell}} = 0$  and it follows that

$$F_i^\ell \equiv \frac{\partial}{\partial u_j^\ell} \psi(|\underline{R}^\ell + \underline{u}^\ell|) = \sum_j A_{ij}^{\ell\ell'} u_j^{\ell'} \quad (2.3.7)$$

Using Fourier transformations and power series expansions, Hardy concludes with an expression for  $G_{ij}$  for cubic lattices

$$G_{ij} = \sum_\ell F_i^\ell R_j^\ell \quad (2.3.8)$$

which is the relationship between the strength matrix and the interatomic potentials.

In principle, the interaction potential between the defect and the atoms of the host lattice can be calculated using the electrostatic theories discussed in the previous section. March and Rousseau (1971) point out that in order to relate the forces  $F_i^\ell$  to the displaced charge, an iterative procedure must be used because initially neither the displaced charge nor the ionic positions about the defect are known. The displaced charge can be calculated for the unrelaxed lattice but then the ions are no longer in equilibrium positions because they are acted upon by the potential due to the displaced charge. When the calculation is finished, the ions will be in new equilibrium positions consistent with the displaced charge.

This is the approach which should be used to describe the strain field of the hydrogen-substitutional defect pair if realistic results are to be obtained. Such a calculation is now possible if the nonlinear

screening approach of Popović (1974) is used to describe the hydrogen ion and a suitable screened pseudopotential is used for the substitutional atom.

#### 2.4 Defect Interaction

Point defect interactions take place because single point defects disturb the perfect lattice both electrostatically and elastically as has been shown in the two preceding sections. At the conclusion of the section on the elastic properties of the defects, the fact that the elastic and electrostatic properties of point defects are closely connected was pointed out. In a similar way, it is not truly possible to separate defect interaction into elastic and electrostatic parts because these are interdependent. However, the development of defect interaction calculations has historically followed these two separate lines. In this section, therefore, the electrostatic and elastic contributions are presented separately. The interrelationships are then pointed out.

The electrostatic contribution to defect interaction is now quite well understood. Corless and March (1961) have shown that the interaction energy for two point charges in a metal can be written

$$\Delta E \approx \frac{1}{2} Z_1 V_{2\text{eff}}(\underline{r}_1 - \underline{r}_2) + \frac{1}{2} Z_2 V_{1\text{eff}}(\underline{r}_2 - \underline{r}_1) \quad (2.4.1)$$

where  $V_{2\text{eff}}(\underline{r}_1 - \underline{r}_2)$  is the self consistent field produced at  $\underline{r}_1$  by the charge  $Z_2 e$  at  $\underline{r}_2$ . This result depends upon limiting the calculation to

first order in the perturbing potentials, and assumes the bare ions are point charges. Ziman (1964) generalized this treatment for distributed charge, showing

$$\Delta E = \frac{1}{2} \int \{Z_1(\underline{r}) V_{2\text{eff}}(\underline{r}) + Z_2(\underline{r}) V_{1\text{eff}}(\underline{r})\} d\underline{r} \quad (2.4.2)$$

where  $Z_1(\underline{r})$  is the density of charge associated with  $Z_1$  and  $V_{2\text{eff}}(\underline{r})$  is the effective potential at  $\underline{r}$  due to the charge  $Z_2$ . If the Fourier transforms of  $Z$  and  $V$  are substituted into the above equation, the interaction can be written

$$\Delta E = \int \frac{4\pi e^2 Z_1(\underline{k}) Z_2(\underline{k}) \exp[i \underline{k} \cdot (\underline{R}_1 - \underline{R}_2)] d\underline{k}}{k^2 \epsilon(k)} \quad (2.4.3)$$

where  $\underline{R}_1 - \underline{R}_2$  is the vector between the centres of the charge distributions. This interaction has the same type of oscillatory character as that in the effective potential previously shown (equation 2.2.5).

The expression above would be valid if the interactions took place at constant volume. However, the total energy of a metal cannot be written in terms of pairwise interactions only but includes terms which are dependent upon the total volume. If there are volume charges due to the interaction then there will be additional terms in the interaction energy.

Elastic interactions between defects have been dealt with in both the continuum model (Eshelby, 1956) and using a discrete lattice (Hardy and Bullough, 1967). Centres of dilatation in an infinite isotropic continuum

cannot interact (Eshelby, 1956). However, the dilatation introduced by the boundary condition at the surface of a finite crystal does cause elastic interaction between such defects. Eshelby shows that this interaction has the form

$$\Delta E = -6v_0(M_1 \Delta V_2^2 + M_2 \Delta V_1^2) / r^6 \quad (2.4.4)$$

where  $v_0$  is the atomic volume,  $\Delta V_i$  is the volume change at the free surface due to the defect  $i$ ,  $M_i$  is the rate of change with atomic concentration of the apparent shear modulus of a crystal containing defects of type  $i$ , and  $r$  is the distance between the defects. This formula is valid only when the separation  $r$  is large enough that the variation of the strain field due to one defect over the extent of the other is small. For cubic crystals Eshelby shows that cubically symmetric defects interact with an energy given by

$$\Delta E = -\frac{15d}{8\pi\gamma^2} \Delta V_1 \Delta V_2 \frac{\phi}{r^3} \quad (2.4.5)$$

where  $d = c_{11} - c_{12} - 2c_{44}$  is a measure of the elastic anisotropy and is small,  $\gamma = K/c_{11}^0$  where  $K$  is the bulk modulus and  $c_{11}^0 = \frac{3}{5}(c_{11} + 2c_{12} + 4c_{44})$  is an "average" of  $c_{11}$  and  $\phi = \ell^4 + m^4 + n^4 - \frac{3}{5}$  where  $\ell, m, n$  are direction cosines of the line joining the defects relative to the crystal axes.

The strength of the interaction therefore depends upon the relative orientation of the defects. Hardy and Bullough (1967) have calculated the

interaction between similar defects in a cubic lattice using a discrete lattice theory. By expanding the energy of a defect according to the equation (2.3.6) already presented and using Fourier transforms, they found that the defect interaction could be written in terms of the Fourier transforms of the forces  $F_i^l$  defined by equation (2.3.7) and the inverse of the Fourier transform of the generalized spring constants. The defect interaction is then given by

$$\Delta E = -\frac{1}{N} \sum_{\mathbf{q}} F_a(-\mathbf{q}) [A(-\mathbf{q})]^{-1} F_b(\mathbf{q}) \quad (2.4.6)$$

where the subscripts a and b refer to the defects a and b. The summation is over the  $\mathbf{q}$  vector of the first Brillouin zone. This formula should describe the interaction energy even at close separations whereas the elastic continuum approval must break down in this range. In the asymptotic limit of large separation, this interaction varies as  $R^{-5}$  where  $R$  is the defect separation and is anisotropic. This is a different result from the  $R^{-6}$  of the isotropic continuum. Another interesting result of this formulation is that the interaction energy calculated for two vacancies by this method not only varies with relative orientation but actually changes sign with distance along one direction (110) even though the interatomic forces are assumed to be nearest neighbour forces only.

## 2.5 Internal Friction

The basis of the measurement of internal friction is the fact that

when a stress is applied to a solid, there is a simultaneous elastic strain followed by a time dependent "anelastic" strain which is a function of the defect structure of the material. If the rate at which the anelastic strain ( $\epsilon_a$ ) develops is proportional to the deviation of the anelastic strain from its equilibrium value ( $\epsilon_0$ ) for a constant stress, then the anelastic strain can be determined from the following equation:

$$\frac{d\epsilon_a}{dt} = \frac{\epsilon_0 - \epsilon_a}{\tau} \quad (2.5.1)$$

Then it follows that

$$\epsilon_a = \epsilon_0(1 - \exp^{-t/\tau}) \quad (2.5.2)$$

where  $\tau$  is the relaxation time (at constant stress). In general, for a given material, there will be a whole range of relaxation times each corresponding to a different type of defect contributing to the time dependent strain.

Since the modulus of compliance  $J$  is defined as the ratio of strain to stress, it is apparent that one modulus is not sufficient to define the properties of the solid. Hence, following Nowick and Berry (1972), we define two moduli  $J_u \equiv \frac{\epsilon_e}{\sigma}$  and  $J_R \equiv \frac{\epsilon_e + \epsilon_0}{\sigma}$ , where the subscripts  $u$  and  $R$  refer to unrelaxed and relaxed respectively and  $\epsilon_e$  is the elastic strain.

It is the dynamic properties of the system that are of interest. The alternating applied stress  $\sigma$  and resulting strain  $\epsilon$  can be described

by the following equations

$$\sigma = \sigma_0 e^{i\omega t} \quad \epsilon = (\epsilon_1 - i\epsilon_2) e^{i\omega t} \quad (2.5.3)$$

where  $\epsilon_1$  and  $\epsilon_2$  are the in-phase and out-of-phase strain components. Now if we define  $J_1 \equiv \frac{\epsilon_1}{\sigma_0}$  and  $J_2 \equiv \frac{\epsilon_2}{\sigma_0}$  then it turns out that  $J_1$  and  $J_2$  are functions of  $\omega$ , the angular frequency, given by the following equation:

$$J_1(\omega) = J_u + \frac{\delta J}{(1 + \omega^2 \tau^2)} \quad (2.5.4)$$

$$J_2(\omega) = \delta J \frac{\omega \tau}{1 + \omega^2 \tau^2} \quad (2.5.5)$$

$$\delta J \equiv J_R - J_u$$

These are the Debye equations which were first derived to describe dielectric relaxation.

It is easy to show that the work done per cycle of the alternating stress  $\sigma$  per unit volume is given by

$$W = \pi \sigma_0 \epsilon_2 = \pi J_2 \sigma_0^2 \quad (2.5.6)$$

The out-of-phase component of the strain is responsible for work being done.

Since the internal friction,  $Q^{-1}$ , is defined as the ratio of the work done per cycle to  $2\pi$  times the maximum energy stored per cycle,

which is  $\frac{1}{2} J_1 \sigma_0^2$ , therefore

$$Q^{-1} = \frac{J_2}{J_1} = \frac{\epsilon_2}{\epsilon_1} = \tan \phi,$$

where  $\phi$  is the phase between stress and strain. In terms of  $J_R$  and  $J_U$  the internal friction is given by

$$Q^{-1} = \delta J \frac{\omega\tau}{J_R + J_U \omega^2\tau^2} \quad (2.5.7)$$

In the case where  $\delta J \ll J_U$  then the internal friction is well represented by a Debye peak

$$Q^{-1} \approx \Delta \frac{\omega\tau}{1 + \omega^2\tau^2} \quad (2.5.8)$$

$$\Delta \approx \frac{\delta J}{J_U}$$

$\Delta$  is the relaxation strength. The height of the internal friction maximum, which occurs for  $\omega\tau = 1$ , is therefore  $\Delta/2$ .

The effect of having more than one process contributing to the development of the anelastic strain at constant stress is reflected in the dynamic moduli  $J_1$  and  $J_2$ . In the case of such multiple relaxations,  $J_1$  and

$J_2$  are given by (Nowick and Berry, 1972)

$$J_1(\omega) = J_u + \sum_{i=1}^n \frac{\delta J^{(i)}}{1 + (\omega\tau^i)^2} \quad (2.5.9)$$

$$J_2(\omega) = \sum_{i=1}^n \delta J^{(i)} \frac{\omega\tau^i}{1 + (\omega\tau^i)^2} \quad (2.5.10)$$

where  $\delta J^{(i)}$  is the contribution to the relaxed compliance from process  $i$  with relaxation time  $\tau^i$ . If all the  $\delta J$ 's are small, then the internal friction will also have the same form as  $J_2(\omega)$ .

If the relaxation process is thermally activated, then the relaxation time  $\tau$  is temperature dependent in the following way:

$$\tau = \tau_0 \exp \frac{\Delta H}{kT}, \quad (2.5.11)$$

where  $\Delta H$  is the activation enthalpy and  $\tau_0^{-1}$  is a frequency factor. In terms of the internal friction measurements, this temperature dependence is of great significance. The expression for the internal friction is symmetric in  $\omega$  and  $\tau$ . This means that if  $\tau$  is fixed, the maximum in the internal friction, which occurs for  $\omega\tau = 1$ , will be found only by varying the frequency. In practice, the range over which the frequency can be varied on a given sample is very limited. However, if  $\tau$  has the temperature dependence indicated by equation (2.5.11), then by varying the temperature  $\tau$  can be brought to the value  $\omega^{-1}$  where there will be an internal friction

maximum due to the process in question. The activation enthalpy,  $\Delta H$ , can be determined by finding the temperature of the internal friction peak at two different frequencies. Then, since in each case

$$\omega = \tau^{-1} = \tau_0^{-1} \exp \left[ -\frac{\Delta H}{kT} \right],$$

therefore

$$\ln \frac{\omega_2}{\omega_1} = \frac{\Delta H}{k} \left[ \frac{1}{T_1} - \frac{1}{T_2} \right] \quad (2.5.12)$$

where  $T_1$  and  $T_2$  are the peak temperatures corresponding to the applied stress frequencies  $\omega_1$  and  $\omega_2$ .

If the value of  $\tau_0$  for the relaxation process is known (and there seem to be values which are characteristic of point defect, dislocation, and interaction effects), then for a given applied frequency, the temperature at which a peak occurs,  $T_p$ , is directly proportional to the activation enthalpy of the process producing the anelastic strain. A plot of  $\Delta H$  vs.  $T_p$  can be made for various values of the product  $\omega\tau_0$ . This is the Wert-Marx plot (Wert and Marx, 1953).

The activation enthalpy may also be found from the width of the peak in  $T^{-1}$  at half maximum height if the peak is a Debye peak. Using the activation enthalpy found in this way and the Wert-Marx plot, the value of  $\tau_0$  for the process may be determined in order to identify it.

### Internal friction due to point defects

The theory of internal friction due to point defects is well developed. The relaxation strength  $\Delta$  and the time constant  $\tau$  can be derived from microscopic defect properties.

The anelastic strain due to point defects can be calculated if the strain fields of the defects and the defect concentrations are known. It is possible to define a tensor which describes the strain field of a point defect by the following equation (Nowick and Heller, 1963):

$$\epsilon_{ij}^d - \epsilon_{ij}^0 = \sum_{p=1}^{n_d} \lambda_{ij}^{(p)} c_p \quad (2.5.13)$$

The superscripts  $d$  and  $0$  on the strain components refer to the crystal with defects and without defects respectively.  $p$  is an index which labels the defect orientation and  $c_p$  is the mole fraction of defects in the  $p$  orientation

$$c_p = v_0 N_p, \quad (2.5.14)$$

where  $v_0$  is the atomic volume and  $N_p$  is the number of defects in the  $p^{\text{th}}$  orientation per unit volume. It follows from equation (2.5.13) that the  $\lambda_{ij}^{(p)}$  are defined by

$$\lambda_{ij}^{(p)} \equiv \frac{\partial \epsilon_{ij}}{\partial c_p} \quad (2.5.15)$$

Since  $\epsilon_{ij}$  is a strain tensor, it must be symmetric and, therefore,  $\lambda_{ij}$  is also symmetric. This means that  $\lambda_{ij}$  may be diagonalized. The diagonal elements  $\lambda_1$ ,  $\lambda_2$  and  $\lambda_3$  are the semi-axes of a strain ellipsoid which has its principal axis oriented at some angle with respect to the crystalline axes. This orientation is dependent upon the positions of the atoms which make up the defect. The symmetry of the defect must be reflected in the symmetry of the strain ellipsoid. The diagonal elements or principal values of the  $\lambda$  tensor are dependent only upon the type of defect, not upon the orientation of the strain ellipsoid. The  $\lambda$  tensor is directly calculable if the strain distribution around the defect is known, as has been done for the single double-force of Huntington and Johnson (1962). Flynn (1972) shows that when the defect lies along the 1 direction, the  $\lambda$  tensor is given by

$$\lambda_1 = \frac{G_{11}}{\mu v_0} + \frac{G_{11}}{3(3\lambda + 2\mu)v_0} \quad (2.5.16)$$

$$\lambda_2 = \lambda_3 = -\frac{G_{11}}{\mu v_0} + \frac{G_{11}}{3(3\lambda + 2\mu)v_0} \quad (2.5.17)$$

For anisotropic material the results of Brudnoy (1974) could be used for calculating the values of the  $\lambda$  tensor.

The possibility of observing point defect reorientation by internal friction is dependent upon several criteria. The basic criterion is that the applied stress must cause a change in the relative free energies of the possible orientations of the defect. This means that, first of all, there

must be more than one position in the primitive unit cell for the defect (or more than 2 positions if the positions are centro-symmetric (Wachtman and Peiser, 1962).

It is possible to calculate the relaxation magnitude  $\Delta$  from simple thermodynamic arguments such as those presented by Nowick and Berry (1972). If the mole fraction of defects of a particular type (e.g. substitutional-interstitial defects) is  $c_0$  and there are  $n_t$  crystallographically equivalent orientations of the  $\lambda$  tensor then

$$\sum_{p=1}^{n_t} c_p = c_0 \quad (2.5.18)$$

When the applied stress is zero, there will be nothing which distinguishes the different orientations, therefore the concentration in each orientation will be  $c_0/n_t$ . If the application of a uniaxial stress  $\sigma_{11}$  to the system changes the distribution of defects among the possible orientations of the  $\lambda$  tensor then the strain (considering only  $\epsilon_{11}$ ) will be given by

$$\epsilon_{11} = J_u \sigma_{11} + \sum_{p=1}^{n_t} \lambda_{11}^{(p)} [c_p - (c_0/n_t)] \quad (2.5.19)$$

The value of  $\lambda_{11}^{(p)}$  is derived from the principal values of the strain ellipsoid by a tensor transformation given by

$$\lambda_{ij}^{(p)} = \sum_{m=1}^3 \alpha_{im}^{(p)} \alpha_{jm}^{(p)} \lambda_m \quad (2.5.20)$$

where  $\lambda_m$  is the value along the principal axis of the ellipsoid that has direction cosine  $\alpha_{km}^{(p)}$  to the  $k^{\text{th}}$  crystal direction when the defect is in orientation  $p$ .

In order to calculate the relaxation strength we need to know  $c_p$  for a given stress. The change in the Gibbs free energy with change in stress of any particular defect with tensor  $\lambda^{(p)}$  must be calculated. The application of Boltzmann statistics then yields the  $c_p$ 's. Nowick and Berry (1972) show that the change in the Gibbs free energy of a defect in orientation  $p$  due to the stress application is given by

$$\Delta G^{(p)} = -v_0 \lambda_{11}^{(p)} \sigma_{11} \quad (2.5.21)$$

for a uniaxial stress, or

$$\Delta G^{(p)} = -v_0 \sum_{ij} \lambda_{ij}^{(p)} \sigma_{ij}$$

in general.

If the different orientations are then allowed to repopulate according to the Boltzmann distribution so that the probability of occupation of an orientation  $p$  is proportional to  $\exp[-\Delta G^{(p)}/kT]$  then the result is

$$\bar{c}_p - \frac{c_0}{n_t} = \frac{c_0 v_0 \sigma_{11}}{n_t kT} \left[ \lambda_{11}^{(p)} - \frac{1}{n_t} \sum_q \lambda_{11}^{(q)} \right] \quad (2.5.22)$$

$\bar{c}_p$  is then the equilibrium value of the concentration of defects in orientation  $p$  under an applied stress  $\sigma_{11}$ . The assumption is made that  $\Delta G^{(p)}/kT \ll 1$  which will be valid at low stress levels. The relaxation of the compliance is then given by substituting equation (2.5.22) into equation (2.5.19)

$$\delta J = \frac{\epsilon_a}{\sigma_{11}} = \frac{c_0 v_0}{n_t kT} \left[ \sum_p (\lambda_{11}^{(p)})^2 - \frac{1}{n_t} \left( \sum_p \lambda_{11}^{(p)} \right)^2 \right] \quad (2.5.23)$$

The internal friction peak height is just  $\delta J/2J$ .

In single crystal specimens, for which the stress axis may be oriented in specific directions relative to the crystal axes, this expression can be calculated if the symmetry of the defect and the principal values of the  $\lambda$  tensor are known. For tetragonal defects (which are expected in the case of hydrogen-substitutional pairs in aluminum) the defect  $\lambda$  tensor has three possible orientations in the cubic lattice. The tetragonal axis of the defect (largest principal value) must lie along one of the cube axes. The other two principal values, which are equal, can be taken to lie along the other cube directions. For this case, the expression in the bracket above reduces to

$$\frac{2}{3} (\lambda_1 - \lambda_2)^2 \quad (2.5.24)$$

if the applied stress is along a cube direction and zero if the applied stress is along the  $\langle 111 \rangle$  direction. The reason for the relaxation of the

modulus being zero for the  $\langle 111 \rangle$  stress orientation is that the stress axis has the same relationship with all three possible orientations of the defect strain ellipsoid and hence cannot cause a change in their relative free energies. Thus no redistribution of defects among the different orientations takes place. In order to find the relaxation  $\delta J$  for an arbitrary orientation of the stress axis with respect to the cube axes, it is possible to follow the above procedure. The general result is (De Batist, 1972).

$$\delta J = \frac{2}{9} \frac{c_0 v_0}{kT} (\lambda_1 - \lambda_2)^2 (1 - 3\Gamma) \quad (2.5.25)$$

$$\text{where } \Gamma = \alpha^2 \beta^2 + \beta^2 \gamma^2 + \gamma^2 \alpha^2 \quad (2.5.26)$$

$\alpha$ ,  $\beta$  and  $\gamma$  are the direction cosines of the stress axis relative to the cube axes.  $\Gamma$  varies from 0 to a maximum of  $1/3$  if the stress axis is along the  $\langle 111 \rangle$  direction.

In order to determine the relaxation strength,  $\Delta$ , for an arbitrary orientation of the stress the value of the compliance modulus  $J$  must also be known. The results of Hearmon (1957) may be used to show that

$$J = s_{11} - 2(s_{11} - s_{12} - \frac{1}{2} s_{44}) \Gamma \quad (2.5.27)$$

where the  $s$ 's are the normal elastic compliance constants referred to the cubic axes. The relaxation strength, given by  $\delta J/J$ , is not therefore a

linear function of  $\Gamma$ .

In polycrystalline samples, the crystal axes of the various crystallites are in random orientations with respect to the stress axis (neglecting texture effects). In order to determine the compliance modulus,  $J$ , and the relaxation of the modulus,  $\delta J$ , some assumption must be made to describe the stress conditions at the grain boundaries. If the stress is assumed to be uniform from grain to grain (the Reuss approximation) then it can be shown (De Batist, 1972) that the resulting modulus and relaxation would be the same as in equations (2.5.27) and (2.5.25) with  $\Gamma = 0.2$ .

The relaxation time,  $\tau$ , for reorientation of tetragonal defects in cubic crystals can be calculated in a straight forward way using rate theory (Nowick and Berry, 1972). If the splitting of the free energy levels of the different orientations due to the stress is small and if the number of defects is constant, then

$$\tau^{-1} = 3\nu \quad (2.5.28)$$

where  $\nu = \nu_0 \exp[-\Delta G_m/kT]$  is the probability per unit time of reorientation from one particular orientation to another.  $\nu_0$  is a frequency factor and  $\Delta G_m$  is the activation free energy. This is the general form for all tetragonal defects in cubic lattices. In order to relate this to atomic jump frequencies, the substitutional-interstitial defect must be examined in more detail. As in Figure 2.1, there are six possible nearest neighbour positions for the hydrogen atom next to the substitutional atom, but there

are only three possible orientations for the defect strain tensor. If the substitutional atom is considered to be at the origin, then hydrogen atoms in octahedral positions at  $\pm \frac{1}{2}, 0, 0$  produce the same  $\lambda$  tensor. If the atomic jump frequency for the hydrogen atom to jump to one of the other sites adjacent to the substitutional impurity is  $w$ , then the frequency of reorientation of the  $\lambda$  tensor must be  $2w$  because there are two sites which produce the same reorientation. Therefore,

$$\tau^{-1} = 6w \quad (2.5.29)$$

The diffusion coefficient of hydrogen can be found in terms of the jump frequency of hydrogen in the normal lattice. If  $w'$  is the rate of jumping of an interstitial from one octahedral site into another octahedral site, then an expression for the diffusion coefficient for the face centred cubic lattice may be found in terms of this jump rate to be (Flynn, 1972)

$$D = w' a^2 \quad (2.5.30)$$

where  $a$  is the lattice parameter. If  $w'$  is the same as  $w$ , then equation (2.5.30) may be substituted into (2.5.29) to get

$$\tau^{-1} = \frac{6D}{a^2} \quad (2.5.31)$$

The temperature dependence of  $\tau^{-1}$  can, therefore, be found from that of the diffusion coefficient. The temperature of an internal friction peak

due to substitutional-interstitial pairs can then be estimated since the peak position is determined by  $\tau^{-1} = 2\pi f$  where  $f$  is the frequency of the applied stress.

## CHAPTER 3

### EXPERIMENTAL APPARATUS

#### 3.1 Introduction

The purpose of this chapter is to describe the apparatus which was used to make internal friction measurements over the temperature range from liquid nitrogen temperature to room temperature.

Briefly, the apparatus includes the composite resonator, the electronic equipment for measurement of the electrical properties of the resonator at resonance, and the equipment for controlling the environment of the resonator in order that sensitive measurements could be made over the wide temperature range.

The composite resonator technique was chosen for the internal friction measurements for two reasons. With careful technique, it can be used to measure damping in the  $Q^{-1} \approx 10^{-6}$  range and measurements can be made at several frequencies simply by using different resonance modes. The fundamental frequency of the resonators used in this work was 35 kHz and measurements could also be made using the third and fifth harmonics. The low background damping was essential because of the small expected size of the internal friction due to hydrogen-substitutional pairs. The use of higher resonant frequencies enables determination of activation energies of thermally activated processes responsible for the internal friction and also the temperature dependence of the relaxation strength  $\Delta$ .

### 3.2(a) The Composite Resonator

The two component resonator with frequency matched components was first used by Balamuth (1934). The two components are the driving quartz crystal and the specimen. A typical 35 kHz resonator is shown in Figure 3.1. The combination is excited into resonance in a longitudinal mode by the application of an alternating voltage at the resonant frequency to electrodes on the faces of the quartz crystal.

The quartz crystals used in these experiments were  $-18.5^\circ$  X-cut crystals of natural quartz which were obtained from the Bliley Electric Company, Erie, Pa. Quartz seems to be the only reasonable material for piezoelectric drives for the composite oscillator. It combines a high electromechanical coupling factor, (so that most of the energy stored per cycle at resonance is in the stress distribution and not in the electric field) with a low damping which is essential for sensitive internal friction measurements because the total damping in the resonator depends also on the damping of the quartz. The  $-18.5^\circ$  X-cut has special significance; there is very good coupling of the electric field in the X direction with uniaxial strain along the length of the bar and almost no coupling to other strain components (Mason, 1950). This results in the generation of reasonably pure longitudinal waves in the rod upon application of an alternating electric field in the X direction.

The quartz crystal is joined to the metallic sample rod with a bond of low melting point solder. The technique for making the bond is described in the following chapter. Other types of bonding materials were tried including various organic materials (gelatine, phenyl salicylate and GE 7031 varnish). All of these had serious disadvantages, including long

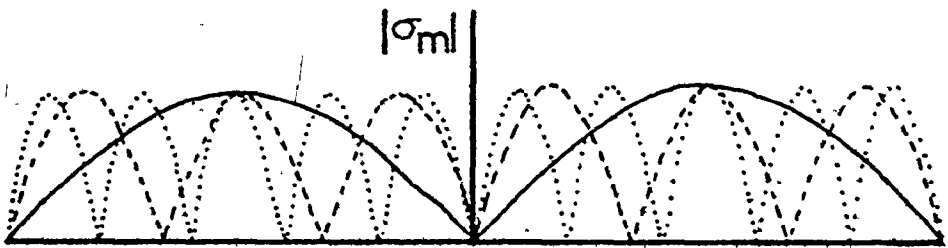
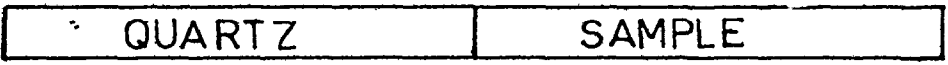
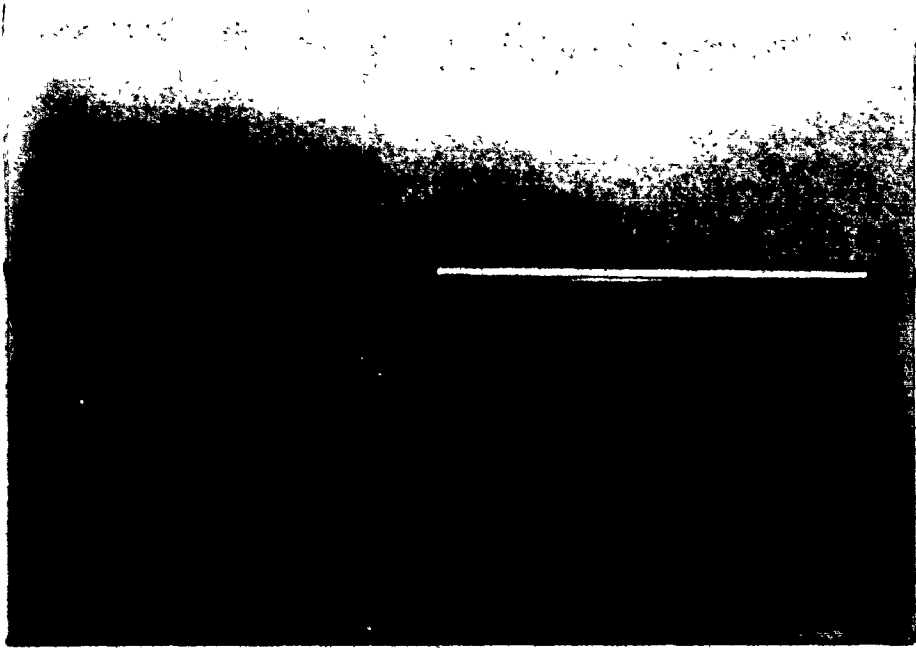
FIGURE 3.1

35 kHz composite resonator showing suspension threads, electrical leads and contacts, and the gold film on the quartz

FIGURE 3.2

Maximum absolute stress distribution in a resonator at resonance

——— fundamental  
----- third harmonic  
..... fifth harmonic



curing times, high damping or lack of the ability to be thermally cycled. The metallic bond necessitates heating the sample to 100°C for a short period but once made it does not change with time, the damping is very low and it can be thermally cycled to liquid nitrogen temperatures without cracking.

Quartz and metallic specimens have quite different thermal expansion coefficients, hence on temperature cycling large thermal stresses can be built up at the interface. It is thought that the metallic bond allows these stresses to be relaxed (by plastic deformation).

The bond material is also important for another reason. At room temperature, if the resonant frequencies of the quartz and specimen are closely matched, the bond occurs at a node of the standing stress wave as shown in Figure 3.2. Even if the internal friction of the bond material is high, the damping in the whole resonator can still be low because the bond is not stressed. However, on cooling the composite resonator, the resonant frequencies of the quartz and specimen are no longer matched due to the differences in the temperature dependence of the elastic moduli and thermal expansion coefficients. This means that the joint material is no longer at a stress node. The internal friction of the bond may now contribute significantly to the total damping in the resonator. The effect is especially large when the resonator is operated on higher harmonics because a change in temperature moves the node the same distance away from the joint for all frequencies but this distance is a larger fraction of the wavelength for higher frequencies. Thus, the stress at the joint will be higher.

The sample is cut so that the resonant frequencies of the quartz alone and of the composite resonator are equal at some temperature between

80 K and 300 K. This assures that the node of the stress wave is never too far from the joint.

Similar considerations of the effect of temperature on nodal position apply to the suspension point, which is ideally a displacement node. As the node moves away from the suspension point with temperature changes acoustic energy can be lost by radiation along the suspension. There have been many different types of suspension reported in the literature (see e.g. Saul and Bauer, 1968; Cady, 1946). Extensive preliminary experiments showed that the wire and pin suspensions which were tried gave large background damping and were very sensitive to the nodal position. The silk thread suspension, which was finally used, was much less sensitive to the nodal position, had a very low background damping and, since it was permanently attached to the crystal, gave reproducible results. The electrical connection to the gold film on the quartz crystal was by very fine (#44 B.S. gauge) copper wires joined to the film with a dab of colloidal silver.

### 3.2(b) Electrical Properties of the Composite Resonator

One of the advantages of using the composite resonator technique is that the resonator is also an electrical device the properties of which can be easily measured and are directly related to the elastic and anelastic properties.

The quartz resonator operating near the resonant frequency has an equivalent electrical circuit (Cady, 1946) which is shown in Figure 3.3 below.

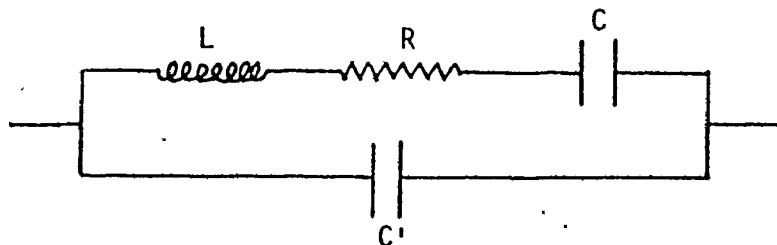


FIGURE 3.3

It consists of a simple series resonant circuit with a parallel capacitance  $C'$  due to the dielectric nature of the quartz. The inductance,  $L$ , resistance,  $R$ , and capacitance,  $C$ , of the series resonant circuit represent the inertial, damping and elastic parts respectively of the mechanical resonator.

In order to demonstrate the behaviour of this equivalent resonator near the resonant frequency, it is instructive to follow Cady's analysis. The admittance,  $Y$ , of the resonator can be written

$$Y = j C' \omega + \frac{R}{R^2 + X^2} - \frac{jX}{R^2 + X^2} \quad (3.2.1)$$

where  $X = (L\omega - \frac{1}{C\omega})$ ,  $j = \sqrt{-1}$

A graphical method may be used to describe the admittance,  $Y_R$ , of the series arm of the resonant circuit (i.e. the last two terms in equation 3.2.1). This method has the advantage that it allows rapid interpretation of more complex circuits (e.g. the bridge circuit to be described). The basic graph is shown in Figure 3.4.

The vector from the origin to a point on the circle is the admittance. The circle is the locus of the admittance as the frequency varies near the

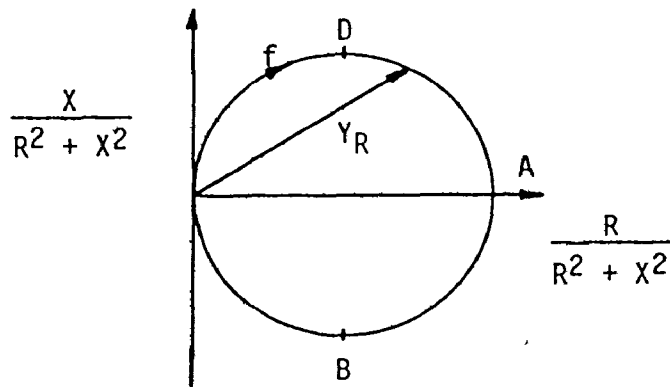


FIGURE 3.4

resonant frequency (the direction of increasing frequency is indicated in the figure). At resonance,  $X$  is zero and the admittance is given by point  $A$  (a real admittance with a value of  $1/R$ ).

Since admittances in parallel are added vectorially, the total admittance of the equivalent resonator is shown in Figure 3.5.

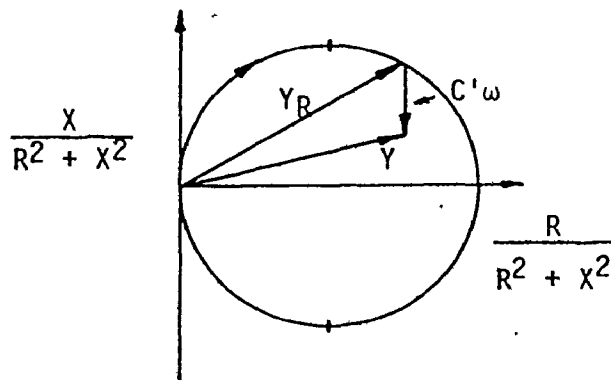


FIGURE 3.5

At each point a vector  $C'\omega$  is added to the vector  $Y_R$  to give the total admittance  $Y$ .

For a given resonator operating at a single frequency, the resistance at resonance,  $R$ , is directly proportional to the total damping  $Q_t^{-1}$  of the composite oscillator. Marx (1951) gives the following relationship between  $Q_t^{-1}$  and  $R$ :

$$Q_t^{-1} = \frac{9.98 \times 10^{-3} b^2 R}{\pi m_t f}, \quad 3.2.2$$

where  $b$  is the width of the electrode face in cm (0.635 cm in our case),  $m_t$  is the total mass of the resonator in grams, and  $f$  is the frequency in Hz. This expression is valid only for  $-18.5^\circ$  X-cut quartz transducers with full length adherent electrodes operating on odd harmonics.  $Q_t^{-1}$  may also be found by measuring the frequencies at the half power points (B and D in Figure 3.4). The values so obtained agreed with Marx's result within about 5%. Robinson (1974) has proposed a different equivalent circuit and his analysis yields results which are about twenty per cent higher than Marx's. Our results have been interpreted using Marx's formulation because of the better agreement with his results.

### 3.3 The Alternating Current Bridge

The bridge circuit is shown schematically in Figure 3.6. This bridge, which is used to measure the resistance of the composite resonator at resonance, is based on that of Saul and Bauer (1967).

The signal generator is a Monsanto 3100 B digital frequency synthesizer with a very pure output (harmonics, spurious signals and line frequency related signals were 40, 70 and 60 dB respectively below the

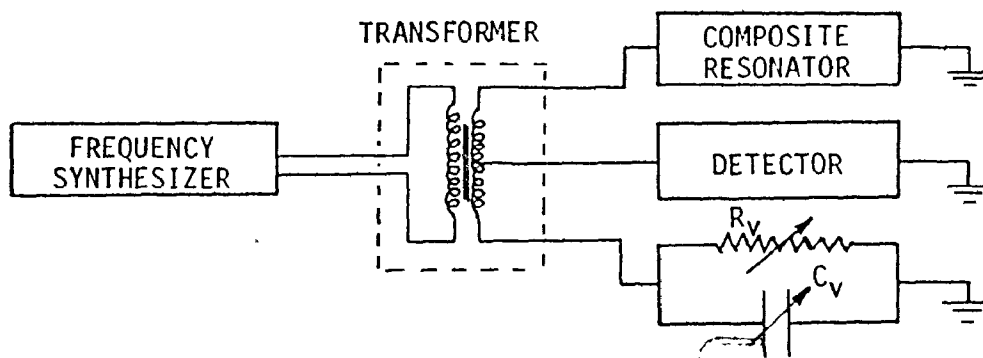


FIGURE 3.6

main output). The frequency can be varied either continuously or in steps of .01 Hz to 100 kHz from DC to 1.3 MHz. The output voltage into a  $50\Omega$  impedance is variable in 10 dB steps from -70 dB to +20 dB with 0 dB corresponding to 223 mV rms. This range was sufficient for all the measurements performed in this work.

The output from the synthesizer is fed into a transformer which provides equal and opposite outputs to the composite resonator and the variable arm of the bridge.

The bridge balance condition is easy to determine. If the secondary coil of the transformer is truly divided in half at the point where the detector is connected, then when the admittances of the resonator and balancing arm are equal the signal at the detector will be null.

The admittance of the resonator near resonance has already been shown to be

$$Y = \frac{R}{R^2 + X^2} + j C \omega - \frac{j X}{R^2 + X^2}$$

C' now includes the parallel capacitance in the leads from the bridge to the resonator in addition to the capacitance of the quartz. The admittance,  $Y_V$ , of the variable balancing arm (a variable resistance,  $R_V$ , in parallel with a variable capacitance  $C_V$ ) is simply

$$Y_V = \frac{1}{R_V} + j \omega C_V$$

At balance the real and imaginary parts of  $Y$  and  $Y_V$  must be equal i.e.:

$$\frac{R}{R^2 + X^2} = \frac{1}{R_V}$$

and 
$$\omega C_V = \omega C' - \frac{X}{R^2 + X^2}$$

At resonance  $X = 0$ , therefore  $R_V = R$  and  $C_V = C'$ . The technique used for achieving this balance condition is described in the following chapter.

The transformer is really the heart of the bridge circuit. It converts the synthesizer signal into two signals of equal magnitude but opposite phase. These two signals supply the composite resonator and the balancing arm. The transformer was wound using #28 B.S. gauge copper wire on a Philips Ferroxcube "H core" transformer core. The windings were varnished to the core using GE 7031 insulating varnish. The resulting transformer had very good characteristics over the frequency range used in the experiments (i.e. 35 to 175 kHz). In order to determine the transformer properties,

several tests were made.

In the first test, the output of the bridge ( to the detector) was shorted with a short copper wire and equal length co-axial cables were used to join the two transformer arms to the dual inputs of a phase sensitive detector (Princeton Applied Research HR-8). The amplitude and phase of each signal was measured (the phase was measured relative to the constant amplitude output of the frequency synthesizer). This test was carried out at various frequencies. In order to account for possible differences in the dual inputs of the phase sensitive detector the inputs were reversed and the amplitude measurements were repeated. The ratio of the amplitudes of the bridge outputs,  $r(\omega)$ , and the difference,  $\phi$ , between the phase angle between the outputs and  $180^\circ$  are shown in Table 3.1 for an output amplitude of -20 dB.

TABLE 3.1

<u>Frequency(kHz)</u>	<u><math>r(\omega)</math></u>	<u><math>\phi(^{\circ})</math></u>
1	0.99 <sub>1</sub>	1.4
10	0.99 <sub>4</sub>	1.2
20	1.00 <sub>1</sub>	0.7
30	1.00 <sub>1</sub>	0.8
40	0.99 <sub>2</sub>	0.7
50	0.99 <sub>6</sub>	1.1
60	0.99 <sub>4</sub>	0.7
70	0.99 <sub>3</sub>	1.4
80	0.98 <sub>2</sub>	1.2
90	0.99 <sub>3</sub>	1.3
100	0.98 <sub>4</sub>	1.0

The results show that the voltages in the two arms of the bridge are within 1.6% and the phases are within 1.4° of being perfectly out of phase. At 35 kHz the transformer outputs are very closely related.

The output impedance of the bridge into the two arms was measured in another test by comparing the voltage developed by the output into an open circuit and into a 93  $\Omega$  termination. With a 20 dB setting on the frequency synthesizer the output of the bridge arms into an open circuit was 2.38 V while a 93  $\Omega$  termination yielded 1.48 V. Therefore the output impedance was 56.6  $\Omega$ . These values were important for the determination of strain amplitudes.

The other main component of the bridge circuit is the decade resistance box. Initially, a commercial decade resistance was used (General Radio 1433-G), the frequency characteristics of which were supposedly well known. However, upon measuring internal frictions which required balancing resistances of 100 k $\Omega$ , severe problems were encountered. The most obvious problem was lack of continuity when changing scales at 100 k $\Omega$ . The reason for this soon became apparent. The resistance box was constructed entirely of wire wound resistors which were connected in series on any decade. Each resistor has an unavoidable capacitance between itself and ground (the case). The effect of having these capacitances was to change the effective resistance of the total resistance setting (i.e. changing the real part of the impedance). This effect was larger as the frequency became higher and made the whole box quite unacceptable for the measurements.

A resistance box was constructed with a range of 0 to 1.1 M $\Omega$  with minimum step size of 10  $\Omega$ , to minimize the effects described above. The resistors used were metal film type resistors of small size with 1% nominal

accuracy. Each of the five decades was made of ten resistors of sequential value from 1 to 10. For any resistance setting, there was at most one resistor per decade being used. The switches used were ceramic wafer switches which were slightly modified by using nylon threaded rods to hold them together and by isolating the knob from the part of the shaft between the wafers. The interior of the box is shown in Figure 3.7. As can be seen, the resistors were placed to minimize the distance to the ground (the case). All these precautions reduced the capacitance to ground.

This resistance box had very good frequency characteristics. It was tested by measuring the resistances of carbon composition resistors as a function of frequency (using the bridge circuit described with the carbon composition resistor replacing the composite resonator). The changes in the measured resistance were small. For example, a resistor which measured 98.4 k $\Omega$  at 1 kHz, balanced at 98.2 k $\Omega$  at 100 kHz and 97.0 k $\Omega$  at 200 kHz. The absolute accuracy of the box was fixed by the use of the 1% resistors. The resistance values were measured using a Keithley 701 digital multimeter and hence corrections could be applied to the values indicated by the settings on the box to give accurate resistance measurement.

The variable capacitance was made up of two butterfly capacitors in parallel with a total range of 220 pf. When accurate capacitance measurements were required, to find the half-power points for example, a commercial, calibrated variable capacitor was used (Jay-Jay Instruments, PVC2).

The detector for the bridge circuit was a PAR HR-8 lock-in amplifier with a type D preamplifier. The HR-8 was used as a tuned amplifier of variable gain, the output of which was observed on a Tectronix 585A oscilloscope. The use of the oscilloscope made the detection of the balance point more

FIGURE 3:7

Interior of the decade resistance box showing the  
arrangement of the switches and resistors



sensitive because some of the noise accompanying the signal could be eliminated by eye.

The sensitivity of the bridge circuit over the range of frequencies used in the experiments was such that changes in resistance of less than 1% or  $5\Omega$  (whichever was greater) could be reliably detected.

### 3.4 Environment

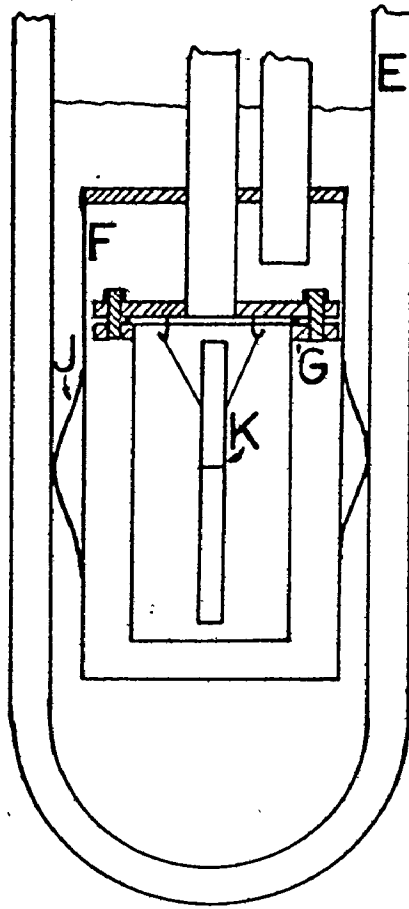
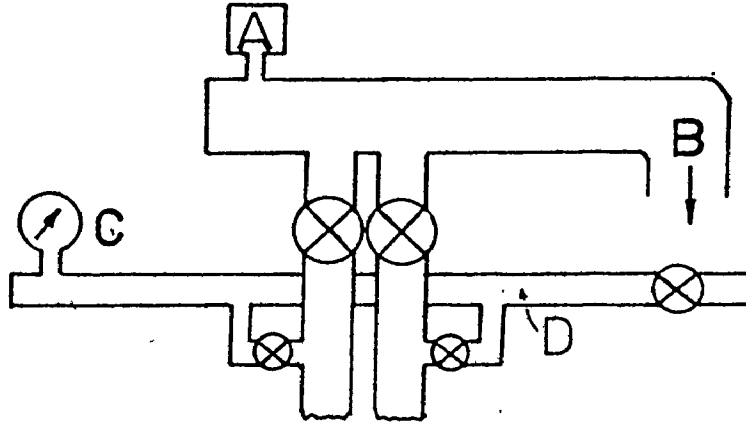
It was necessary to design and construct a cryostat in order to make internal friction measurements over the temperature range from 80 to 300 K. The design, simple yet effective, is shown in Figure 3.8. The cryostat consists of two concentric copper cans suspended by thin walled stainless steel tubes which are the vacuum lines. A small oil vapour diffusion pump can maintain a  $10^{-5}$  torr vacuum when necessary. The line to the fore pump is fixed to the wall in order to reduce the transmission of vibration from the pump to the cryostat. The cryostat is cooled by liquid nitrogen which is contained in a glass dewar surrounding the outer copper can.

The composite resonator is suspended by the silk suspension from three hooks in the inner can. The temperature of the sample is controlled by controlling the temperature of the inner can. Thermal contact between the sample and the inner can is maintained by helium gas at a pressure of 0.1 torr. Also in the inside can is a "dummy" sample which is also thermally isolated from the can except for the exchange gas. A copper-constantan thermocouple is varnished to this sample, and the temperature indicated by this thermocouple is taken to be the sample temperature. On the outer surface of the inside can a  $135\Omega$  copper resistance thermometer (Dauphinee and Preston-Thomas, 1954) and a  $240\Omega$  manganin heater are concentrically

FIGURE 3.8

Schematic diagram of the cryostat

- A - Penning gauge
- B - to vacuum pumps
- C - manometer
- D - He exchange gas system
- E - glass dewar
- F - outer can with Wood's metal joint
- G - Flange on inner can for indium seal
- J - springs for vibration prevention
- K - resonator - suspended from hooks



and non-inductively wound. The copper thermometer serves as the temperature sensor for a temperature controller which powers the heater. An aluminized mylar film covers these wires in order to reduce radiant heat loss. The inner can is made vacuum tight by an indium seal whereas a space-saving Wood's metal joint is used for the outside can.

The temperature controller is a commercial unit (Shinko DIC-PR) which was designed for use with a  $100\Omega$  platinum resistance thermometer as the sensor. The controller uses a simple bridge system with a three lead configuration for the sensor. The purpose of the three leads is to eliminate effects of lead resistance on the temperature sensed by the instrument. Since the copper resistance thermometer used as the sensor varied from  $19.5\Omega$  to  $135\Omega$  in going from 77 K to 300 K, a modification of the leads was made in order to enable the temperature controller to respond to this range of resistance. The modification consists of an additional ten turn  $100\Omega$  potentiometer which may be effectively added in series, either to the resistance of the copper thermometer or to the balancing resistance in the temperature controller itself. If the actual resistance of the copper thermometer is less than  $100\Omega$  then sufficient resistance is added to bring the total resistance to  $100\Omega$ . If the resistance of the copper thermometer is greater than  $100\Omega$  then resistance is added to the balancing resistor in the controller to bring the total resistance to that of the copper thermometer. Although this procedure does mean that for low temperatures the sensor forms only a small part of the total resistance sensed by the controller, the controller is sensitive enough to control the temperature over the whole range of temperatures to better than  $0.1^\circ\text{K}$  for periods of many hours.

## CHAPTER 4

### EXPERIMENTAL TECHNIQUE

The object of this chapter is to describe the techniques which were used to prepare samples and measure small dampings. The sample preparation involved making alloys, growing single crystals and hydrogen charging. The techniques for obtaining very small dampings were developed so that dampings of  $Q^{-1} \approx 10^{-6}$  could be measured at three frequencies.

#### 4.1 Sample Preparation

##### a) Pure aluminum samples

Two types of aluminum samples were prepared: single crystals of particular orientations and polycrystalline samples. The starting material for the single crystals was a  $\frac{1}{2}$ " rod of 99.9999% nominal purity aluminum. The polycrystalline samples were made from Cominco 99.9999% grade aluminum cut from 1" cubes and swaged to the desired  $\frac{1}{4}$ " diameter.

##### i) Single crystal preparation

The aluminum single crystals prepared for the internal friction measurements were of about 7 cm in length and had square cross sections of side 0.63 cm ( $\frac{1}{4}$ "). The length requirement made it improbable that such crystals could be cut from even a large single crystal of random orientation. Consequently, the technique devised was to grow crystals of the correct shape of random orientation, reorient the tip to the desired orientation as

described below and regrow the crystal into the new orientation (Rutter, 1968).

The randomly oriented crystals of about 18 cm length were grown by the Bridgman technique using a split mould of high purity graphite and a furnace atmosphere of flowing argon. The starting material,  $\frac{1}{2}$ " diameter rod, was placed at the top of the mould and allowed to melt into it. The rate of growth, determined by the upward velocity of the furnace, was approximately 2.5 cm per hour. The orientation of the crystal axis was then found by means of a Laue back reflection X-ray photograph. In order to reorient the crystal tip, a short portion (2 cm) of the crystal just above the tip was chemically thinned to about 1.5 mm diameter using hot, concentrated sodium hydroxide. A bend was made in this thinned section so that a Laue photograph of the tip, taken with the X-ray beam parallel to the main axis of the crystal, showed the tip to be in the desired orientation. The crystal was then placed in a powder mould as shown in Figure 4.1. The graphite powder provides good thermal contact between the tip and the bottom of the mould which reduces the probability of melting the tip. The thinned neck also limits the heat flow into the tip. The neck is not in the graphite powder so that it will melt and not just recrystallize. The remainder of the crystal is surrounded by alumina powder (200 mesh) of high purity. This is the soft mould technique described by Noggle (1953). The mould is placed in the furnace tube at a known position and the hot furnace is lowered in steps until the neck of the crystal, but not the lower tip, is melted. The upward motion of the furnace is then started to grow the crystal.

The crystals were etched in Tucker's etch to verify that they were single crystals and the orientation was determined by another Laue photograph

FIGURE 4.1

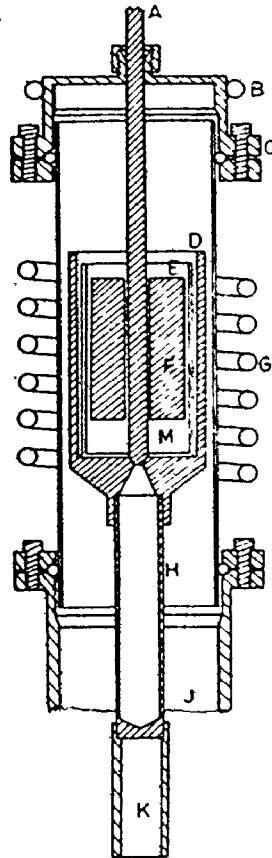
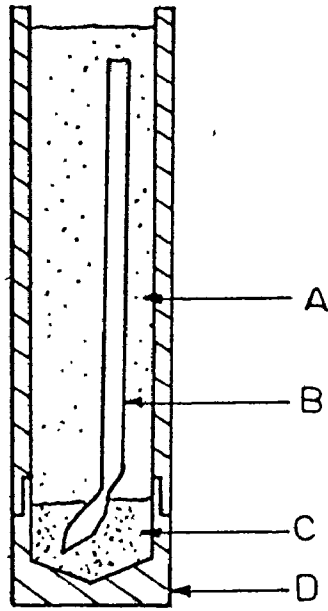
Powder mould (in section)

- A - alumina powder
- B - aluminum crystal
- C - graphite powder
- D - graphite shell

FIGURE 4.2

Alloy preparation furnace

- A - graphite rod
- B - water cooling
- C - vacuum flange with O-ring  
onto quartz tube
- D - graphite cup
- E - alumina crucible
- F - graphite float
- G - R.F. coils
- H - graphite mould
- J - to vacuum pump
- K - support
- M - melt



to check that the orientation was within a few degrees of that desired. The surface condition of the crystals obtained in this way was in general very good and the dimensions were also close to those desired with a slight increase in the square edge dimension at the top of the crystal.

ii) Polycrystalline sample preparation

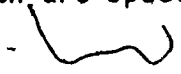
High purity polycrystalline samples were prepared very simply from 1" cubes of 99.9999% Al. The cubes were cut into pieces  $\frac{1}{2}$ " x  $\frac{1}{2}$ " and etched in Tucker's etch, and were swaged down to the desired diameter (.63 cm) in successive steps. The surface was abraded between steps to prevent fins, which formed on the sample, from being folded into it. The samples were then etched again with Tucker's etch and annealed in vacuum at 600°C.

b) Aluminum alloy samples

The aluminum alloy samples were prepared by vacuum casting in an induction furnace. The starting materials for the alloys were 99.999% pure aluminum and copper, and 99.99% pure magnesium.

A cross section of the apparatus is shown in Figure 4.2. The starting materials were placed in the alumina crucible, which was sealed at the bottom by the graphite rod. After obtaining a roughing-pump vacuum in the quartz tube, the induction furnace was started. When the melt was well mixed (after five minutes in the molten state) the graphite rod was raised and the metal flowed into the mould under the additional head provided by the graphite float. The cast alloy was then swaged down to the desired diameter (0.63 cm) in the way used for the pure aluminum rod.

The aluminum copper alloys were analysed using atomic absorption flame spectrophotometry while the aluminum magnesium alloys were analysed with arc spectroscopy.



The aluminum copper single crystal was grown in the same way as the pure aluminum crystal except that the powder mould technique was also used for the initial single crystal growth before reorientation.

c) Heat treatment and hydrogen charging

All heat treatments were done in a vertical furnace (Popovič, 1974). The furnace tube could be evacuated to  $10^{-5}$  torr or a gas could be continuously passed through it. Samples which were annealed in vacuum were removed from the furnace immediately after breaking the vacuum by admitting helium gas.

For hydrogen charging the sample was suspended in the furnace and hydrogen gas was passed through the furnace at atmospheric pressure at a slow rate of about  $10 \text{ cm}^3$  per minute. The hydrogen gas was used either straight from the cylinder or was saturated with water vapour by bubbling it through water. Specimens were cooled by removing them from the furnace and allowing them to cool in air or by quenching them directly into water at room temperature.

d) Gas analysis

The apparatus and technique used for the analysis of hydrogen retained in the samples are described in Appendix B.

e) End preparation

Following the heat treatment, the ends of the specimen were ground on 400 grit silicon carbide paper with water lubricant. The holder used to support the sample during polishing is shown in Figure 4.3. The sample was held in position in the holder with a small piece of plasticene. This

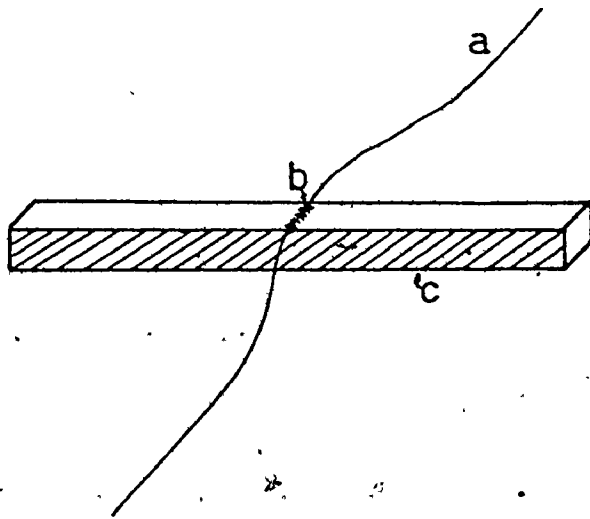
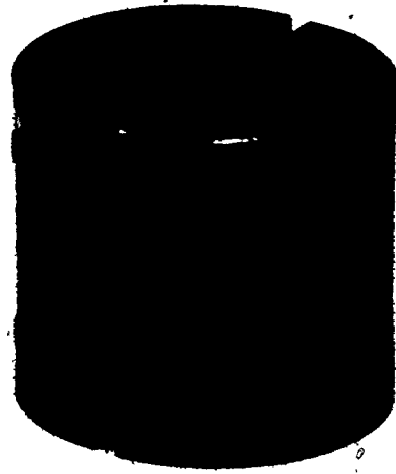
FIGURE 4.3

Sample holder for end polishing

FIGURE 4.4

Initial step in making silk suspension

- a - silk thread
- b - dilute varnish
- c - evaporated gold electrode



method of grinding produced flat and parallel ends on the sample but deviations from these conditions did not produce a large effect on the measured damping.

#### 4.2 Quartz Crystal Preparation

It was necessary to reduce the damping in the quartz crystal to a minimum. This was done by using very thin gold-film electrodes, a silk-thread suspension and #44 B.S. gauge copper wire leads.

The quartz crystals were received from the supplier in the correct shape with the X-faces indicated by pencil marks. They were then ground on all sides on 400 grit silicon carbide paper using the sample holder described before for grinding the end faces. They were then etched in concentrated HF for 5 minutes at room temperature and washed thoroughly with distilled water. This etching procedure is thought to reduce the damping (Cady, 1946). Degreasing with n-pentane preceded the evaporation of gold onto the X-faces. The evaporation was done in a vacuum of  $5 \times 10^{-5}$  torr in a Varian evaporator using a 10 cm distance from the evaporator tungsten basket to the quartz surface. No attempt was made to get a uniform film by moving the quartz crystal during evaporation. Typical resistances from one end of the film to the other were a few ohms. The surface did not reflect specularly due to the prior etching. The film adhered to the quartz surface very well and did not noticeably deteriorate with careful handling.

After the gold evaporation was done, the silk suspension was made. Two silk strands about 20 cm long made up of approximately 40 fibres each were obtained by dividing a silk thread. The centres of these strands were

then varnished across the centres of the quartz crystal faces on which there was no gold film as shown in Figure 4.4. The varnish used was GE 7031 diluted with 50:50 ethanol:toluene. The width of the varnish in the direction of the long axis of the crystal was kept to a minimum of about 1 mm. When the varnish was dry, it was baked on the V heater, described later, at 100°C for a half hour. The ends of one of the silk strands were then joined together taking care that the tension in each side was the same when the crystal was suspended. Loops were made in the ends of the strands and adjusted with the crystal suspended from the three hooks of the inner can of the cryostat. The adjustment was made so that the crystal would hang vertically. The three strand suspension was used so that vibrations of the can would not set up "swinging" oscillations of the crystal.

The #44 B.S. gauge wires used for the leads to the crystal were joined to the gold films on the quartz crystal using Electrodag (Acheson Colloids Ltd.), a silver colloidal suspension which was diluted with acetone. The bare wire was laid on the centre of the gold film on the quartz and small amounts of Electrodag were dabbed onto the contact point. After drying, the excess was removed by gentle scraping. The contact obtained in this way was good at the four frequencies used in the experiments. It could be heated to more than 100°C without deterioration and was strong enough to withstand small stresses which could occur when the inner can was put into position around the suspended resonator.

These small quantities of Electrodag are at the maximum of the stress distribution of the standing wave. A comparison of the damping of a crystal for which a small amount of Electrodag was used with one using more Electrodag is shown in Figure 4.5. There are no large differences. The

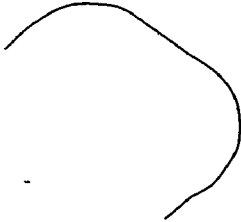


FIGURE 4.5

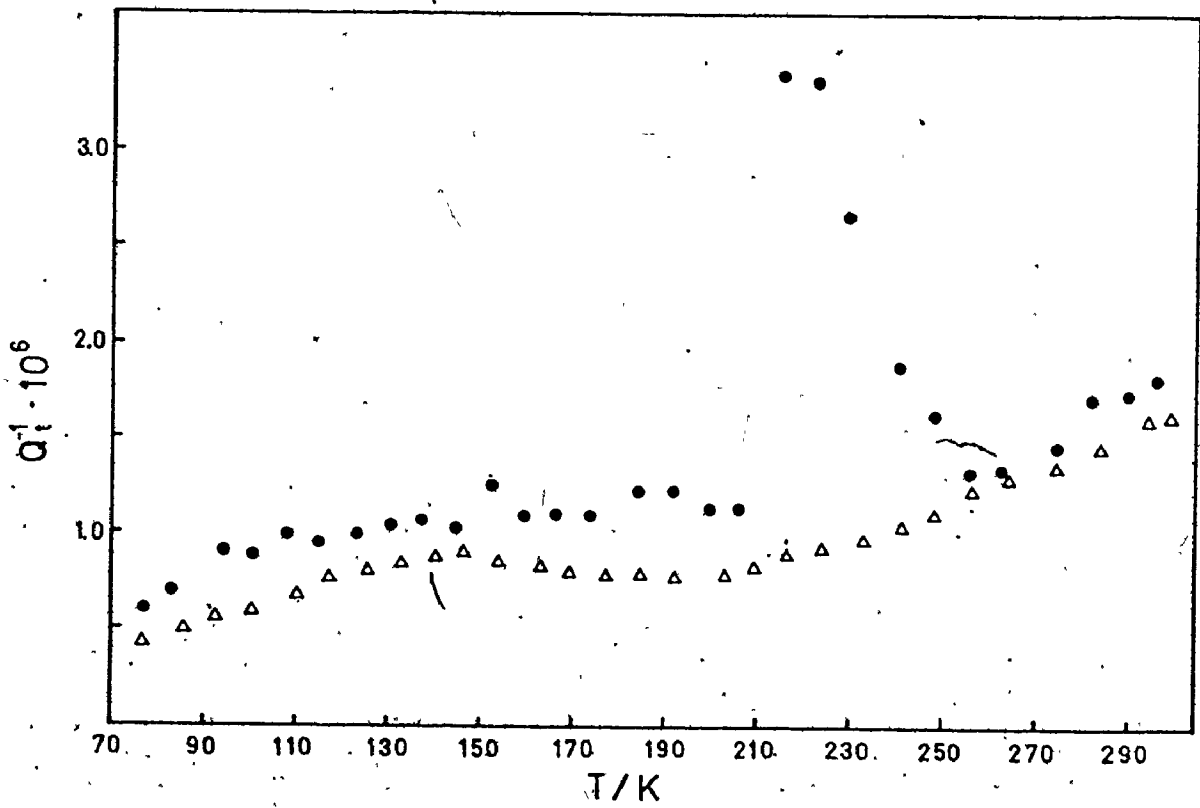
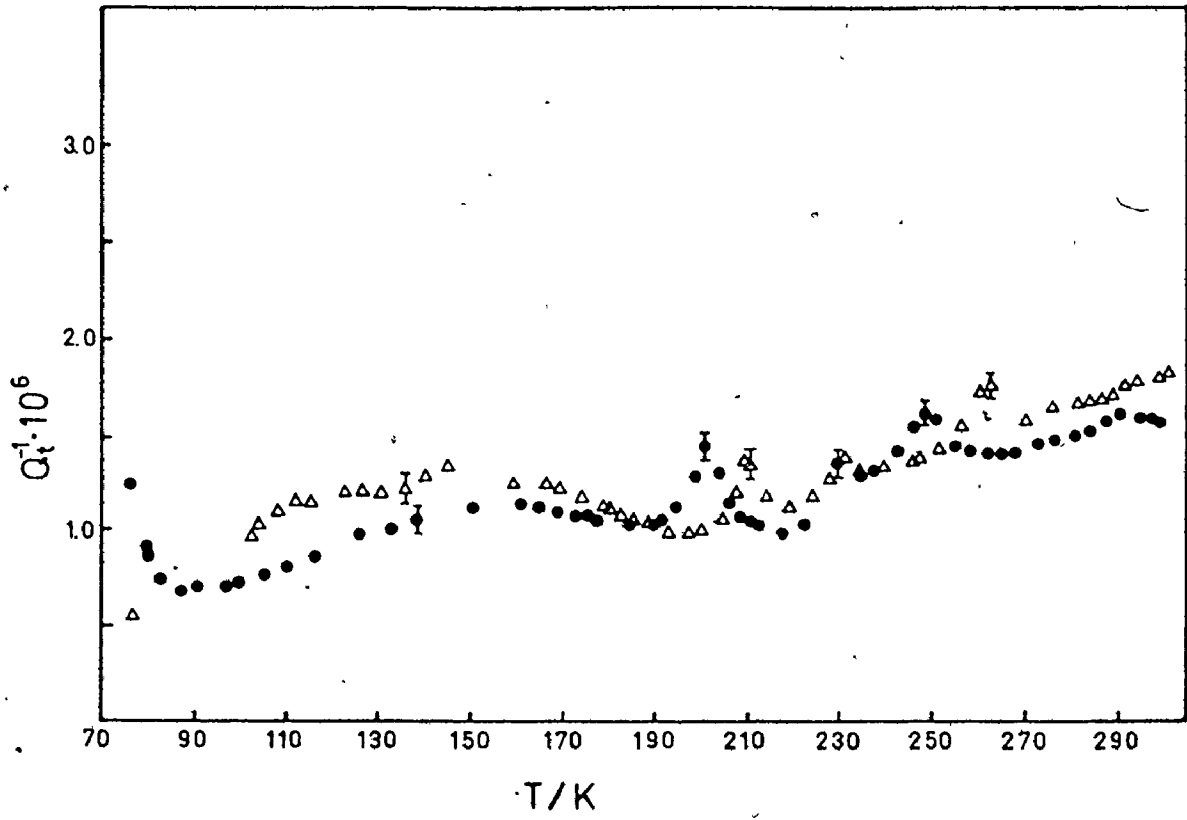
Damping spectrum of a composite oscillator before and after addition of colloidal silver onto gold face

- initial measurement
- △ after addition of colloidal silver (joint unchanged)

FIGURE 4.6

Damping spectrum of a composite resonator showing the effect of a slightly damaged suspension

- initial run
- △ after repairing suspension (joint unchanged)



Electrodag did not affect the damping. During the course of the work, another contact method was tried using indium pressed onto the gold film and copper wire. The damping due to the indium was much higher than that with the Electrodag.

The important characteristic of the suspension and contact method described above is its reproducible, low damping. The flexibility of the suspension made it resistant to slight knocks which occurred when other parts of the cryostat were being assembled. Another suspension which was tried (spring loaded copper pin contacts) was not reproducible for the reason that slight knocks changed the pin position and the damping was very sensitive to the pin position. The fact that the final suspension and contacts were permanent parts of the transducer also eliminated another possible source of irreproducibility, namely the placement of the suspension on successive experiments.

Occasionally, spurious internal friction measurements resulted from a damaged suspension. One such result is shown in Figure 4.6. The large peak at 220 K disappeared upon changing the suspension. The suspension which was responsible for the peak was visibly damaged--one of the silk threads had pulled away from the crystal, removing some varnish with it.

a) The joint between the quartz transducer and the sample

The most critical part of the whole composite resonator is the joint. A technique for making a good joint was developed as were several criteria for determining the joint characteristics, and hence the validity of the measured damping spectrum.

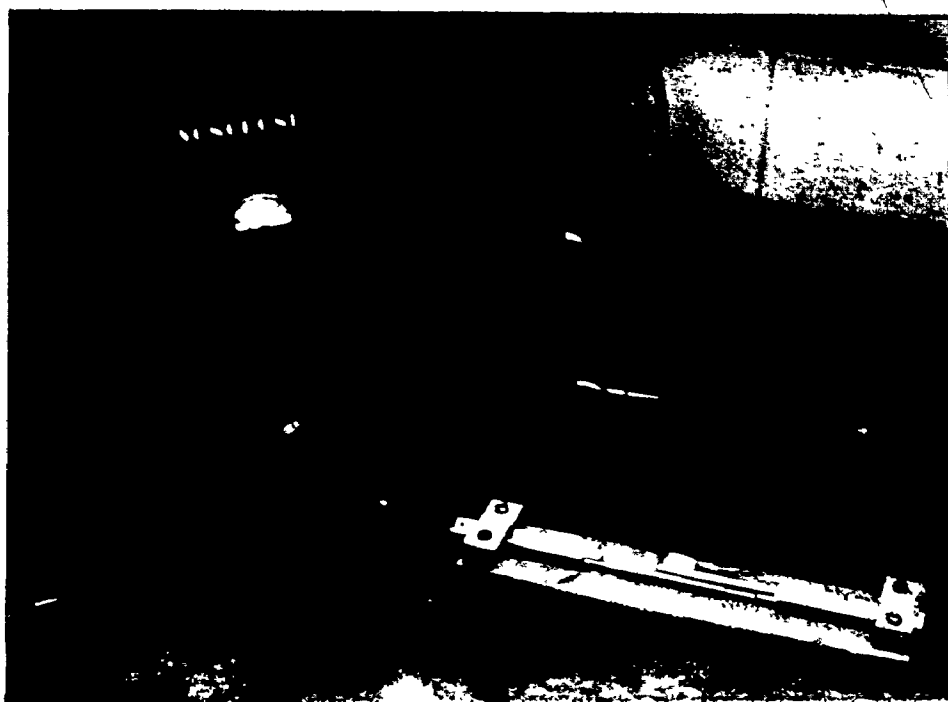
The basic requirements of the joint have already been outlined in Chapter 3. When several materials (GE 7031 varnish, gelatin, phenyl salicylate) proved to lack one or more of the requirements (low damping on the fundamental, third and fifth harmonics, ability to be thermally cycled, short curing time), a metallic joint appeared to be the solution. The idea of the metallic joint was taken from the thesis of M. Puls (1970) who used a pure gallium joint for pulse-echo measurements of ultrasonic attenuation. He found that the joint had good transmission properties over a wide frequency range at MHz frequencies. A pure gallium joint was attempted but was disappointing because there was structure in the damping spectrum due to the gallium. The gallium also interacted with the aluminum and appeared to lift the oxide layer. Since liquid gallium is known to cause embrittlement of aluminum alloys attempts at making a gallium joint were discontinued. A low melting point alloy (m.p. 91.5°C) with component metals not known to embrittle aluminum was finally chosen. The composition of this ternary eutectic was Bi 51.6 wt%, Pb 40.2% and Cd 8.2%. This material was used for all the results presented in this work.

The temperature controlled trough shown in Figure 4.7 was built to align the sample and quartz transducer while they were being joined. The trough, which was made of aluminum, was heated with a manganin heater varnished to the back. The temperature at the surface of the trough was controlled to within a few degrees using a thermocouple and controller (Shinko NIC-D).

Since the eutectic joint material did not readily wet either the quartz or the aluminum samples, an ultrasonic soldering unit (Sonobond

FIGURE 4.7

The temperature controlled trough, used for assembling resonators,  
with a resonator in position.  
The ultrasonic soldering unit is also shown



Model S-3-HE) was used to produce a film of solder adhering to both these surfaces before they were joined. For the quartz transducer, the effect of the ultrasound was to allow the eutectic to flow into the rough surface created by the HF etch. The action of the ultrasound on the aluminum was thought to be the breaking up of the oxide film which prevented the eutectic from wetting the surface. The disadvantage of the ultrasound was the production of dislocations in the soft aluminum samples. In annealed aluminum samples, the Niblett-Wilks peak due to dislocations was small but was clearly visible in the internal friction spectrum after making the joint using the ultrasonic unit.

The procedure for making the joint was as follows. The ends of the two components to be joined together were cleaned with n-pentane and placed on the cold trough. The trough was heated to 105°C and held there for five minutes to allow the components to reach the same temperature. The end of the hot soldering unit was cleaned with tissue and a small amount of eutectic was melted onto it. The quartz crystal was held by hand (using folded tissue insulation) and the eutectic was applied with the ultrasound on. When a uniform film was produced on the end face, the quartz was returned to the trough and the same procedure was carried out for the aluminum. Excess eutectic on the quartz face was wiped off with tissue and the two components were pushed together. All samples were held near 100°C for a total of 900 seconds unless otherwise mentioned. This included time to remake the joint if problems developed during the first attempt. The heater for the trough was then turned off and the resonator was allowed to cool. When cool, the resonator was suspended from the hooks in the cryostat and

the #44 wire leads from the cryostat were soldered to the leads in the cryostat. Measurements at room temperature could then be started.

b) Checks of the joint and suspension

The joint and suspension were checked by the measurements in air at room temperature. If the total damping was low on all four frequencies (subharmonic, fundamental, third and fifth harmonics) and if there were no spurious resonances near the fundamental frequency then the joint was assumed to be good. Since the air has a very large effect on the damping of low  $Q^{-1}$  specimens, low total damping on the fundamental frequency (35 kHz) means a balancing resistance of about  $10\text{ k}\Omega$ .

The damping on the subharmonic (at approximately 17.3 kHz) was most sensitive to both bad joints and faulty suspensions because this mode puts the joint at a maximum in the strain distribution and the suspension far from a displacement node. Bad joints were characterized by a very large damping (balancing resistance greater than  $60\text{ k}\Omega$ ).

The spurious resonances mentioned above require additional explanation. Sometimes, a joint with low damping on the four frequencies exhibited additional resonances near the fundamental frequency. The widths ( $\Delta f$ ) of these resonances between half power points were generally much larger than that of the true fundamental. The cause of the additional resonances must be excitation of modes other than the longitudinal one. If the joint was changed, these resonances would usually disappear. Temperature dependent measurements of the internal friction of resonators with double resonances were carried out, but the results were considered invalid because these effects sometimes produced spurious peaks in the internal

friction spectrum (see Chapter 5).

Faults in the suspension could also be checked with room temperature measurements. Slightly tapping the frame supporting the cryostat resulted in small oscillations of the whole resonator. If the suspension was faulty, these small oscillations were sufficient to cause large instabilities in the bridge balance condition. When such instabilities were detected, the suspension was very carefully checked using a magnifying glass.

#### 4.3 Measurement Technique

The electrical characteristics of the bridge have been described. The object of this section is to describe the procedure used to balance the bridge on resonance, which is basically that of Saul and Bauer (1967).

Initially, the decade resistor was switched to open circuit and the frequency of the synthesizer was set far from resonance (to about 25 kHz in most cases). The balancing capacitance was adjusted to give the minimum output from the bridge, as observed on the oscilloscope (CRO). This procedure balanced the capacitance of the quartz crystal and the leads with the variable capacitor  $C_v$ . The frequency of the synthesizer was then swept over the range where the resonance was expected. This was done using the variable decade in place of either the 100 or 1000 Hertz digital decade. The presence of the resonance showed as a maximum in the output on the CRO. Once the resonant frequency was found, the variable decade was substituted for the 10 or the one Hertz digital decade depending upon the frequency width ( $\Delta f$ ) of the resonant peak which is itself determined by the damping.

The frequency at which the maximum in the bridge output occurred

was close to, but not exactly, the resonant frequency. This means that in order to balance the bridge on resonance the frequency had to be changed. In practice this was easily accomplished by first changing the decade resistance and then sweeping the frequency through the resonance and repeating this procedure until a satisfactory balance was obtained. It was in obtaining this balance that the CRO was particularly useful as it was possible to visually distinguish signal from noise. At balance the signal appeared to have twice the resonant frequency because the synthesizer produced harmonic components (down 40 dB from the main output) for which the bridge was not balanced and these were amplified to some extent by the tuned amplifier.

When the best balance was achieved, the values of the decade resistance, frequency and output amplitude of the synthesizer were recorded.

The results shown in Chapter 5 are measurements of the internal friction as a function of temperature. These spectra were obtained in several different ways. In most cases some of the steps described above could be left out after the initial measurements were made. The capacitance balance did not change appreciably over the whole temperature range and it was not necessary to alter it unless the damping became very large, in which case small errors in the capacitance balance affected the measured resistance. These effects can be easily understood using the graphical method described in Chapter 3.

Room temperature measurements were performed immediately after allowing the joint to cool, suspending the composite oscillator and connecting the leads. If checking the joint and suspension, as above, showed them to be reasonably good, then the two cans of the cryostat were attached. It was

necessary to use a level to align the outer can, which had the Wood's metal seal, so that it did not touch the inner one. The system was then evacuated for one or two hours until a vacuum in the  $10^{-4}$  torr range was achieved. Helium gas was admitted into the exchange gas reservoir to a pressure of 100 torr after first flushing the reservoir several times with helium gas. This reservoir was simply a valved off length of copper pipe with a pressure gauge attached which could be connected to either of the cans of the cryostat. The glass dewar was positioned and filled with liquid nitrogen. A deflection plate near the nitrogen inlet and copper-beryllium springs which were attached to the outer can and which pressed against the glass dewar prevented any large oscillations of the cryostat cans during this operation. A small quantity of helium gas was allowed into the inner can as exchange gas. The pressure drop in the reservoir was two torr which gave an exchange gas pressure in the inner can which was sufficient to maintain good thermal contact between the sample and the can at all temperatures. This exchange gas increased the damping factor,  $Q^{-1}$ , by about  $5 \times 10^{-8}$ . The internal friction was then measured at all four frequencies and the results were recorded.

Several different procedures were used to obtain the internal friction spectrum. At the beginning of the work, the composite resonator was cooled slowly (overnight) by radiation from the inner to outer can (at liquid nitrogen temperature) or more quickly (about two hours) by admitting some exchange gas into the space between the inner and outer can. When the resonator reached liquid nitrogen temperature, measurements were commenced. If the internal friction was to be measured at all four

frequencies, then a step heating method was used. The effective set-point temperature of the controller was changed by altering the resistance of the ten turn potentiometer in the sensor leads and the heater power was adjusted to achieve the fastest possible approach to the desired temperature. When the rate of temperature change slowed enough that measurements could be easily made, the internal friction was measured on all four frequencies. Of course, since the resonant frequencies were temperature dependent, at each new temperature the resonances had to be found. This could usually be done without open circuiting the decade balancing resistance. The output amplitude of the synthesizer at each frequency was carefully recorded. If measurements were taken every four degrees, the total time to do the spectrum from 50 K to 300 K was about twelve to fourteen hours.

Measurements of the internal friction on one mode could be done while continuously heating the resonator. The results of Appendix C indicate that changing temperature should not affect the measurements. The only criterion was that the rate of temperature change was slow enough that good balances could be achieved. This required continuously changing the frequency of the synthesizer and maintaining balance conditions by altering the decade resistance.

Since the joint between specimen and quartz sometimes deteriorated during the thermal cycling, thus invalidating the measurements and wasting time, it was decided to do measurements initially on the fundamental frequency during continuous cooling from room temperature. In this way the whole spectrum could be determined in a matter of a few hours depending upon the cooling rate which was controlled by the exchange gas pressure

between the cryostat cans. Any interesting features of the spectrum obtained in this way were examined more closely using the step heating method so that measurements could be made at the third and fifth harmonic frequencies.

## CHAPTER 5

### RESULTS

This chapter first describes the methods used to treat the data. The results of preliminary experiments which determined the size of the internal friction of the quartz, suspension and joint are then reported. The main body of results follows. These are measurements of the internal friction of high purity aluminum--both single crystal and polycrystalline samples, the aluminum alloys (AlCu and AlMg) and two commercial aluminum alloys (7075 and 6061). Comparisons of measurements performed after vacuum annealing and after hydrogen charging are made.

#### 5.1 Treatment of the Data

The data obtained from the measurements consisted of resistance values, thermocouple voltages, synthesizer output amplitudes and frequencies. The first three of these were transformed to obtain the internal friction, temperature and strain amplitude respectively. The frequencies could have been transformed to yield the modulus variations (Saul and Bauer, 1967) but this was not done.

Marx's expression relating  $Q^{-1}$  and  $R$  (equation 3.2.2) is used to obtain the internal friction of the composite oscillator from the measured resistance value at resonance. The specimen internal friction,  $Q_s^{-1}$ , is found by subtraction of the contribution due to the quartz crystal,  $Q_q^{-1}$ , according to the following expression (Marx, 1951):

$$Q_s^{-1} = \frac{m_s + m_q}{m_s} Q_t^{-1} - \frac{m_q}{m_s} Q_q^{-1} \quad (5.1.1)$$

where  $Q_t^{-1}$  is the total damping of the resonator,  $m_q$  and  $m_s$  are the masses of the quartz crystal and the specimen respectively. This expression is easily derived by considering both the energy stored and that lost per stress cycle in each component. It is interesting to note that the contribution of the quartz becomes less important as the specimen mass is increased. However, in the case of aluminum alloys, the sample and quartz transducer are of approximately the same mass.

The maximum strain amplitude of the sample can be easily determined from the voltage applied to the resonator by the bridge circuit and the damping of the resonator. According to Marx (1951)<sup>1</sup>, the maximum transducer strain is given by

$$\epsilon_q = (2.24 \times 10^4) \frac{hV}{b\ell fR}$$

where  $h$  is the harmonic,  $b$  and  $\ell$  are the breadth and length respectively of the electrodes,  $f$  is the frequency,  $V$  is the applied voltage in rms volts and  $R$  is the resistance. This expression could not be verified because there was no independent method of measuring the strain amplitude. The specimen strain is found by equating the displacements at the interface

---

<sup>1</sup>Robinson (1974) again finds a discrepancy within Marx's expression but we have used Marx's work for consistency.

between specimen and transducer. Then,

$$\epsilon_s l_s = \epsilon_q l_q$$

where  $l_s$  and  $l_q$  are the lengths of the frequency matched specimen and transducer.

The equipment used to measure the internal friction was not well suited to measurements at constant strain amplitude. The synthesizer output voltage had to be altered manually in order to maintain constant maximum strain amplitude when the internal friction changed. Hence, in most cases, the synthesizer output was fixed unless the damping changed by more than a factor of five. Accordingly, the maximum strain amplitude varied inversely as the resistance at resonance. Since the measurements were usually done at very low strain amplitudes, where the damping was strain independent, therefore the variation in strain amplitude did not affect the resulting internal friction spectrum. For each spectrum, the strain amplitude was calculated only at the position of minimum damping over the temperature range examined.

## 5.2 Results of Preliminary Experiments

### a) The suspension

The first experiments were performed in order to determine the damping of the quartz transducer alone. Typical results for the quartz crystal are shown in Figure 5.1. The measurements of internal friction

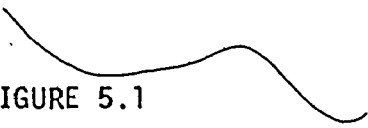


FIGURE 5.1

Quartz transducer damping measured by step heating

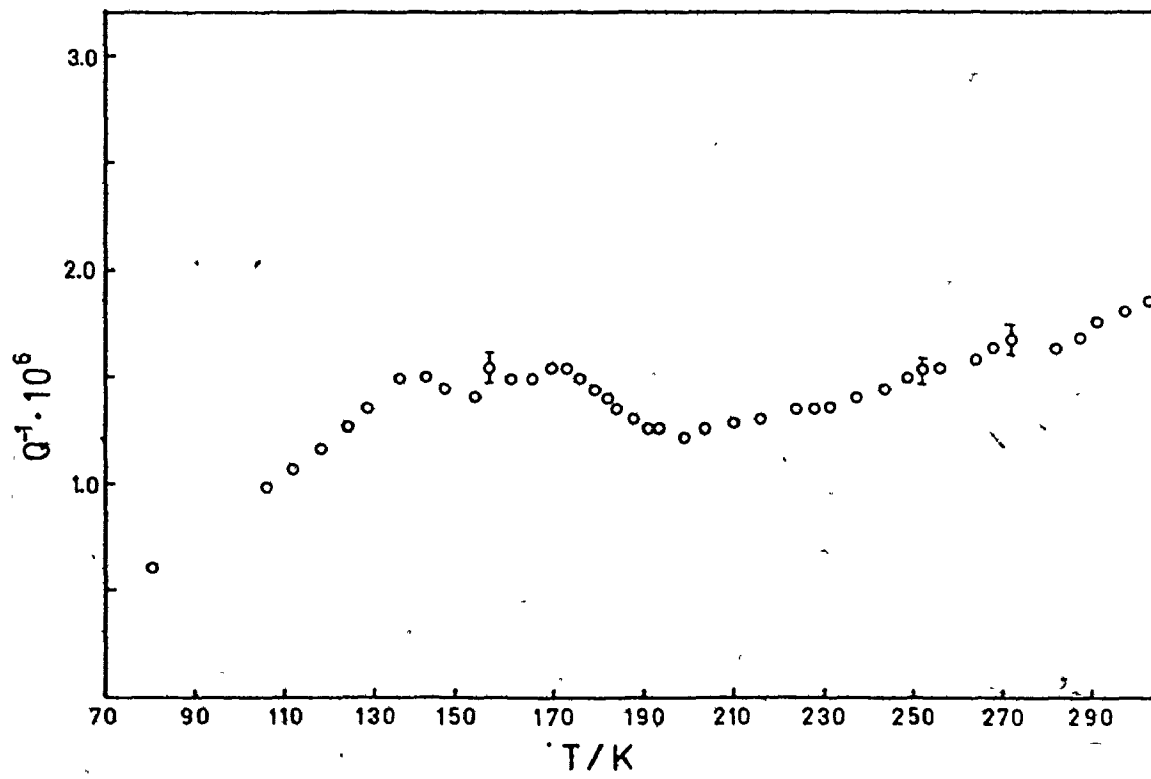
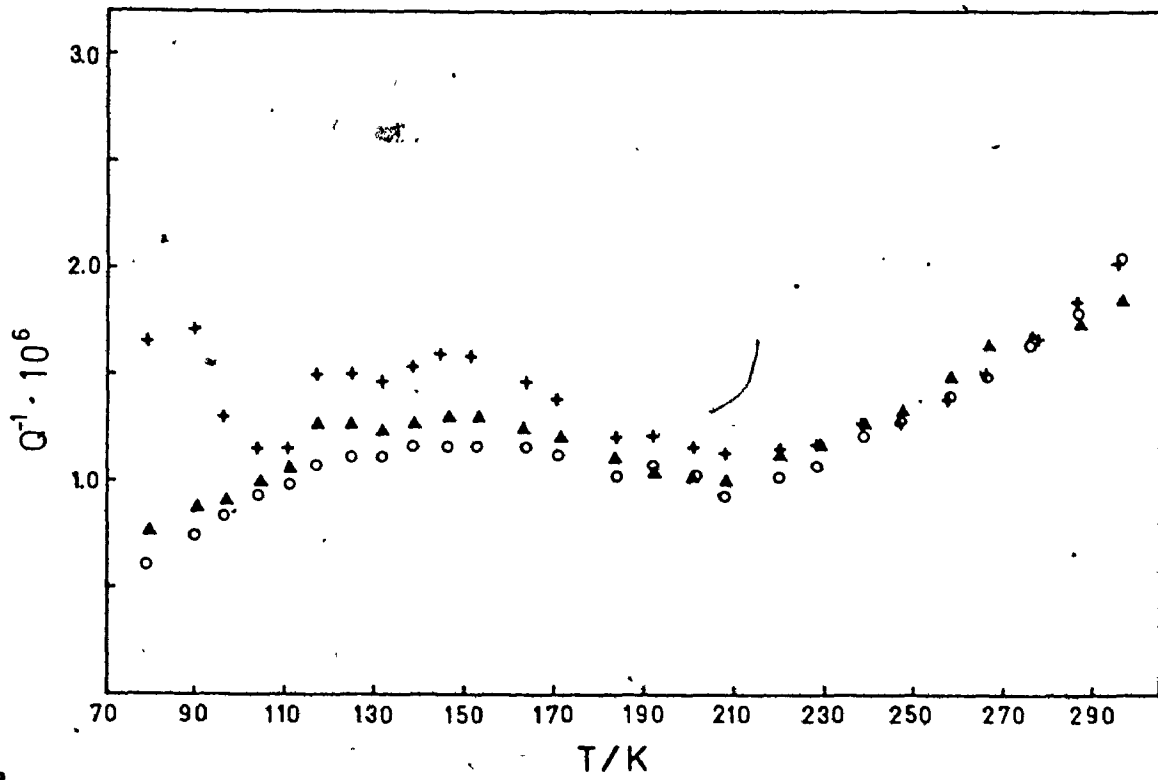
○	fundamental	$\epsilon_m = 1.6 \times 10^{-7}$
▲	third harmonic	$\epsilon_m = 1.7 \times 10^{-7}$
+	fifth harmonic	$\epsilon_m = 8.2 \times 10^{-8}$

error bars are about the size of the points.

FIGURE 5.2

Quartz transducer damping measured during continuous cooling

○	fundamental.	$\epsilon_m = 1.8 \times 10^{-7}$
---	--------------	-----------------------------------



on the fundamental, third and fifth harmonics were obtained by the step heating method, i.e. equilibrating the sample at each new temperature and then measuring damping at all three frequencies. The internal friction,  $Q^{-1}$ , is less than  $2 \times 10^{-6}$  over almost the complete temperature range in each mode. Additional results for the first harmonic are shown in Figure 5.2. These were obtained during continuous cooling of the transducer. The suspension had been completely changed between these two results; the thickness of the silk thread being almost doubled for the results of Figure 5.2. The values of  $Q^{-1}$  are within  $3 \times 10^{-7}$ . This demonstrates the excellent reproducibility of the silk suspension and the accuracy of measurements made during continuous cooling rather than the more time consuming step heating.

b) The joint between quartz and sample

Two preliminary experiments with quartz crystals were performed to examine the joint. In the first experiment, two quartz crystals of the same frequency (34.9 kHz) were joined using the eutectic solder. Since the crystals were closely matched, the joint was at a strain node for all temperatures. This not only examines the joint under optimum conditions, but can also be used to check the expression given by Marx (equation 5.1.1) that was used to obtain the internal friction of all the aluminum samples. The curves shown in Figure 5.3 are the measured curves for the quartz sample using equation 5.1.1 to correct for the damping in the quartz transducer (using the values of Figure 5.1 for the transducer). A comparison with the transducer results of Figure 5.1 shows that the quartz

FIGURE 5.3

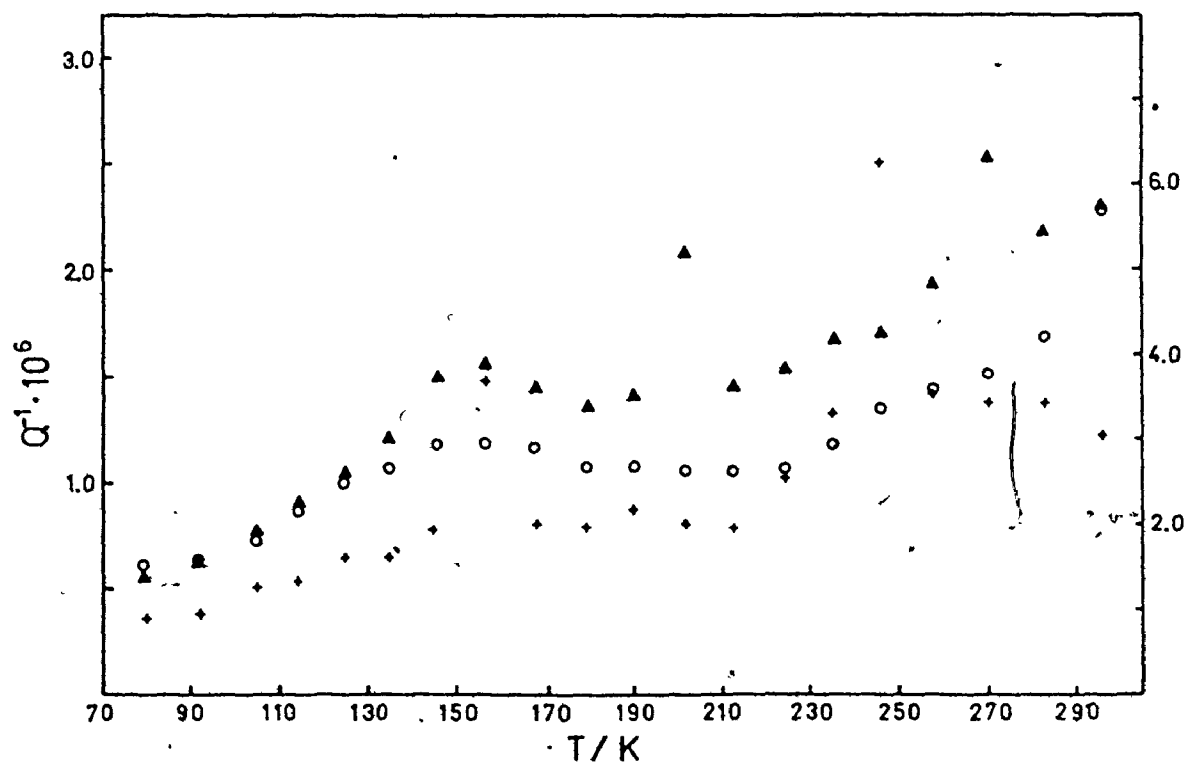
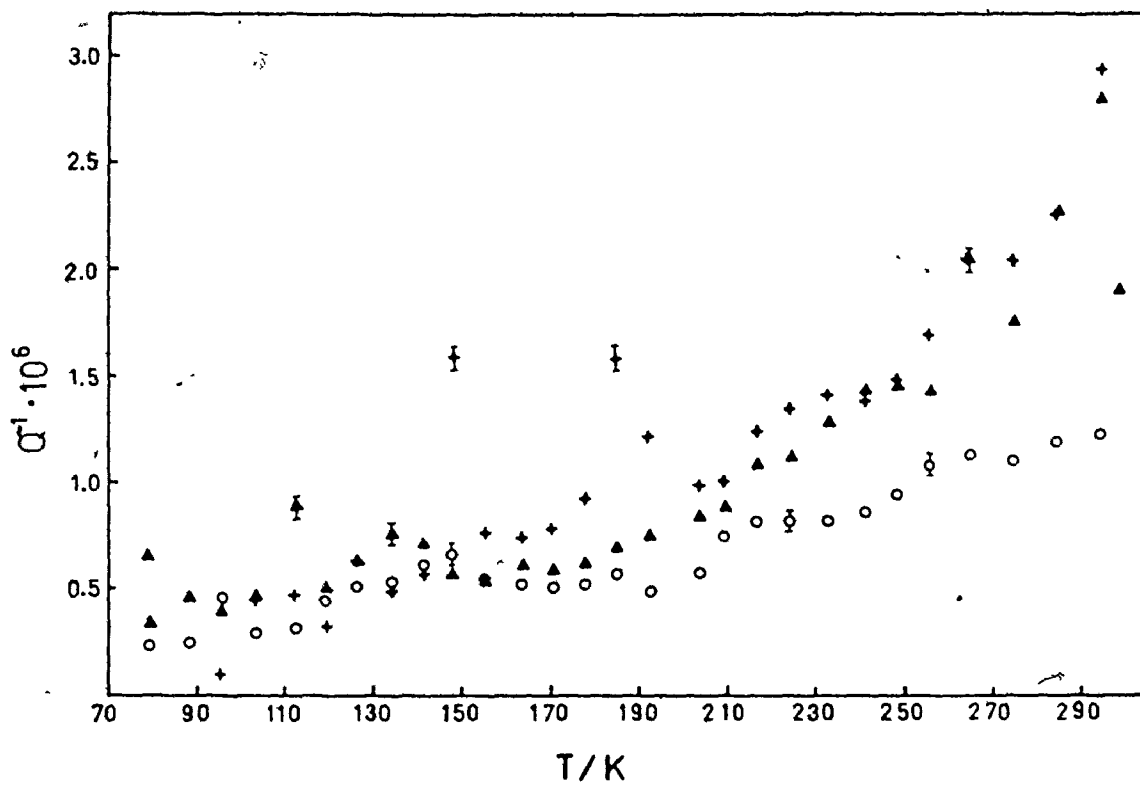
Internal friction of quartz sample - frequency matched to transducer

Q	fundamental	$\epsilon_m = 1.5 \times 10^{-7}$
▲	third harmonic	$\epsilon_m = 1.3 \times 10^{-7}$
+	fifth harmonic	$\epsilon_m = 7.8 \times 10^{-8}$

FIGURE 5.4

Damping of composite oscillator made of unevenly matched quartz crystals

○	fundamental	$\epsilon_m = 1.0 \times 10^{-7}$	} (left hand scale)
▲	third harmonic	$\epsilon_m = 3.9 \times 10^{-8}$	
+	fifth harmonic	$\epsilon_m = 5.0 \times 10^{-8}$	- (right hand scale)



specimen has a much lower damping than the transducer alone, but at high temperature the specimen has an apparently higher damping on the third and fifth harmonics. This indicates that at low temperature the observed damping of the transducer alone is probably limited by the suspension. In fact, the apparent peak in Figure 5.1 at 135 K must also be due to the suspension because it is not present in the quartz specimen curves of Figure 5.3 and it does increase when the suspension thickness was doubled from Figure 5.1 to Figure 5.2. The higher damping measured in the quartz sample above 220 K is probably caused by the soldered joint, but the value is still very low.

Since the modulus and thermal expansion coefficients of quartz and aluminum do not have the same temperature dependence, it is not possible to have the joint at the strain node at all temperatures. Thus, a second set of experiments with a quartz crystal specimen was performed to examine this. Two quartz crystals of slightly different lengths (7.3 and 7.1 cm) were joined using the eutectic solder. This arrangement ensured that the joint was not at the strain node at any temperature. The results for the total damping are shown in Figure 5.4. The damping is less than  $2 \times 10^{-6}$  over almost the whole range on the fundamental and third harmonic but is larger for the fifth harmonic. This shows that, even when the joint is not at the strain node, the effect on the total damping due to the joint can still be small.

Several other measurements of the internal friction spectrum of these same quartz crystals with other joints were made using the continuous cooling technique in order to determine joint reproducibility, effect of

thermal cycling, etc. The total damping curves are shown in Figure 5.5. Slightly larger measurement errors are inherent in the continuous cooling method because the synthesizer frequency must be continuously changed to match the change in resonant frequency with temperature. When the damping is low, transient effects due to switching and changing frequency become more pronounced. The possible error in the resistance measurements is therefore approximately  $\pm 20\Omega$ . This leads to errors of  $\pm .05 \times 10^{-6}$  in the total damping. When the specimen damping is extracted from the total damping curves, these errors become more pronounced. The specimen damping curve for one case is shown in Figure 5.6 (cf. Figure 5.3). The variations in the specimen damping are not accounted for by the possible error, nor are there similar variations present in the results of Figure 5.3. Therefore, these variations must be due to the joint or suspension or both.

The results of Figure 5.5 curves a and b are for one particular joint and curves c and d are for another joint. The differences in the total damping between these two different joints are no bigger than the differences between successive runs on the same joint.

#### c) Criteria for validity of measured peaks

The preliminary results demonstrate the capabilities of the technique. Measurements of specimen internal friction in the  $Q^{-1} = 10^{-6}$  range can be made at three frequencies. Although the effects of the joint and suspension are usually very small, they can introduce variations in the internal friction measurements which are also of size  $Q^{-1} = 1 \times 10^{-6}$ . These variations are not reproducible on successive runs. It is this irreproducibility which

FIGURE 5.5

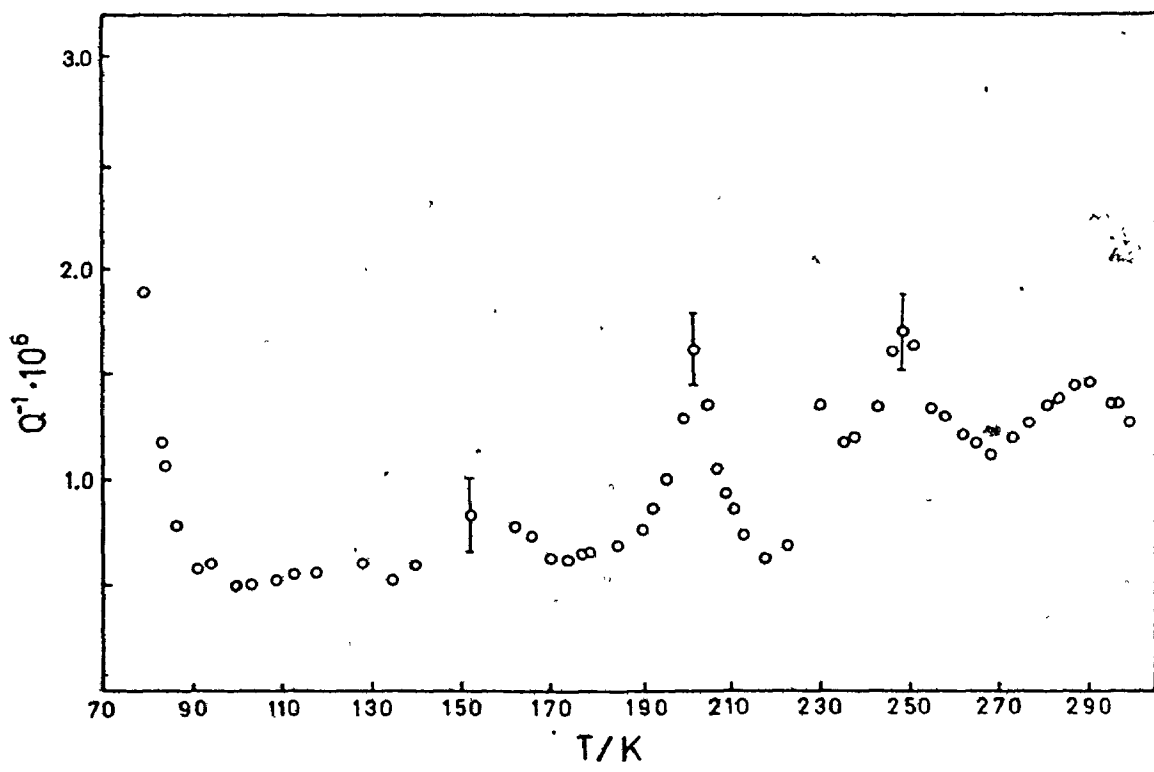
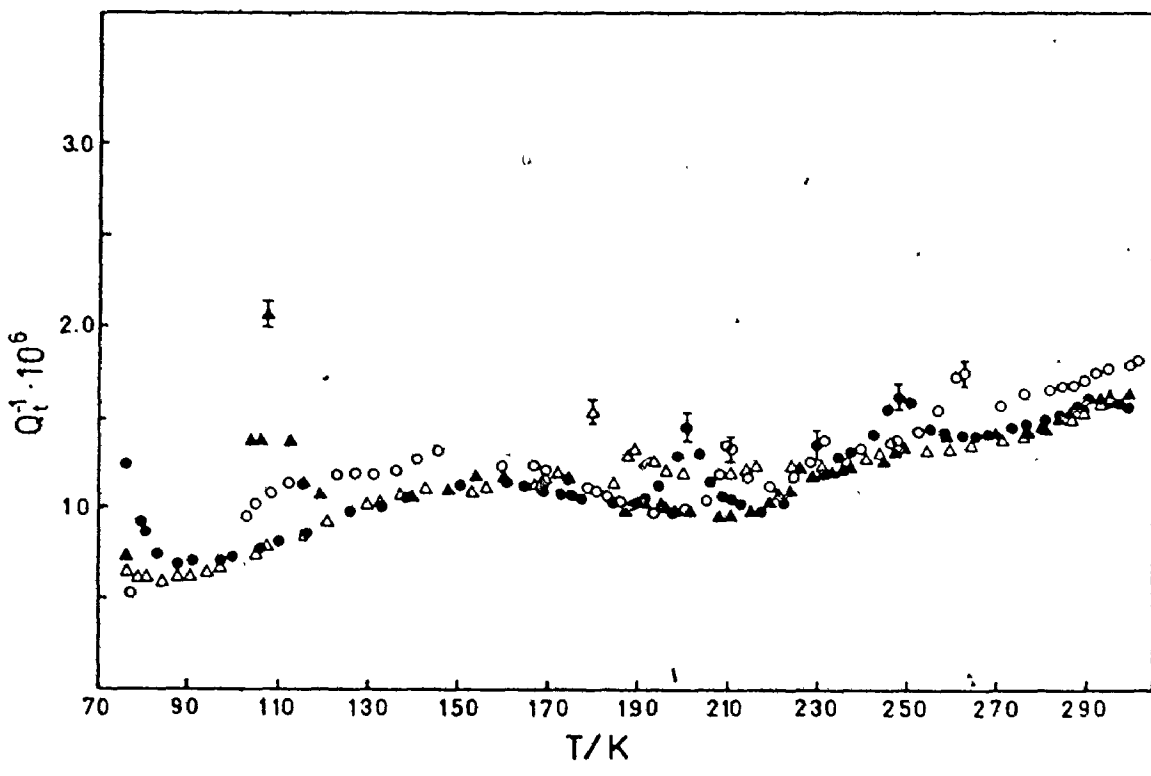
Total damping of unevenly matched quartz resonators measured  
by continuous cooling

○ a } one joint  
○ b }  
△ c } another joint  
△ d }

$\epsilon_m$  in all cases  $\approx 1.2 \times 10^{-7}$

FIGURE 5.6

Quartz specimen internal friction determined from  
curve (a) in Figure 5.5



makes necessary a careful examination of the internal friction results for the metallic specimens.

These preliminary experiments and other experiences with metallic samples led to the development of several criteria which were later used in determining whether or not structures in a particular internal friction spectrum were real, i.e. due to the specimen, or spurious, i.e. due to other causes.

The first criterion developed was a condition on the frequencies of various modes. Resonators which exhibited structures in the internal friction spectrum when cooled also had to reproduce the same resonant frequencies when measurements were repeated at room temperature. If measurements were done at slightly different temperature (as was usually the case) then the differences of the frequencies for a given mode before and after measuring the spectrum had to be proportional to the frequency.

Since operation of the composite resonator at half the fundamental frequency of the transducer maximizes the strain at the joint, measurements at this subharmonic frequency were very sensitive to changes in the joint. There was often a correspondence between apparent "spikes" in the internal friction spectrum and frequency changes at room temperature of the subharmonic frequency. Structure obtained in such cases was not considered in the analysis. However, it was assumed that the absence of structure in cases where the frequencies were not reproducible was real. This follows from the assumption that anything that causes the joint or suspension to be less than ideal will create additional damping.

The second criterion for real internal friction structure on the

fundamental was the necessity of corresponding peaks on the third and fifth harmonics. The peak temperature can, of course, be expected to shift with changing frequency consistent with the fact that the relaxation times for the defect reorientation are temperature dependent. The peak height may be quite different at the different frequencies because the strain distribution in the specimen is not the same for different modes. Specimen inhomogeneity can then cause peak height changes with mode change.

The third criterion applied to structure in the internal friction spectrum concerned the peak widths at half maximum height. Using the Debye model this width can be related to the activation energy for the process responsible for the peak. If the activation energy for the peak obtained in this way was much too high for the temperature at which the peak occurred (using the Wert-Marx criterion [Chapter 2]) then the validity of the peak was suspect:

### 5.3 Pure Aluminum Results

Measurements of the internal friction spectrum of pure aluminum charged with hydrogen were made so that effects due to the presence of substitutional solutes in the alloy specimens could be separated from other effects.

The results of the internal friction measurements on a <100> aluminum single crystal cooled in air from a hydrogen-water vapour atmosphere at 600°C, are shown as curve a in Figure 5.7. These results were obtained by the continuous cooling technique at a cooling rate of

FIGURE 5.7

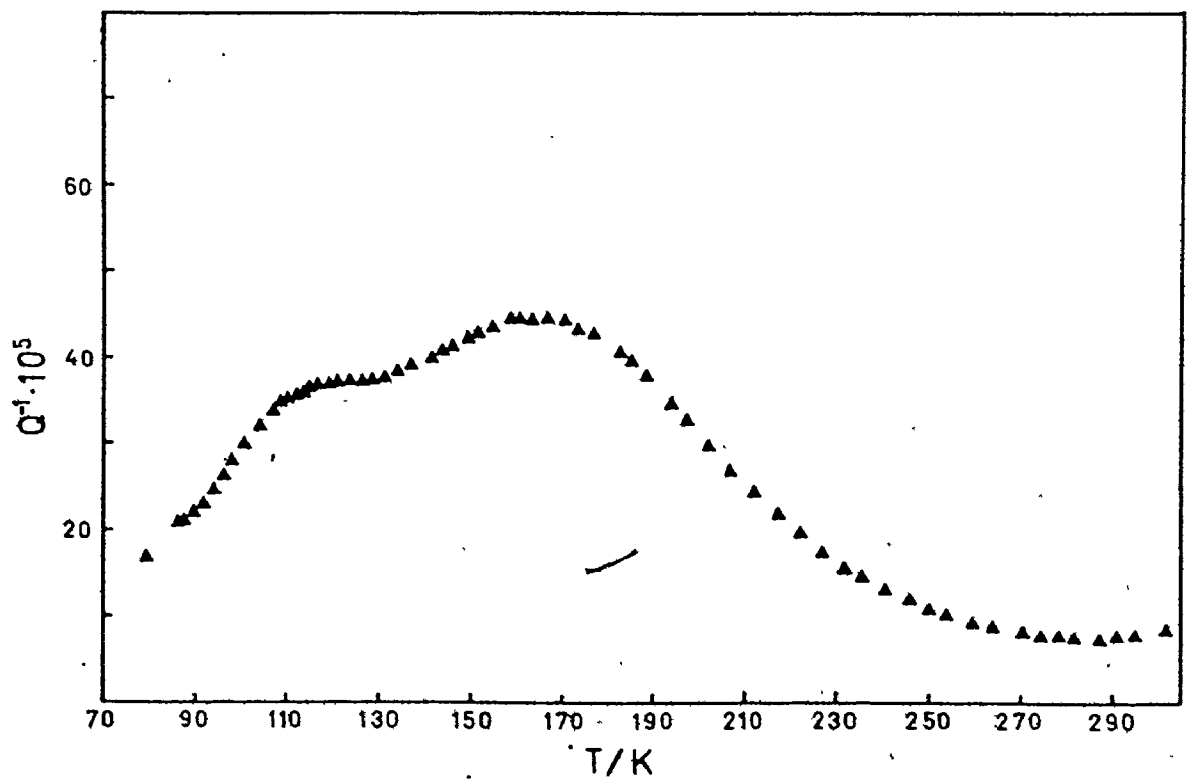
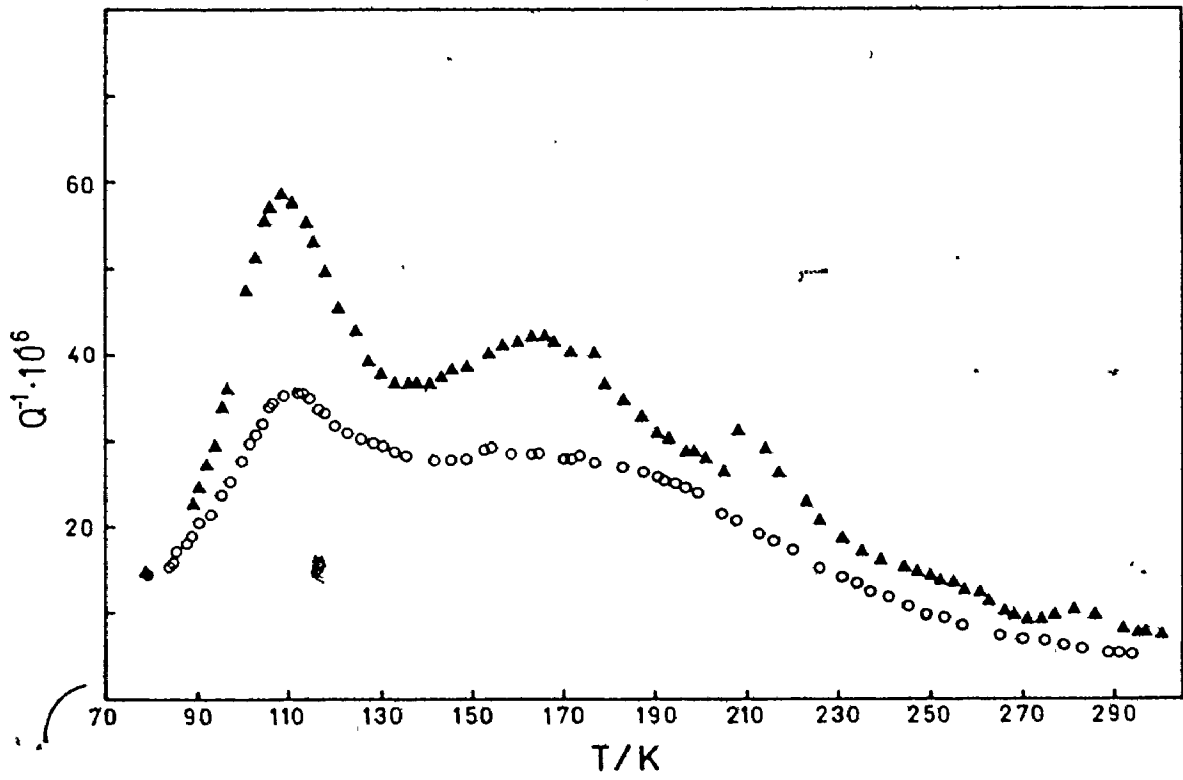
Internal friction of Al <100> single crystal

- (a) hydrogen annealed  $\epsilon_m = 2.2 \times 10^{-8}$   
▲ (b) vacuum annealed  $\epsilon_m = 1.7 \times 10^{-8}$

FIGURE 5.8

Internal friction of polycrystalline Al following  
room temperature deformation

$$\epsilon_m \approx 3.1 \times 10^{-9}$$



about 2°/minute. Results of measurements on the same crystal after cooling in air from vacuum annealing at 600°C are shown as curve b. The structures in the spectra below 200 K are similar except that the peak heights are different. The large peak at 110 K has been identified (see Appendix A) as the Niblett-Wilks peak. The peak at 165 K is the Bordoni peak. These peaks are the result of slight deformation caused by handling and making the joint. The peak at 210 K in the vacuum annealed sample corresponded to an instrumental instability. Since the low temperature peaks are so sensitive to handling, it is not unexpected that the two spectra are not identical.

Some internal friction spectra were also measured for deformed aluminum polycrystalline samples both with and without hydrogen. The main body of these results is presented in Appendix A. A representative curve for a deformed sample without hydrogen is shown in Figure 5.8. These results were obtained after annealing the sample in vacuum and cooling it in air. The sample was then joined to the quartz and deformed by twisting to a surface shear strain of about 1%. The general level of the damping is about ten times the level of the undeformed single crystal samples and again the structure exhibits two peaks below 200 K. The Bordoni peak is predominant for these deformed samples. The results of Appendix A show that there was no qualitative difference between samples charged in hydrogen and those annealed in vacuum.

#### 5.4 Aluminum Copper Alloys

Internal friction measurements of aluminum copper alloys were performed on two different samples. One sample was polycrystalline with an average grain size of between two and three millimetres and the second sample was a single crystal. The compositions, determined by atomic absorption flame spectrophotometry, were 0.68 and 0.42 at.% respectively.

The results for the polycrystalline sample are shown in Figures 5.9 and 5.10. The sample was annealed in a vacuum of  $10^{-5}$  torr at  $600^{\circ}\text{C}$  for a period of two weeks before the measurements of Figure 5.9. It was removed from the furnace and allowed to cool in air. Measurements were performed during both cooling and heating (done in steps) at three frequencies. The cooling rates exceeded  $2^{\circ}/\text{minute}$  between measurements while the heating rates were slightly smaller. The results for the fundamental (about 35 kHz) and the third harmonic frequencies are shown. The maximum strain amplitude (determined from the applied voltage and the damping) was  $7.14 \times 10^{-8}$  for the fundamental, at the minimum in the damping at 210 K, and  $5.06 \times 10^{-7}$  for the third harmonic. Since the measurements were made when the sample temperature and hence the frequency was constant, the estimated possible errors in the resistance measurement are 1% or  $5\Omega$ , whichever is larger. The error bars representing this error are indicated on the figure. This is not the total possible error because there are possible errors in the value of the damping of the quartz which is involved in the calculation of the specimen damping. The differences in  $Q^{-1}$  between heating and cooling are as much as  $0.7 \times 10^{-6}$  which are not accounted for by

FIGURE 5.9

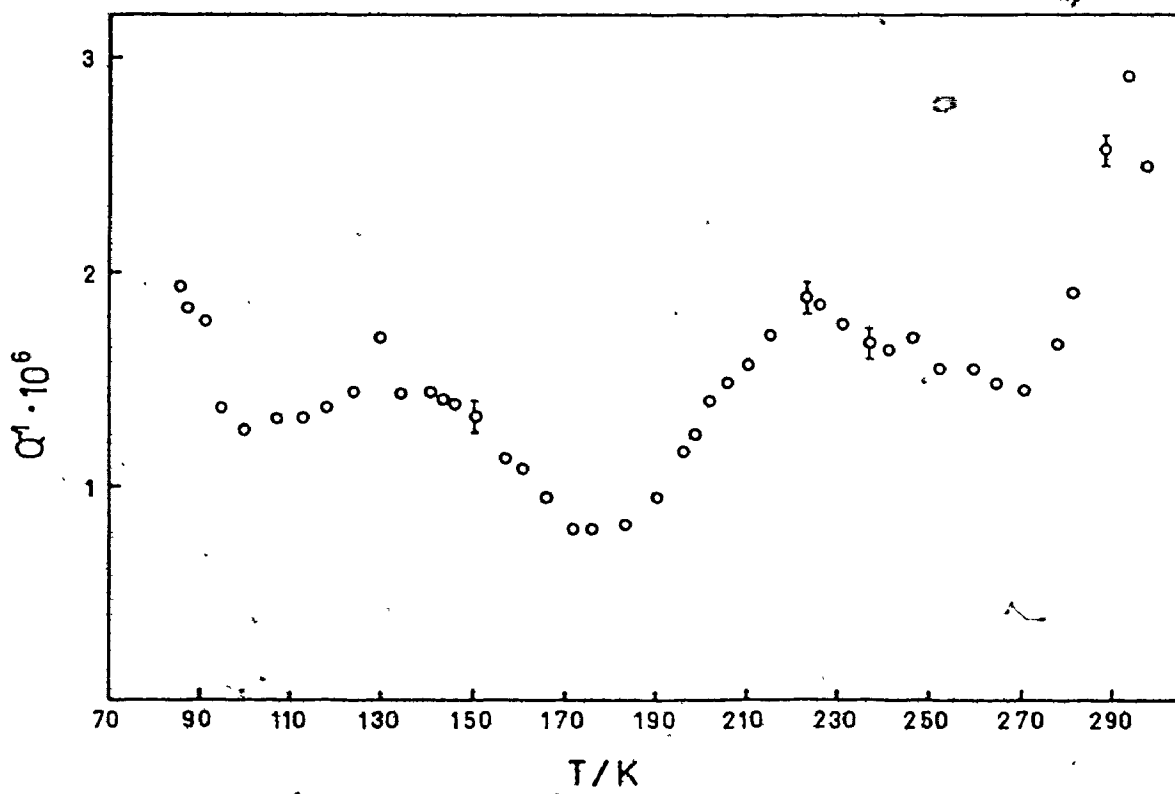
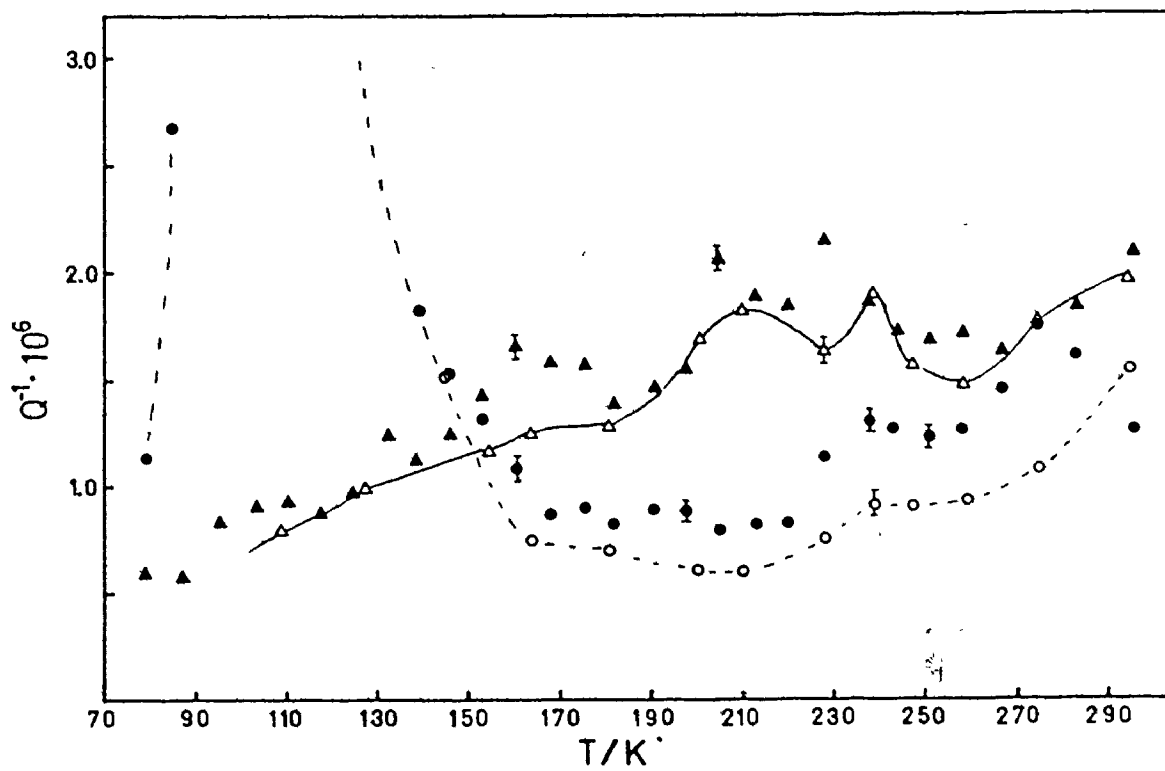
Internal friction of an Al Cu polycrystalline sample. Vacuum annealed

- fundamental - cooling curve  $\epsilon_m = 7.1 \times 10^{-8}$
- " - heating curve
- △ third harmonic - cooling curve  $\epsilon_m = 5.1 \times 10^{-7}$
- ▲ " " - heating curve

FIGURE 5.10

Internal friction of the same sample as in  
Figure 5.9 - hydrogen annealed and quenched

$$\epsilon_m = 2.1 \times 10^{-7}$$



the possible error in the measurement. It is possible that there was some joint deterioration during the measurement as the subharmonic frequency was not monitored for this run but the other frequencies (fundamental, third and fifth harmonics) were within the error of the frequency measurement (1 Hz) when the resonator returned to room temperature. The rapid rise in the damping of the fundamental with decreasing temperature below 160 K was accompanied by the appearance of a second resonance at nearly the same frequency. The measurements at the third harmonic are included in Figure 5.9 in order to show that this increase in the damping on the fundamental is not due to internal friction processes in the sample. Similarly, since the small, apparent peaks at 240 K and 275 K on the fundamental are not matched by corresponding peaks on the third harmonic, they also must be spurious. The cooling curve, which exhibits no structure as large as  $0.5 \times 10^{-6}$  above 150 K, is therefore taken to be the representative curve for this sample.

This same sample was annealed in a flowing hydrogen atmosphere at 600°C and then quenched directly into water at room temperature. The joint to the quartz transducer was made with a total time at 100°C of about 700 seconds. Measurements of the internal friction spectrum were made only at the fundamental frequency as the sample was continuously cooled at a rate varying from 0.7°/minute initially to 0.25°/minute at low temperatures. The resulting internal friction spectrum is shown in Figure 5.10. As the continuous cooling technique was used, the possible error of the resistance measurement was estimated to be  $\pm 15\Omega$  and is reflected in possible errors in the internal friction indicated by the error bars. The maximum strain

amplitude was  $2.10 \times 10^{-7}$ . The internal friction is less than  $3 \times 10^{-6}$  over the whole temperature range, as it was for the same sample before charging with hydrogen. There are four structures in the spectrum which deserve comment. The peak at 293 K is too narrow to satisfy the Wert-Marx relation. The peak at 220 K with a height of about  $0.8 \times 10^{-6}$  will be discussed in conjunction with the single crystal results. There is a small peak (about  $0.5 \times 10^{-6}$ ) at 140 K which is in the range of the normal Bordoni peak. The rise in the damping below 95 K is thought to be due to joint deterioration as the balance of the bridge was difficult in this temperature range. On returning to room temperature, the frequency of the subharmonic had dropped by 4.5 Hz although its resistance at resonance was still less than 50 K $\Omega$ .

Since there was a small peak at 220 K after putting hydrogen in the polycrystalline sample, a single crystal with optimum orientation for sensitivity to tetragonal defects was grown. The cylindrical axis of the specimen was approximately  $4^\circ$  from  $\langle 100 \rangle$  crystalline direction. The crystal was annealed in vacuum at  $600^\circ\text{C}$  for 24 hours and air cooled. When the joint was made, the total time at  $100^\circ\text{C}$  was about 1200 seconds. The resulting internal friction spectrum, obtained by cooling in steps is shown as curve (a) in Figure 5.11. The cooling rate between points was similar to that for the vacuum annealed polycrystalline sample. The maximum strain amplitude was  $8.6 \times 10^{-8}$ . There is no structure in this curve as large as  $0.3 \times 10^{-6}$  although the general level of internal friction is actually higher than in the polycrystalline sample.

FIGURE 5.11

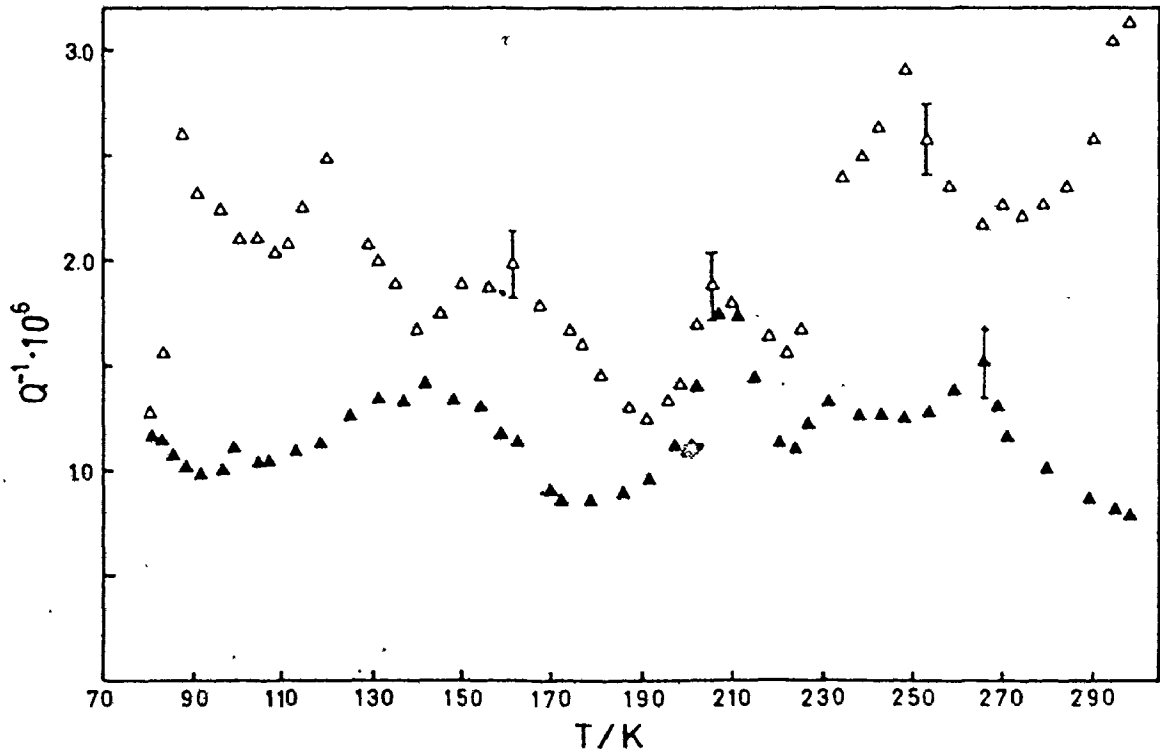
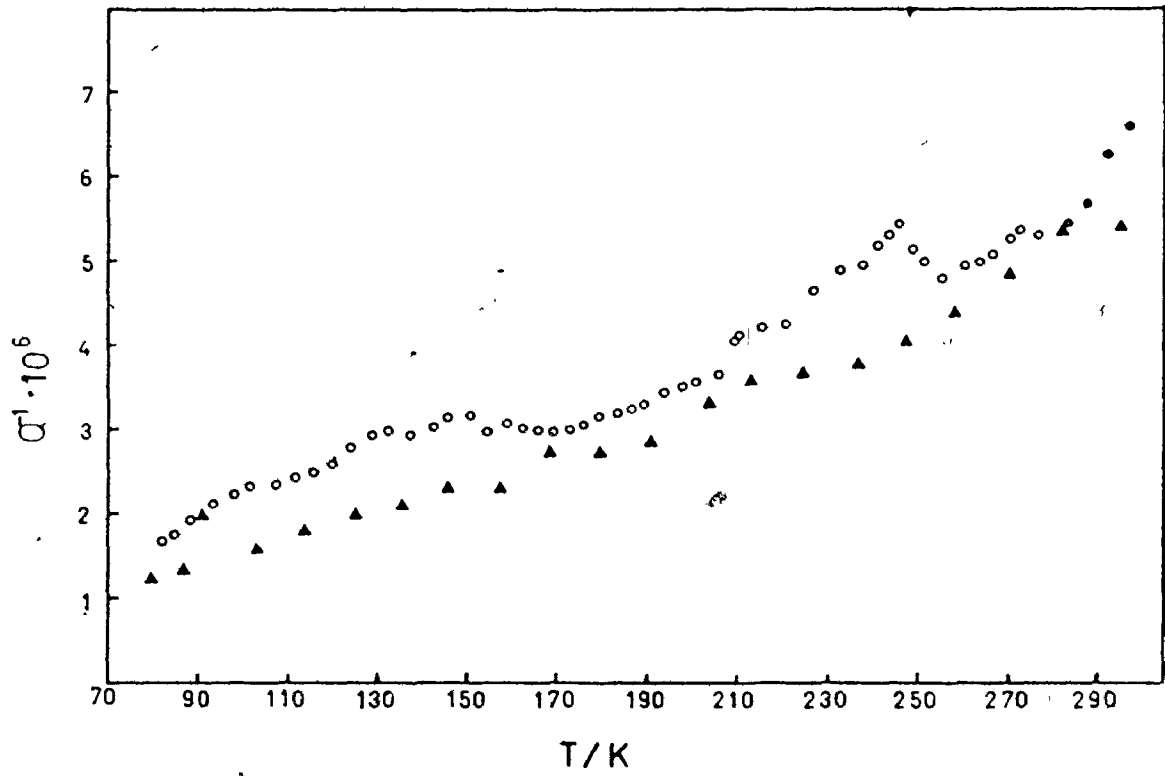
Internal friction of the Al Cu single crystal

- ▲ (a) vacuum annealed  $\epsilon_m = 8.6 \times 10^{-8}$
- (b) hydrogen annealed and quenched  $\epsilon_m = 1.6 \times 10^{-7}$

FIGURE 5.12

Internal friction of the Al 0.16 at.% Mg polycrystalline sample -  
annealed in helium

- △ (a) initial measurement  $\epsilon_m = 8.1 \times 10^{-8}$
- ▲ (b) after changing the joint



The sample was subsequently heated in a flowing hydrogen atmosphere at 600°C and quenched into water. The joint was made more rapidly with the sample at 100°C for only 360 seconds. The cooling rate during measurement was always less than 1°/minute. The results are shown as curve (b) in Figure 5.11. The maximum strain amplitude was  $1.6 \times 10^{-7}$ . The general level of damping is about the same as for the sample annealed in vacuum, except for a broad peak at about 140 K with maximum height of about  $0.5 \times 10^{-6}$  and some structure between 210 and 250 K, the significant feature of which is a peak at 246 K with maximum height about  $0.8 \times 10^{-6}$ . If a comparison is made with the polycrystalline sample, it is apparent that this peak does not correspond to any peak in the polycrystalline sample, nor does the 220 K peak in the polycrystalline sample have a corresponding peak in this spectrum. For this reason, neither of these peaks is considered to be due to hydrogen. In addition, the actual size of the peaks in both cases was no bigger than the structures observed in the quartz-quartz combination of Figure 5.5.

### 5.5 Aluminum Magnesium Alloys

Internal friction measurements were made using the continuous cooling method on polycrystals of aluminum magnesium alloys of two different compositions, which were determined to be 0.16 and 0.54 atomic per cent magnesium.

The results for the aluminum 0.16 at.% magnesium sample annealed in a flowing helium atmosphere at 600°C and cooled in air are shown as

curve a in Figure 5.12. A flowing helium atmosphere was used, instead of vacuum, for the aluminum magnesium alloys in order to reduce the loss of magnesium from the sample during the annealing treatment. The maximum strain amplitude used during the measurements was  $8.1 \times 10^{-8}$ . The cooling rate was relatively large (as high as  $3^\circ/\text{minute}$ ). Consequently, the possible error in the resistance measurement at balance was estimated to be  $\pm 30\Omega$ . The corresponding error in the internal friction is indicated by the error bar in the figure. There are several peaks in the internal friction spectrum. The most prominent peak is at 248 K with a maximum height of about  $1 \times 10^{-6}$ . Smaller peaks which are only slightly larger than the estimated error bars occur at 205 K, 160 K, 120 K and 88 K. After returning the resonator to room temperature, the frequency of the subharmonic had changed relative to the fundamental by 3 Hz. The measurements were repeated after remaking the joint. The resulting spectrum is shown as curve (b) in Figure 5.12. The cooling rate was approximately the same as for the previous run, consequently the errors of measurement are the same. The only peak which is repeated in both spectra is the peak at about 205 K. The frequency of the subharmonic had changed by 52 Hz relative to the fundamental and the resistance at balance of the subharmonic was very large ( $90\text{ K}\Omega$ ) after returning the resonator to room temperature.

The sample was subsequently annealed in an atmosphere of hydrogen and water vapour (obtained by bubbling hydrogen through water at room temperature) at  $600^\circ\text{C}$  for a period of twelve hours. The sample was cooled in air and then heated to  $100^\circ\text{C}$  for about 900 seconds while the joint was made. The resulting internal friction spectrum is shown as curve (a) in

Figure 5.13. The maximum strain amplitude was  $8.5 \times 10^{-8}$ . There are two peaks in the spectrum. One at 245 K with a height of  $\sim 1 \times 10^{-6}$  and a second at 160 K with a height of  $0.5 \times 10^{-6}$ . As the cooling rate was similar to previous runs, the error bars are approximately the same size. The frequencies of the various modes upon returning to room temperature had not changed by more than 1 Hz.

In order to examine the effect of a faster quench that would possibly retain more of the hydrogen in the lattice, the same sample was again annealed at 600°C in a hydrogen atmosphere and then quenched directly into water at room temperature. The results are shown as curve (b) in Figure 5.13. A slower cooling rate of less than 1°/minute was used during the measurements. Consequently, the error bars are somewhat reduced. The maximum strain amplitude was  $5.4 \times 10^{-8}$ . The damping at low temperature is seen to be considerably higher than in the previous measurements but there is no structure on the curve which is greater than  $0.5 \times 10^{-6}$ . The frequencies of the various modes were within 1 Hz of the initial values after the resonator was returned to room temperature.

The results of measurements of the internal friction spectrum of the 0.54 at.% magnesium sample are shown in Figure 5.14. The sample was annealed at 600°C in flowing helium and cooled in air prior to measurements shown as curve (a). The maximum strain amplitude during measurement was  $1.2 \times 10^{-7}$ . The cooling rate was as high as 3°/minute and consequently the error bars are again quite large. There is a peak at 153 K with a height of  $1.4 \times 10^{-6}$  and two smaller peaks at 190 K and 252 K which are almost within the error bars. On returning the resonator to ambient

FIGURE 5.13

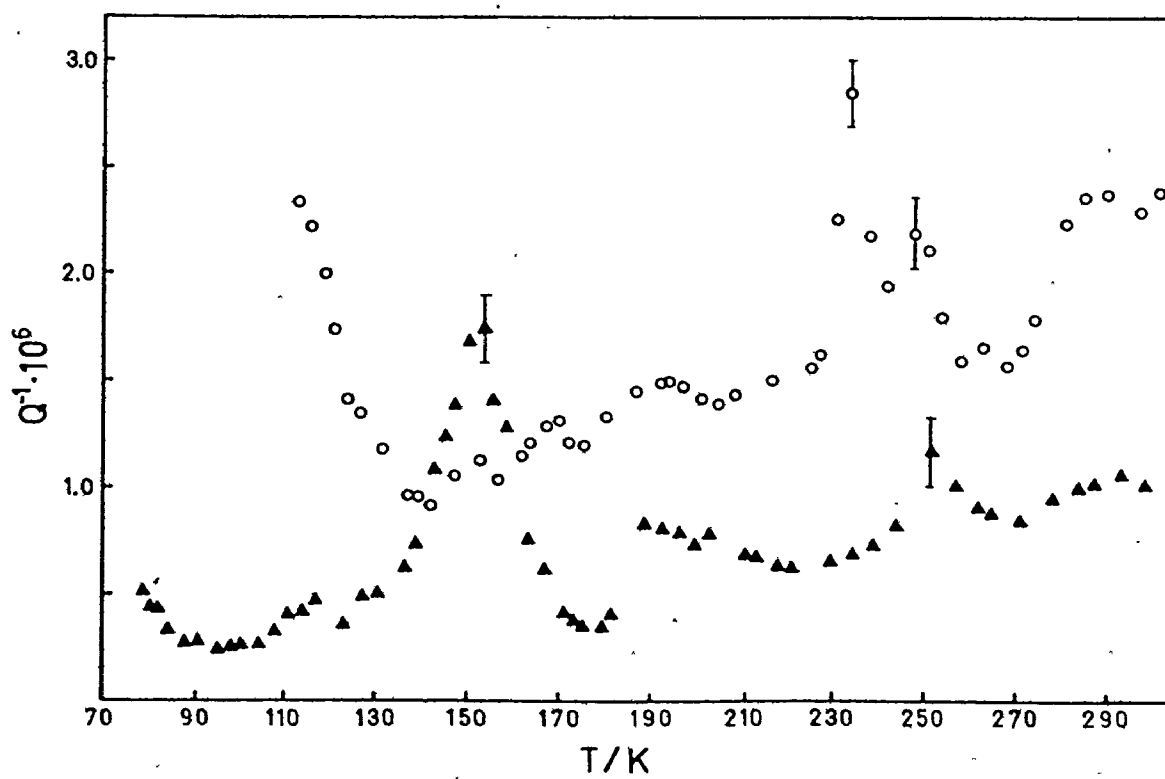
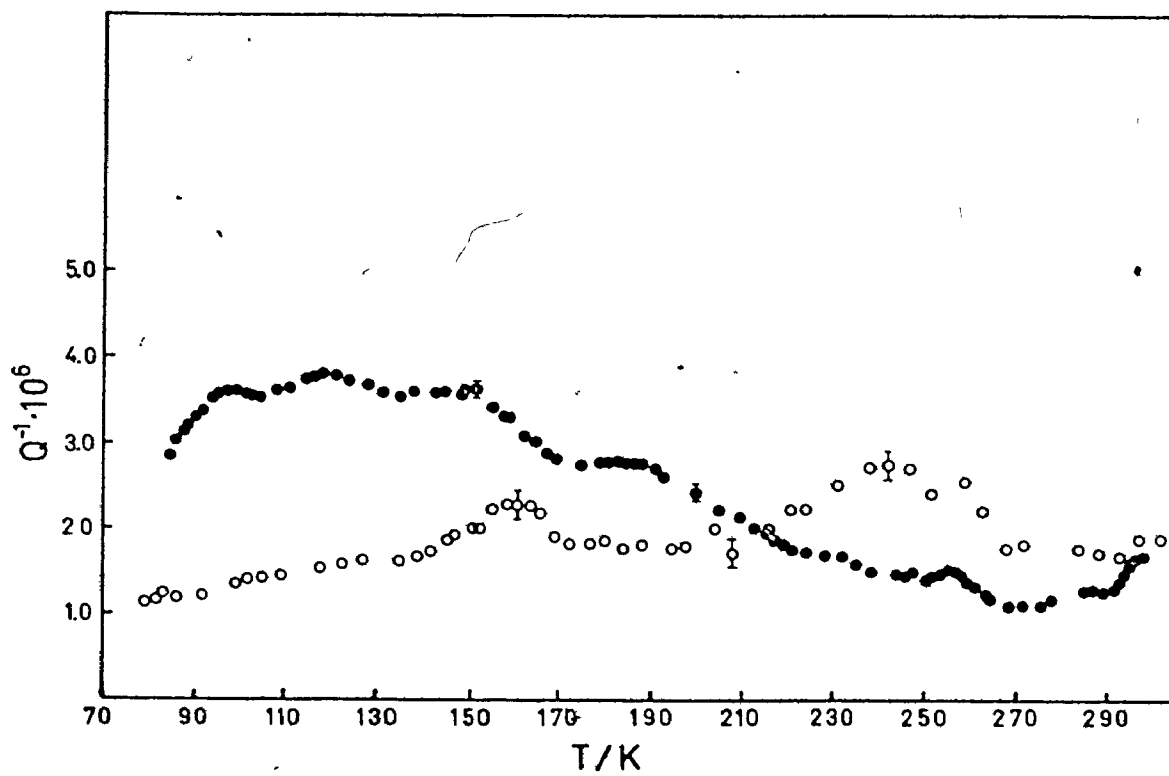
Internal friction of Al 0.16 at.% Mg polycrystalline sample -  
hydrogen charged

- (a) air cooled  $\epsilon_m = 8.5 \times 10^{-8}$
- (b) quenched  $\epsilon_m = 5.4 \times 10^{-8}$

FIGURE 5.14

Internal friction of Al 0.54 at.% Mg polycrystalline sample

- ▲ (a) annealed in helium  $\epsilon_m = 1.2 \times 10^{-7}$
- (b) annealed in hydrogen  $\epsilon_m = 6.2 \times 10^{-8}$



temperature the frequency of the subharmonic was observed to have changed by 11 Hz indicating that the joint had deteriorated somewhat.

The sample was annealed for twelve hours in a hydrogen-water vapour atmosphere at 600°C and allowed to cool in air before taking the measurements shown in curve (b). The maximum strain amplitude was  $6.2 \times 10^{-8}$  and the initial cooling rate was again about 3°/minute. The spectrum shows a rapidly rising internal friction below 130 K which was accompanied by the presence of a second resonance near the fundamental frequency. This is similar to the behaviour of the aluminum-copper sample shown in Figure 5.9. There is also some structure between 230 K and 255 K with a prominent sharp peak at 234 K. This peak is too narrow for the Wert-Marx plot. The remaining structure is not very different from the sample after the helium anneal except that the sharp peak at 153 K is absent. The frequency of the subharmonic after returning to room temperature was within 1 Hz of the starting value.

## 5.6 Commercial Alloys

Internal friction measurements were made on two commercial alloys, 7075 and 6061 the compositions of which are shown in Table 5.1.

The internal friction measurements of the 7075 sample, shown as curve (a) in Figure 5.15, were obtained after the sample was machined to size from a  $\frac{1}{2}$ " diameter rod of material in the as-received T6 condition. The results, obtained by continuous cooling at a rate of less than 1°/minute, show a low damping (less than  $4 \times 10^{-6}$ ) over the whole temperature range with one prominent peak at 152 K of height  $1.8 \times 10^{-6}$ . This peak could be the

TABLE 5.1

SOLUTE CONTENT OF COMMERCIAL ALLOYS  
IN WEIGHT PER CENT

	Mg	Cu	Zn	Si	Cr
7075 <sup>a</sup>	2.57	1.21	6.23	-	
7075 <sup>b</sup>	2.5	1.6	5.6		0.3
6061 <sup>b</sup>	1.0	.25	-	0.6	0.25

a - by atomic absorption

b - nominal composition

Bordoni peak resulting from the deformation during machining. The maximum strain amplitude during the measurement was  $5.2 \times 10^{-8}$ . The room temperature frequencies of the various modes remained unchanged after the experiment.

The results shown as curve (b) in the same figure were obtained with the same sample under the same conditions except that the whole resonator, after degreasing the surface in pentane, had been placed in a hydrogen atmosphere at 1800 psi at room temperature for eleven days. The differences between the two curves are smaller than  $0.2 \times 10^{-6}$ .

A similar sample of the same material was annealed in a hydrogen atmosphere at 560°C for 48 hours and quenched into water at room temperature. The low annealing temperature was required because of the low solidus temperature for the alloy (less than 600°C). The material was observed to have several large blisters following the anneal and voids visible to the unaided eye were found when the sample was cut after the internal friction

FIGURE 5.15

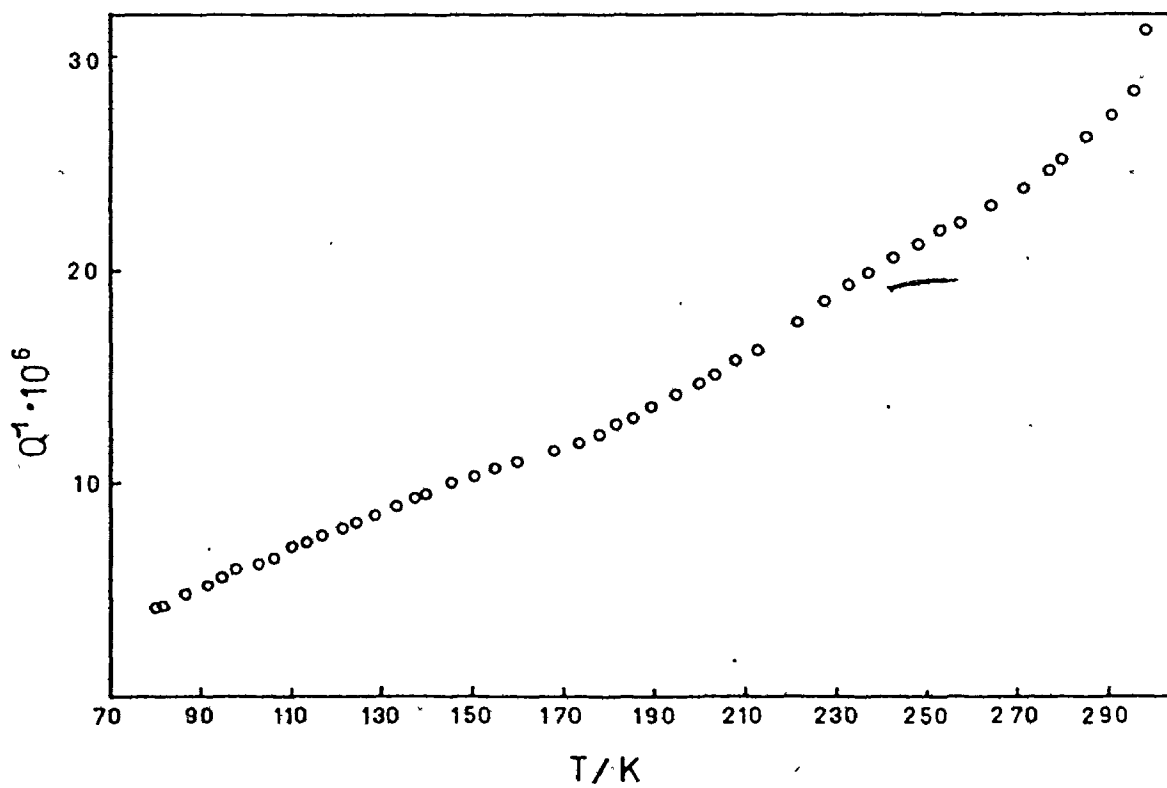
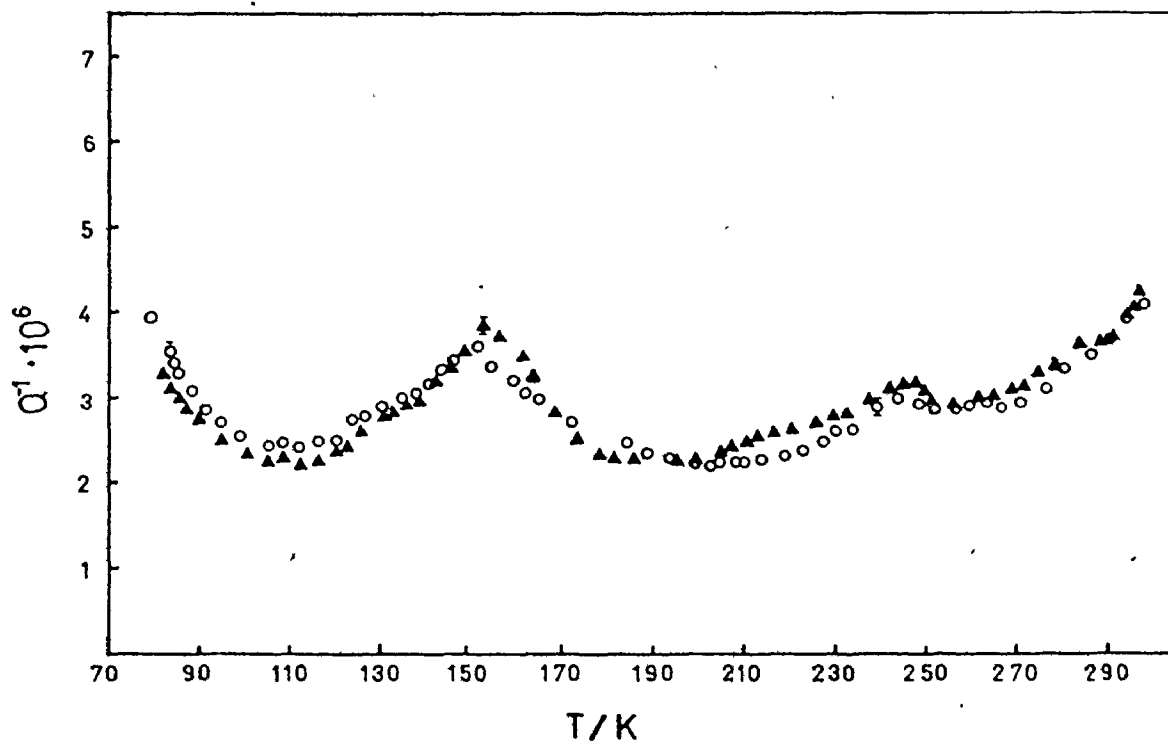
Internal friction of 7075 T6 aluminum

- ▲ (a) as machined  $\epsilon_m = 5.2 \times 10^{-8}$
- (b) after hydrogen treatment

FIGURE 5.16

Internal friction of 7075 aluminum after  
hydrogen anneal at 560°C

$$\epsilon_m = 1.2 \times 10^{-7}$$



experiment. The internal friction spectrum of this sample is shown in Figure 5.16. The cooling rate was the same as for the previous 7075 sample and the maximum strain amplitude was  $1.2 \times 10^{-7}$ . The damping is much higher than in the unannealed sample but is monotonically decreasing, any structure being less than  $1 \times 10^{-6}$ . The frequency of the subharmonic on returning to room temperature was within 1 Hz of the value before the experiment.

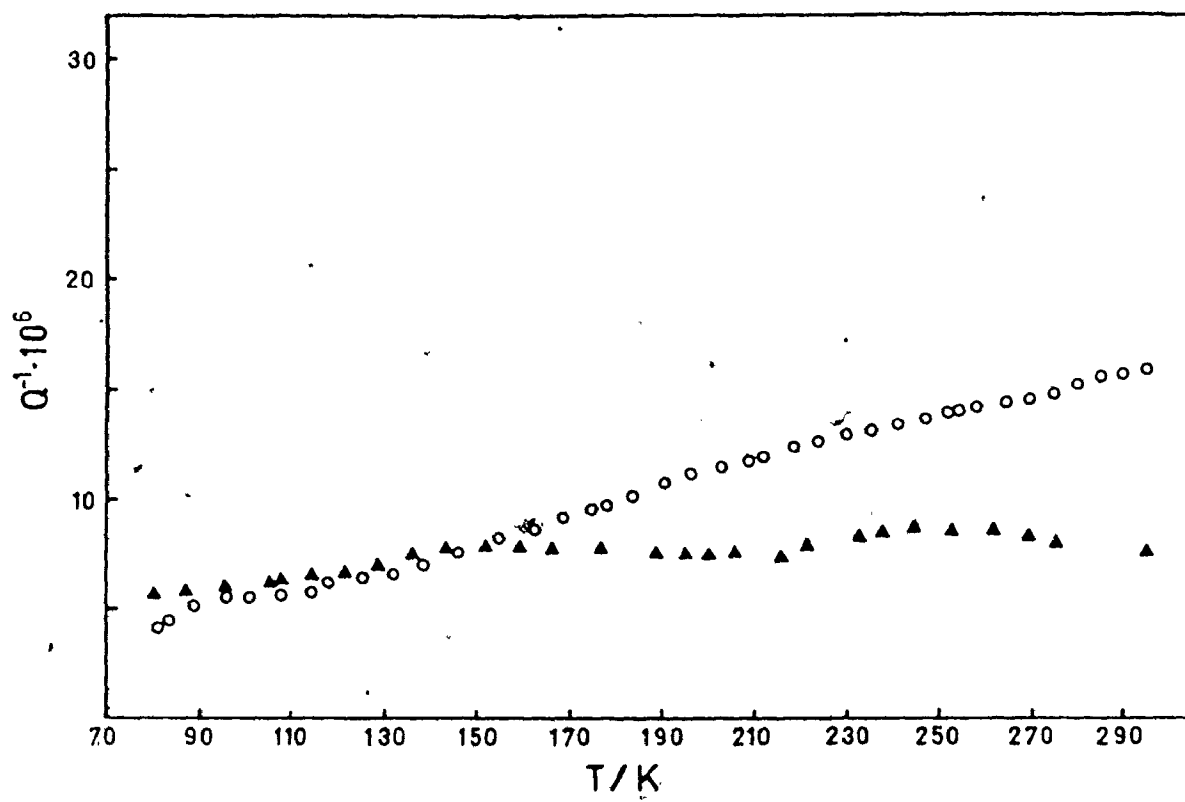
The results of measurements on the 6061 alloy are shown in Figure 5.17. Curve (a) of the figure was obtained with a specimen which had been annealed in vacuum at  $580^{\circ}\text{C}$  and allowed to cool in air. The measurements were made using the step heating method. The third harmonic results are shown because spurious peaks were present on the fundamental. The maximum strain amplitude was  $2.8 \times 10^{-7}$ .

A similar sample was annealed at  $600^{\circ}\text{C}$  in a hydrogen atmosphere and quenched into water. The spectrum was measured by continuous cooling at a rate of less than  $1^{\circ}/\text{minute}$ . The maximum strain amplitude was  $1.6 \times 10^{-7}$ . As with the 7075 sample in the same condition, the damping decreases monotonically and is larger than in the slowly cooled case. There are no distinct peaks in the curve as large as  $1 \times 10^{-6}$  except for one at about 92 K which is about this size. The variations below 118 K are thought to be due to the deterioration of the resonator. The quartz crystal was observed to be cracked near the joint on returning to room temperature. Since there was a slight discontinuity in the frequency vs. temperature curve for the fundamental mode at 118 K, the crack is presumed to have occurred at that temperature. The frequency change involved on the

FIGURE 5.17

Internal friction of 6061 aluminum

- ▲ third harmonic - sample annealed in vacuum  $\epsilon_m = 2.8 \times 10^{-7}$
- fundamental - " " " hydrogen  $\epsilon_m = 1.6 \times 10^{-7}$



fundamental was only about 4 Hz but upon returning to room temperature, the subharmonic had changed by almost 600 Hz. This shows the sensitivity of the subharmonic to joint condition.

## CHAPTER 6

### DISCUSSION

#### 6.1 General Discussion

The object of this work was to determine parameters which characterize the defect pair composed of an interstitial hydrogen atom bound to a substitutional solute atom in an aluminum matrix. The main quantity of interest was the binding energy of the pair because this could be compared with theoretical calculations which are feasible for the aluminum alloy system because it has a relatively simple electronic structure. In this chapter, the internal friction results are used to put upper limits on the pair binding energy.

An expression for the peak height was presented in the second chapter and it is recalled here

$$\text{Peak height} = \frac{1}{2} \frac{\delta J}{J} = \frac{1}{9} \frac{c_0 v_0}{kT J} (\lambda_1 - \lambda_2)^2 (1 - 3\Gamma) \quad (6.1.1)$$

A preliminary calculation of the expected peak height for a random polycrystal yielded a value of  $Q_{\text{max}}^{-1} \approx 10^{-6}$  for a pair concentration of  $5 \times 10^{-7}$  atomic fraction and a value of the defect strain anisotropy,  $(\lambda_1 - \lambda_2)$ , of 0.34 at the expected peak temperature of 230 K. This concentration of

pairs would result from a binding energy of 0.12 eV for a substitutional solute concentration of 0.5 at.%. Although this maximum peak height was very small, the measurements have shown that it would have been easily measurable with the perfected techniques which were used to make the internal friction measurements. In fact, it will be shown that peaks as small as  $0.2 \times 10^{-6}$  would have been observable. This high sensitivity was achieved by the perfection of the metallic joint between the quartz transducer and metal samples which also allowed measurements at the third and fifth harmonics. These higher frequency measurements, essential for binding energy measurements, were also used in conjunction with subharmonic frequency measurements as a criterion for eliminating spurious internal friction peaks from measurements at the fundamental frequency.

The expression for the peak height clearly shows the dependence of the height upon concentration (which in turn depends upon the binding energy according to equation (2.1.9)) and the strain anisotropy ( $\lambda_1 - \lambda_2$ ). Before examining these parameters in detail, there are two more obvious possibilities for the absence of peaks in the internal friction spectra.

The first possibility is that no hydrogen dissolved in the sample during the high temperature annealing in hydrogen-water vapour mixtures. This possibility can be rejected using experimental evidence. First of all, there was visual evidence in some of the samples--notably the pure aluminum samples and the 7075 sample--of blistering and void formation in the sample interior. These blisters, in the aluminum samples, did not appear during vacuum annealing. Gas analysis was performed by vacuum extraction (at Alcan International Laboratories, Kingston, Canada) on one of the Al-Mg

samples. The results indicated a hydrogen content which was more than 80% of the expected value, even though this sample had been cooled relatively slowly by simply withdrawing it from the furnace. Further gas analysis results were performed with a new analysis system and are reported in Appendix B. In that study, samples, which had been charged in deuterium and water quenched, were used in order to distinguish surface adsorbed water from dissolved deuterium. The results indicate that there definitely was deuterium in the samples although further calibration of ion pump speeds is necessary to quantitatively measure the deuterium content. Other experimenters (Eichenauer, 1968 and Shimomura and Yoshida, 1967) made no special surface treatment to promote the dissolution of hydrogen in aluminum samples at high temperature. Absolute values of hydrogen content would not have been necessary to determine the binding energy of the hydrogen substitutional solute pairs if the peak shape could be measured at all three frequencies.

The second possibility for the absence of an internal friction peak is that, for some reason or other, the apparatus was incapable of measuring internal friction. Internal friction measurements of deformed aluminum were made, in part, to refute this argument. The main body of the results on deformed aluminum are reported in Appendix A. These indicate that internal friction measurements could certainly be made even at very low strain amplitude ( $3 \times 10^{-9}$ ) and that they compare very well with previous measurements of similar material made by other experimentalists, in terms of peak heights and activation energies.

The observation of a peak also depends upon the relaxation time,  $\tau$ ,

being equal to the reciprocal of the applied stress angular frequency,  $2\pi f$ , at some point within the measurement temperature range. This problem is discussed in the following section.

The sensitivity of the results, as shown by the preliminary measurements and the limits on the observable peak height for the different alloys, are discussed in the third section.

Since a knowledge of the strain anisotropy ( $\lambda_1 - \lambda_2$ ) of the defect is required in order to determine the binding energy limits, in the fourth section a value for this parameter is estimated by comparison with other systems.

The upper limits of the binding energies between hydrogen and substitutional solutes were determined for each alloy in the following section using the estimated value of ( $\lambda_1 - \lambda_2$ ) obtained in the previous section.

In the next section, the commercial alloy results are compared with those of Gest and Troiano (1974) who observed a peak attributed to hydrogen substitutional defects. Finally, the distribution of hydrogen in aluminum is discussed.

## 6.2 Peak Temperature

The expected peak temperature was determined from high temperature measurements of the diffusion coefficient of hydrogen in pure aluminum. Since the relaxation time,  $\tau$ , for the reorientation of the defect by hydrogen atom jumping, must be equal to the reciprocal of the angular frequency of the applied stress,  $(2\pi f)^{-1}$ , the expected temperature can be

found for any frequency when  $\tau$  is obtained from equation (2.5.31). The diffusion data of Eichenauer et al. (1961) could be represented by the equation

$$D = 0.11 \exp \left[ - \frac{0.424 \text{ eV}}{kT} \right] \text{ cm}^2 \text{ sec}^{-1}$$

This data covered a very large temperature range from 300 to 600°C and was obtained during outgassing experiments. The peak temperature determined using this equation for a 35 kHz applied stress frequency was 230 K. Earlier diffusion coefficient measurements, also by Eichenauer et al. (1957), could be represented by a slightly different equation which yielded an expected peak temperature of 250 K which was still well within the measurement temperature range. The assumption upon which equation (2.5.31) is based is that the jump frequencies of hydrogen atoms resulting in reorientation of the substitutional-interstitial (s-i) pair is the same as in the perfect lattice. This means either that the classical attempt frequency and activation energy are unchanged or that they both change in such a way that the jump frequency remains constant. If there is a binding energy between hydrogen and the substitutional solute, then the saddle point energy between sites adjacent to the substitutional atom is changed from the normal saddle point energy by an amount equal to the binding energy if the attempt frequency remains the same. This assumption seems to be verified in practice in several different lattices. For example, H diffuses in pure Ni with an activation energy of 0.41 eV (Ebisuzaki et al., 1967). Magnetic after-effect measurements on dilute NiFe alloys (Adler, 1965) containing

H yield an activation energy for H-Fe pair reorientation of 0.36 eV and the observed peak temperature for the effect is within a few degrees of that which is predicted using high temperature diffusion data for pure Ni. Similarly, in b.c.c. materials, the temperature of the s-i peak can be very close to the normal Snoek peak temperature (Fast et al., 1961).

In Zr, Ritchie et al. (1976) has recently found that oxygen-substitutional atom pairs reorient with an activation energy which is in good agreement with other oxygen diffusion measurements.

### 6.3 Sensitivity of the Measurements

Preliminary experimental results using quartz crystal combinations have shown that the resonators and the technique can be used for sample dampings in the  $Q^{-1} \approx 10^{-7}$  range. Although the precision of individual measurements was 1% or  $Q^{-1} = 5 \times 10^{-8}$  (whichever was larger) in the cases where the cooling rate was less than 1°/minute, there were always variations in the internal friction over the temperature range examined which were significantly larger than this estimated error of measurement. The continuous cooling measurements of quartz crystal combinations (Figure 5.5) show these changes very clearly. These peaks were not reproducible from one run to the next even in the cases where the joint was not altered (although thermal cycling of the joint during measurement could be considered as an alteration of the joint because of the large stresses involved). The variations are thought to be due to the joint and suspension and not to internal friction processes in the samples. Both quartz specimens and aluminum alloy samples exhibited variations which were approximately the

same size. In examining the aluminum alloy results for possible peaks due to hydrogen-substitutional atom pairs, two reasonable assumptions have been applied. The first assumption is that the temperature of the s-i peak for a particular substitutional solute will be independent of the solute concentration. This is equivalent to assuming that the environment of each s-i pair is the same, which should be valid for the low solute concentrations used in these alloys. The second assumption is that the width of the peak in  $T^{-1}$  at half maximum height should be commensurate with the expected activation energy of 0.424 eV (which is the activation energy for hydrogen diffusion found by Eichenauer et al., 1961), using a Debye peak. Internal friction peaks caused by point defects, tend to be wider than the normal Debye peaks because of distributions in activation energy,  $Q$ , or time constant,  $\tau_0$ , and therefore, very narrow peaks must be due to effects other than s-i pairs. These two assumptions have been applied in comparing internal friction spectra for different specimens containing the same substitutional solute. Each different type of alloy is discussed in turn.

a) The aluminum copper alloys

As pointed out in the last chapter, there are no peaks which are common in the spectra of the hydrogen charged polycrystalline and single crystal AlCu samples (shown in Figures 5.10 and 5.11). The peak at 220 K in the polycrystalline sample has no counterpart in the single crystal specimen; in fact, there appears to be a minimum at 220 K in the single crystal sample. The peak at 246 K in the single crystal does not exist in the polycrystalline sample. The low temperature peaks in the 130 to 150 K range are presumably the Bordoni peaks which appear in the pure aluminum

samples (Figure 5.8) but are greatly reduced in size here. If there was a common peak in the two spectra, it would have to be near 230 K. The maximum size of peak which could be obscured by the damping caused by joint and suspension is one with  $Q^{-1} \approx 0.3 \times 10^{-6}$  in both cases.

b) The aluminum-magnesium alloys

As in the aluminum copper case, there are no peaks which are common to all of the hydrogen charged alloys, for which the results are shown in Figures 5.13 and 5.14. The 0.16 at.% Mg alloy, which was quenched from a hydrogen atmosphere and measured during slow continuous cooling, showed very small variations in the internal friction. Peaks larger than  $Q^{-1} \approx 0.2 \times 10^{-6}$  would be detectable in this spectrum. The limit for the 0.54 at.% Mg sample is about the same size because the variations between 230 and 250 K consist of two peaks which are too narrow to be a Debye peak with the expected activation energy and they also occur in the uncharged 0.16 at.% Mg sample.

c) The commercial alloys

The background internal friction in both commercial alloys quenched from hydrogen atmosphere was much larger than for the laboratory prepared samples. However, the spectra are both monotonically decreasing as can be seen from Figures 5.16 and 5.17. For both the 6061 and 7075 alloys the maximum peak size is about  $Q^{-1} \approx 1 \times 10^{-6}$ .

A comparison of the internal friction spectrum of the 7075 alloy after room temperature exposure to 1800 psig of hydrogen with the same alloy before exposure, Figure 5.15, shows that there were no changes caused by the

exposure which were as large as  $Q^{-1} \approx 0.2 \times 10^{-6}$ . This is in contradiction to the results of Gest and Troiano (1974), who found a peak almost five thousand times this size at 130 K and 100 kHz. This will be discussed in the final section of this chapter.

#### 6.4 The Strain Anisotropy ( $\lambda_1 - \lambda_2$ ) for the Hydrogen-Substitutional Pair

In order to obtain a reasonable value for the strain anisotropy ( $\lambda_1 - \lambda_2$ ) of the hydrogen-substitutional defect pair in aluminum alloys, a comparison has been made with other close-packed metals which have been studied experimentally and some reasonable arguments using additional information are presented.

The number of s-i pairs in f.c.c. metals which have been studied closely enough that values of ( $\lambda_1 - \lambda_2$ ) could be determined is unfortunately very small. Kê and Tsien (1956) used a low frequency torsion pendulum method to study the f.c.c. Fe-Mn-C system. From their work it is possible to derive a value of  $|\lambda_1 - \lambda_2|$  for the C-Mn pair in iron to be 0.082. The same system has been studied by Kandarpa and Spretnak (1969), also with the torsion pendulum technique, and their results yield a value of 0.09<sub>9</sub>, which is very close to that of Kê and Tsien. Internal friction attributed to hydrogen-substitutional solute pairs in several stainless steels has been observed by Peterson et al. (1969) using a composite resonator technique. The main alloying elements were chromium and nickel. Samples which were cathodically charged with hydrogen exhibited large peaks at about 200 K at a frequency of 80 kHz. In order to determine a value for  $|\lambda_1 - \lambda_2|$  for the defect, the samples were assumed to be random polycrystals (as was assumed

for the Fe-Mn-C case). The dissolved hydrogen content was assumed to be that which would be in equilibrium with hydrogen gas at a pressure equal to the yield strength of the material at the temperature of the internal friction peak. The value of  $|\lambda_1 - \lambda_2|$  determined in this way for the s-i pair was 0.28. The assumed dissolved hydrogen content is not unreasonable. The cathodic charging was observed by Peterson et al. to be accompanied by substantial deformation as measured by X-ray line broadening and occasional surface blistering. In b.c.c. iron, Beck et al (1966) observed a critical hydrogen content, which corresponded to a hydrogen pressure much less than the yield strength, above which irreversible damage of the metal took place. It seems likely that this damage is caused by hydrogen precipitation at internal faults in the lattice.

In order to determine a value of  $|\lambda_1 - \lambda_2|$  for the aluminum alloys, some additional information has been used. Gupta and Weinig (1962) have examined s-i peaks in another close packed material (h.c.p. titanium containing interstitial oxygen and various substitutional impurities). They found that the relaxation strength depended upon the relative atomic sizes of the substitutional and host atoms. The distortion of the octahedral site is larger when the substitutional atom is a much different size from the host. A similar size effect might be expected in f.c.c. materials which are also close packed and exhibit no normal Snoek effect. The alloy components of stainless steel, Cr and Ni, have effective atomic diameters which are within 3% of that of iron according to partial molar volume measurements of Straalsund and Bates (1974). Therefore the relative distortion of the octahedral site occupied by the hydrogen atom in Peterson's work should be less than in the aluminum alloys

which were studied in this work since the apparent diameters of Cu, Mg and Si differ from those of aluminum in aluminum alloys by -12.2%, +10.1% and -4.5% respectively (Pearson, 1958).

The size of the interstitial atom should also have an effect on the value of the strain anisotropy ( $\lambda_1 - \lambda_2$ ). In a limiting case in which the interstitial has no effect on neighbouring atoms, the strain anisotropy ( $\lambda_1 - \lambda_2$ ) must vanish. The sum of the principal values of the  $\lambda$  tensor is related to the change in the lattice parameter per unit defect concentration according to the following equation given by Nowick and Berry (1972)

$$\frac{1}{a} \frac{da}{dc} = \frac{1}{3} (\lambda_1 + 2\lambda_2)$$

Therefore,  $\lambda_1 + 2\lambda_2$  must increase for larger interstitials.

If  $\lambda_1$  and  $\lambda_2$  were both small, the difference could not be very large but if they are large then there is a possibility that the difference will also be large. What, then, is the evidence for hydrogen being a large interstitial in aluminum? Since there are no measurements of lattice parameter changes due to hydrogen in aluminum because the concentrations are so small, the relaxation about single hydrogen atoms has not been measured directly. However, an indication that the relaxation may be quite large results from combining theoretical work by Wagner (1971) and solubility measurements in molten alloys. Wagner has shown that the rate of change of solubility of an interstitial, such as hydrogen, with substitutional solute content measured at constant pressure differs from the

rate of change of solubility which would be measured at constant volume. The expression he develops is

$$\left[ \frac{\partial \ln S}{\partial c_i} \right]_{T,P,c_i \rightarrow 0} = \left[ \frac{\partial \ln S}{\partial c_i} \right]_{T,V,c_i \rightarrow 0} + \frac{\bar{V}_H B (\partial V_M / \partial c_i)_{T,P}}{V_1^0 RT} \quad (6.4.1)$$

Where  $S$  is the solubility of hydrogen,  $c_i$  is the atomic fraction of substitutional solute,  $\bar{V}_H$  is the partial molar volume of hydrogen,  $V_1^0$  and  $V_M$  are the molar volume of the host and alloy respectively and  $B$  is the bulk modulus. The first term on the right handside is an indication of interactions between the hydrogen and substitutional atoms and is the dominant term for hydrogen in binary copper alloys (Wagner, 1971). In the molten aluminum alloys, the rate of change of solubility with substitutional content at constant pressure is the same sign as  $\left( \frac{\partial V_M}{\partial c_i} \right)_{T,P}$  i.e. solute elements which decrease the molar volume of the alloy, such as copper and silicon, also decrease the hydrogen solubility. This indicates that the partial molar value of hydrogen,  $V_H$ , could be substantial (at least it is positive). If the first term on the right hand side is assumed to be small, which is equivalent to neglecting interaction between hydrogen and substitutional solutes, then a molar volume for hydrogen in liquid aluminum may be determined. This was done using the solubility data of Opie and Grant (1950), the liquid compressibility of Ascarelli (1968) and the lattice parameter data for solid alloys of Pearson (1958). The results for both Al Cu and Al Si indicate a similar hydrogen partial molar volume (9.95 cm<sup>3</sup> for Al Si and 8.84 cm<sup>3</sup> for Al Cu). Since the forces due to the electronic

interactions at the nearest neighbour distance between hydrogen and Si are expected to be of different sign from those between hydrogen and Cu, the fact that the partial molar volumes are similar indicates that neglecting the interaction term for the molten alloys in equation (6.4.1) is not unreasonable. Since the molar volume of liquid aluminum at the melting point is  $11.3 \text{ cm}^3$ , the partial molar volume of hydrogen is a very large fraction (0.83) of that for aluminum. Since there seems to be such a large partial molar volume in the liquid alloys, the distortions about the interstitial in the solid metal could be quite large. As a comparison, in the iron-carbon system, the partial molar volume of carbon in the liquid (Widawski and Sauerwald, 1930) and in austenite (Ridley and Stuart, 1970) are about the same size:  $3.5$  and  $3.78 \text{ cm}^3$  respectively. In austenite, the carbon occupies about half (0.52) an atomic volume.

In summary, the experimental evidence indicates that the size of hydrogen in aluminum is a large fraction of an atomic volume. Also, the apparent size differences between aluminum and the substitutional atoms investigated are quite large. It is expected, therefore, that the strain anisotropy will be substantially larger than for C in Fe Mn. The estimate of the value of  $|\lambda_1 - \lambda_2|$  for hydrogen-substitutional solute pairs in aluminum which will be used in the determination of the binding energy is 0.25. This is about the same size as that deduced from Peterson's work.

### 6.5 Hydrogen-Substitutional Solute Binding Energy

It is possible to estimate a value for the maximum binding energy of hydrogen to the substitutional solute from the maximum peak height values

already determined in § 6.3. The maximum peak height is related to the s-i pair concentration through equation 6.1.1. The value of  $|\lambda_1 - \lambda_2|$  has been estimated in § 6.4 to be 0.25. The other parameters in the equation are known:  $J$  has been taken to be  $E^{-1}$ , the inverse of the Young's modulus (obtained from resonant frequency, length and density of the sample);  $v_0$  is the atomic volume of aluminum; and  $P$  is the orientation factor for the sample, which has been assumed to be 0.2 for polycrystalline samples and 0 for the  $\langle 100 \rangle$  Al Cu single crystal. The maximum pair concentration,  $c_0$ , can then be calculated at the expected peak temperature of 230 K. The values of the pair concentration for each alloy calculated using equation 6.1.1 with the assumption mentioned are shown in Table 6.5.1.

Ideally, the hydrogen introduced into the sample at high temperature remains in solution when the sample is quenched. As long as the quantity of hydrogen lost through the surface of the sample is small, the hydrogen content of the lattice can be determined. The activity of hydrogen in a quenched sample at low temperature is then very high relative to a hydrogen pressure of one atmosphere. Several investigations of hydrogen solubility in solid pure aluminum have been made (Ransley and Neufeld, 1945; Eichenauer and Pebler, 1957 and Eichenauer, 1968). These studies indicate that the solubility in pure aluminum in equilibrium with hydrogen gas at one atmosphere pressure at 600°C is about  $0.023 \text{ cm}^3 \text{ H}_2(\text{S.T.P.})/100 \text{ g Al}$ . This is equivalent to an atomic fraction of hydrogen of  $5.7 \times 10^{-7}$ . The solubility in solid aluminum alloys has not been as carefully studied, but several molten alloys have been studied by Opie and Grant (1950) and by Baukloh and Oesterlen (1938). These measurements indicated that copper

and silicon solutes decreased the hydrogen solubility while the presence of magnesium increased it. However, since the substitutional solute contents of the Al Cu and Al Mg alloys studied were less than 1 at.%, the change in solubility of hydrogen in the alloys was expected to be quite small. As a first approximation, the hydrogen solubility at 600°C can be assumed to be the same for the alloys as for the pure aluminum. If the hydrogen remains in solution after the quench, then the number of hydrogen-substitutional pairs at any temperature is directly dependent upon the binding energy according to equation 2.1.9. This equation assumes the hydrogen is either in the perfect lattice or next to a substitutional impurity. The fraction,  $f$ , of the total hydrogen content which is in interstitial sites adjacent to the substitutional impurities can be found from 2.1.10 to be

$$f = \frac{6 c_i \exp \Delta G_b / kT}{1 - 6 c_i + 6 c_i \exp \Delta G_b / kT}$$

This fraction is also the ratio of the number of pairs,  $c_0$ , determined from the internal friction results, and the total hydrogen content,  $c_T$ . The maximum binding energy is found by rearranging the equation for  $f$  to give

$$\Delta G_b = kT \ln \frac{f(1 - 6 c_i)}{6 c_i(1 - f)}$$

The temperature,  $T$ , in this equation is taken to be the expected peak temperature since that is the temperature for which  $f$  has been calculated.

The value of the total hydrogen content,  $c_T$ , the resulting fraction  $f$  and the calculated maximum binding energies are recorded in Table 6.5.1. The value of the total hydrogen content for the Al 0.54 at.% Mg sample is that determined by subsequent gas analysis. It is slightly lower than for the other laboratory prepared samples because this sample was air cooled and not water quenched. The commercial alloy results are not included in the table because the internal friction peak size limit ( $1 \times 10^{-6}$ ) was larger than the peak which would be obtained if all the hydrogen was at substitutional sites (using the estimated value of  $|\lambda_1 - \lambda_2|$  of 0.25).

TABLE 6.5.1

<u>Alloy</u>	<u><math>c_0(\lambda_1 - \lambda_2)^2</math></u>	<u><math>c_i</math></u>	<u><math>c_0</math></u>	<u><math>c(\text{Total})</math></u>	<u><math>f</math></u>	<u><math>\Delta G_b(\text{eV})</math></u>
Al Cu polycrystal	$1.8 \times 10^{-8}$	.0068	$2.88 \times 10^{-7}$	$5.7 \times 10^{-7}$	.50 <sub>5</sub>	.06 <sub>3</sub>
Al Cu single crystal	$7.2 \times 10^{-9}$	.0042	$1.15 \times 10^{-7}$	$5.7 \times 10^{-7}$	.20 <sub>1</sub>	.04 <sub>5</sub>
Al Mg .1 at.%	$1.2 \times 10^{-8}$	.0016	$1.92 \times 10^{-7}$	$5.7 \times 10^{-7}$	.33 <sub>6</sub>	.07 <sub>8</sub>
Al Mg 0.5	$1.2 \times 10^{-8}$	.0054	$1.92 \times 10^{-7}$	$4.9 \times 10^{-7}$	.39 <sub>2</sub>	.05 <sub>8</sub>

The values of the binding energy could be compared with theoretical values obtained using the approach outlined in Chapter 2. However, these calculations have not yet been done. Since the value of  $|\lambda_1 - \lambda_2|$  is also critical to the binding energy determinations, theoretical verification of

the estimated value is desirable.

## 6.6 The 7075 Alloy Results

Gest and Troiano (1974) reported internal friction measurements of a 7075-T6 alloy which had been hydrogen charged for eleven days under a 2000 psi hydrogen atmosphere. Employing the two component resonator technique at an applied stress frequency of 100 kHz, they found a very large peak,  $Q_{\max}^{-1} > 10^{-3}$ , at a temperature of 130 K. They attributed this peak to hydrogen-substitutional pairs.

The results presented in Chapter 5 for this same alloy (Figure 5.15) show no indication of such a peak. The internal friction of the sample remained virtually unchanged (changes less than  $2 \times 10^{-7}$  in  $Q^{-1}$ ) after charging the sample for the same period of time at 1800 psi  $H_2$ . The background damping of our measurements was apparently lower by almost two orders of magnitude. Also, the frequencies of the various modes remained unchanged after thermal cycling thus indicating that the joint had not deteriorated.

Annealing the alloy at 560°C in a hydrogen atmosphere followed by quenching in water at room temperature also failed to produce any peak as large as  $Q^{-1} = 10^{-6}$  (Figure 5.16). The annealing treatment caused blistering, thus indicating that hydrogen had certainly been present in the alloy at the charging temperature.

Our measurements of the hydrogen charged 7075 alloy are consistent with all the other results presented in this thesis. Since the sensitivity

of the measurement was significantly better than that of Gest and Troiano, their results must be due to some effect other than substitutional-hydrogen pairing. The peak which they observed is in the same temperature range as some of the deformation produced peaks in aluminum (Appendix A).

There was no attempt made to try to reproduce the results of Gest and Troiano on deformed and hydrogen charged 7075 alloy. Their results, on close examination, seem to show that the only effect of the hydrogen charging was to raise the general level of damping. The size of all structure in the spectrum remained unchanged.

#### 6.7 Hydrogen Distribution in Aluminum

The values of the maximum binding energy are dependent upon the assumptions which have been made. The simple model of a distribution of hydrogen between normal lattice interstices and those next to substitutional atoms is only an approximation. If the hydrogen is distributed in some other way, then the problem of determining a maximum binding energy becomes much more difficult. There are several other positions which hydrogen could occupy:

##### a) Grain boundaries

Eichenauer's (1968) solubility measurements have shown that, as the grain size of pure aluminum gets larger during the hydrogen anneals used to determine the solubility, the solubility decreases. This implies that there could be a significant amount of hydrogen at grain boundaries. However, a comparison of these results with his previous results

(Eichenauer et al., 1961) also indicates that increasing the sample purity decreased the solubility.

b) Dislocations

Measurements of solubility in deformed aluminum (Eborall and Ransley, 1945) have shown that the solubility at 600°C can be increased by a factor of about four in cold rolled, commercial purity aluminum from which it can be inferred that there is binding of hydrogen to dislocations. Further evidence of the binding of hydrogen to dislocations can be seen in the work of Foster et al. (1963) who used tritium autoradiography to determine the position of this hydrogen isotope in pure aluminum. They found that samples which were deformed at room temperature before charging with tritium at 600°C showed tritium present at what had been dislocation pile-ups in slip bands even though the matrix had recrystallized. This means that the tritium was significantly bound to the dislocations even at the charging temperature.

c) Vacancies

Hydrogen could also be bound to vacancies as was suggested by the theoretical work of Popović et al. (1976). The vacancy content at 600°C in pure aluminum is  $4.4 \times 10^{-4}$  (Simmons and Balluffi, 1960). This is a factor of almost  $10^3$  greater than the hydrogen solubility at one atmosphere pressure at the same temperature. If there were a significant binding energy between hydrogen and vacancies, the actual quantity of unassociated interstitial hydrogen could be substantially less than the  $5.7 \times 10^{-7}$  atomic fraction measured by Eichenauer. A hydrogen-vacancy interaction has also been

postulated in order to explain the enhanced nucleation of voids in aluminum foils quenched from hydrogen atmospheres (Shimomura and Yoshida, 1967). Hydrogen trapping by vacancies and voids would reduce the quantity in the perfect lattice and therefore reduce the number of s-i pairs which could be observed by internal friction.

The values of the binding energy which were determined in § 6.5 are therefore the "least upper bounds" of the binding energy between hydrogen and substitutional solutes.

## CHAPTER 7

### SUMMARY AND CONCLUSIONS

1. A very sensitive internal friction spectrometer based on the composite resonator was constructed for measurements, at kHz frequencies, of the internal friction of metallic specimens in the temperature range from 80 to 300 K. The spectrometer was capable of measuring specimen dampings in the  $Q^{-1} \approx 10^{-7}$  range. Changes in damping of 1% could be easily measured for damping greater than  $Q^{-1} = 5 \times 10^{-6}$ .
2. The two component resonator technique was refined by using a low melting point metallic joining material between the quartz transducer and the specimen. The joint so obtained had excellent characteristics including very low damping, no curing time, ability to withstand thermal cycling between 300 and 80 K, and reasonable reproducibility (in terms of damping in the  $10^{-6}$  range). The joint also allowed measurements to be made at the third and fifth harmonics. A method of testing the joint which involved making measurements at half the fundamental frequency was developed.
3. The sensitivity and reproducibility of measurements was verified by measurements of damping of quartz crystal specimens. Low damping measurements were limited by the suspension and the joint at low and high temperatures respectively.

4. Several pure aluminum and aluminum alloy samples were made and some single crystals of certain orientations were grown.
5. Internal friction measurements were made of the aluminum and alloy samples after vacuum annealing at 600°C and after hydrogen charging at 600°C. The measurements were made between 300 K and 80 K in order to detect possible hydrogen-substitutional solute pair reorientation. Strain amplitudes for most measurements were less than  $10^{-7}$ . The resulting internal friction spectra were used to calculate values for the binding energy between hydrogen and substitutional solutes. The maximum binding energies consistent with the measurements, the assumed hydrogen distribution and the estimated defect anisotropy were 0.04<sub>5</sub> eV and 0.05<sub>8</sub> eV for the H-Cu and H-Mg pairs in aluminum respectively.
6. Measurements of the internal friction of two commercial aluminum alloys (7075 and 6061) were made over the same temperature range. The results of measurements of the 7075 sample after exposure to hydrogen gas at room temperature were compared with those of Gest and Troiano (1974). The background damping in our specimen was almost two orders of magnitude smaller but there was no peak attributable to hydrogen-substitutional solute pairs.
7. The simple model of distribution of hydrogen between normal interstitial sites and sites adjacent to substitutional impurity does not account for hydrogen bound to grain boundaries, dislocations or vacancies. If the binding energy of hydrogen to these defect sites is much higher

than the binding energy to substitutional solutes, then a model of the hydrogen distribution which incorporates these other defects would result in higher limits on the binding energy values determined from the internal friction measurements.

## APPENDIX A

### INTERNAL FRICTION IN HYDROGEN CHARGED AND DEFORMED ALUMINUM

The results of measurements of the internal friction of 99.9999% pure aluminum which was deformed at room temperature after either vacuum annealing at 600°C or annealing in a wet hydrogen atmosphere at 600°C are reported in this appendix. Some of these measurements have been presented in Chapter 5. The object of doing these measurements was to determine if there were any noticeable effects of prior hydrogen charging on the damping spectrum of deformed aluminum. However, the results also show, beyond doubt, that the two component resonator technique used for all measurements reported in the thesis, does indeed produce reliable results.

Internal friction effects associated with dislocation-interstitial interactions have been observed in both b.c.c. and f.c.c. materials. There are many different effects which are ascribed to these interactions. A good review of these has been made by De Batist (1972). One such effect is the "cold-work" peak in b.c.c. materials which is thought to be caused by the dragging of interstitial solute by moving dislocations (Schoeck, 1963). Other effects include both amplitude and time dependent damping which results from the thermomechanical depinning of dislocations.

Dissolved hydrogen may interact with dislocations in aluminum to produce a measurable effect on the internal friction. There is evidence for such interaction in both b.c.c. (Gibala, 1967) and f.c.c. (Combette, 1972) metals. The f.c.c. systems which have been studied include nickel, copper,

palladium and a type 310 stainless steel. A comparison of the effects in different metals does not yield a consistent picture of the behaviour of hydrogen. The measurements on both Ni and Cu were performed using strain amplitudes which were greater than  $10^{-5}$ . These strains produce amplitude dependent damping which makes damping measurements difficult using the technique described in the fourth chapter. The measurements in the stainless steel case (Peterson et al., 1969) were made using a similar composite resonator technique but the strain amplitude used for the measurements was not reported.

#### Technique

The preparation of the polycrystalline aluminum samples was described in Chapter 4. Hydrogen was introduced into the samples by annealing in wet hydrogen atmospheres at 600°C. Samples annealed in hydrogen exhibited several large surface blisters upon removal from the furnace.

Samples were deformed after the joint between specimen and transducer had been made and tested. Deformation was by torsion, which was manually applied to the sample only. Resulting strains were measured approximately from the rotation of an inscribed pencil mark drawn parallel to the cylindrical axis before and after torsion.

Internal friction measurements were performed using the same techniques as described in Chapter 4. The strain amplitudes were calculated only at the maximum strain amplitude for each spectrum.

## Results

In order to test the reproducibility of the effects of deformation on the internal friction spectrum of a vacuum annealed aluminum polycrystal, the sample was twice subjected to the same treatment. After vacuum annealing at 600°C (resulting in a grain size of  $\sim 1$   $\mu$ m), the joint to the transducer was made and tested. The sample was deformed to a surface shear strain of slightly more than 1%. Internal friction measurements were made during continuous cooling at a maximum rate of 1° per minute. The two sets of results are shown in Figure 1. The results have been normalized to give the same maximum peak height. In both cases the maximum strain amplitude was less than  $10^{-8}$ . The results clearly show two peaks: one at 110 K and the other at about 165 K. Only the lower temperature peak appeared in the undeformed samples and the magnitude of the peak was much reduced. These peaks are thought to be the Niblett-Wilks peak (110 K) and the Bordoni peak (160 K).

The sample was then annealed in a wet hydrogen atmosphere at 600°C and air cooled. The surface of the sample was observed to be slightly blistered by several blisters a few  $\mu$ m in diameter. The joint to the transducer was made and then the specimen was twisted to a 1% shear strain. After 2.5 hours at room temperature, the measurements at the fundamental frequency were commenced using the continuous cooling technique at an initial cooling rate of slightly more than 1° per minute and a maximum strain amplitude of  $3.6 \times 10^{-9}$ . The results are shown in Figure 2. The narrow peak superimposed upon the Bordoni peak at 160 K was due to an imperfect joint and did not recur in any measurements of samples given the

FIGURE 1

Normalized internal friction of a vacuum annealed aluminum polycrystal deformed at room temperature

○ first measurement  $Q_{\max}^{-1} = 4.5 \times 10^{-4}$   
 $\epsilon_m = 3.1 \times 10^{-9}$

▲ following vacuum annealing and deformation a second time

$$Q_{\max}^{-1} = 2.1 \times 10^{-4}$$
$$\epsilon_m = 5.2 \times 10^{-9}$$

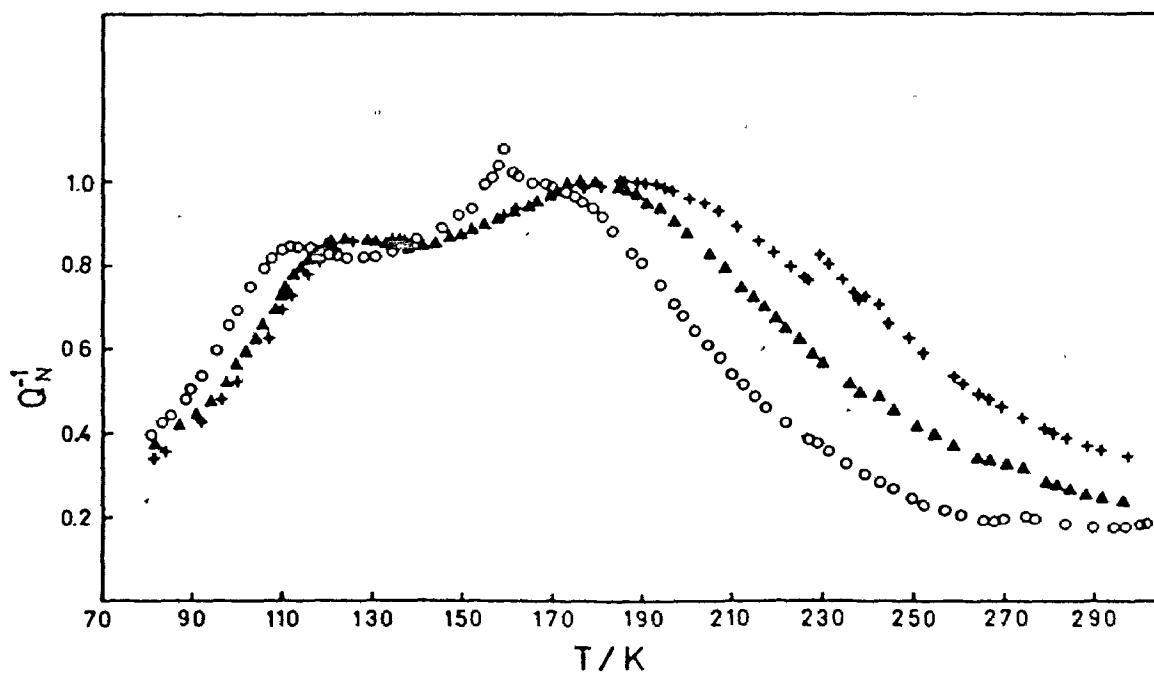
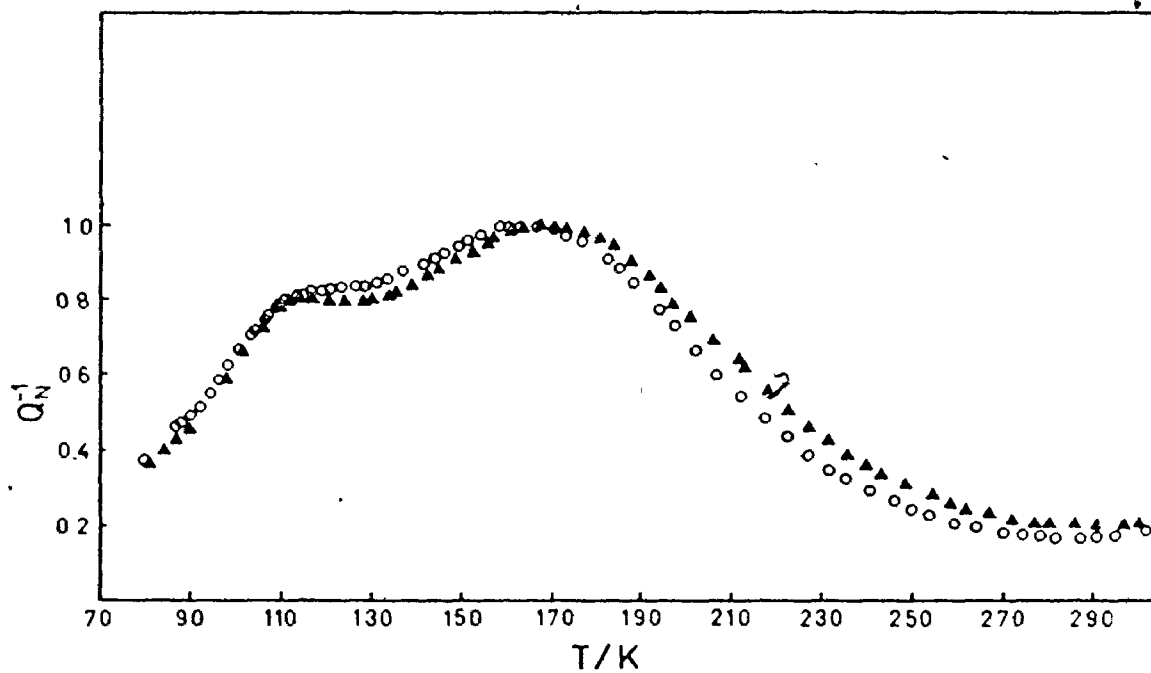
FIGURE 2

Normalized internal friction of a hydrogen charged aluminum polycrystal deformed at room temperature

○ fundamental  $Q_{\max}^{-1} = 4.8 \times 10^{-4}$   
 $\epsilon_m = 3.6 \times 10^{-9}$

▲ third harmonic  $Q_{\max}^{-1} = 3.8 \times 10^{-4}$   
 $\epsilon_m = 1.1 \times 10^{-8}$

+ fifth harmonic  $Q_{\max}^{-1} = 3.3 \times 10^{-4}$   
 $\epsilon_m = 3.4 \times 10^{-9}$



same treatment. A comparison with the results of Figure 1 indicates that, at these strain amplitudes, the effect of hydrogen is negligible.

Measurements were also made at the third and fifth harmonics using the same continuous cooling technique. These results are included in Figure 2 and they have again been normalized for easier comparison. The shifts in the peak temperatures with increasing frequency are apparent and were used to determine the activation energy of each peak. These activation energies were  $0.10 \pm 0.01_5$  eV and  $0.18 \pm .03_2$  eV for the Niblett-Wilks and Bordoni peaks respectively.

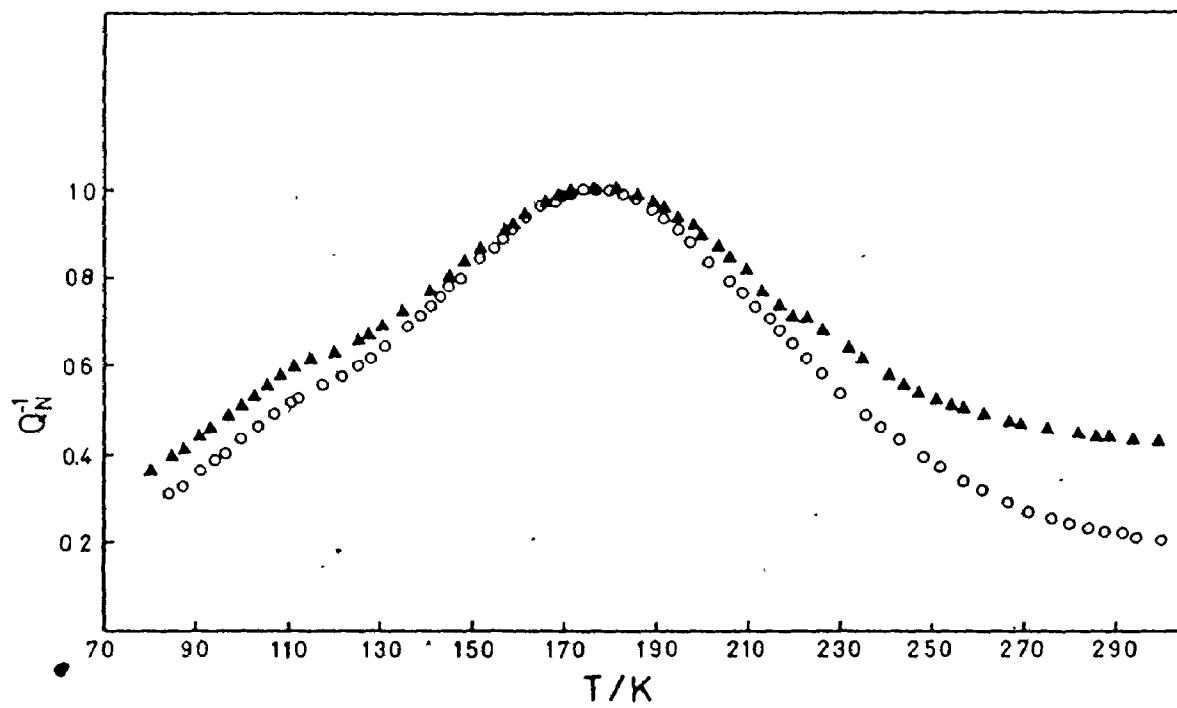
In order to retain more hydrogen in the aluminum, another sample was quenched into water after being hydrogen charged at 600°C. Again the joint to the transducer was made before the 1% deformation. Measurements were made during continuous cooling at a rate of less than 1° per minute, the maximum strain amplitude was  $9.4 \times 10^{-9}$ . These results, shown in Figure 3, exhibit a large peak at 175 K and a slight hump in the damping in the temperature range of the previous Niblett-Wilks peaks. Although there is a substantial change in shape from the previous results, this is not due to hydrogen but to the change in sample (the two samples were not identical). Measurements of this same sample with deformation after vacuum annealing yielded similar results.

Internal friction measurements were repeated on this sample at a much higher strain amplitude ( $5.2 \times 10^{-6}$  maximum). These are also included in Figure 3 and have been normalized for better comparison. The higher amplitude causes slight changes in the shape of the spectrum at both high and low temperature. Measurements at the higher amplitude were difficult to

FIGURE 3

Normalized internal friction of a hydrogen charged aluminum polycrystal after room temperature deformation

$$\begin{aligned} \circ \quad Q_{\max}^{-1} &= 1.0 \times 10^{-3} \\ \epsilon_m &= 9.4 \times 10^{-9} \\ \blacktriangle \quad Q_{\max}^{-1} &= 9.7 \times 10^{-4} \\ \epsilon_m &= 5.2 \times 10^{-6} \end{aligned}$$



perform because of the amplitude dependence of the damping caused by dislocation unpinning. This resulted in a large frequency shift in the resonant frequency of composite oscillator when resonance was achieved.

### Discussion

The object of these experiments was to determine the effect of prior hydrogen charging on the internal friction spectrum of deformed aluminum and also to test the composite resonator technique. The results indicate that, for the strain amplitudes which were used in these experiments ( $5.2 \times 10^{-6}$  maximum), there is no evidence of any effect of hydrogen charging. However, this does not necessarily imply that there is no effect. In order to detect the effects due to hydrogen, it may be necessary to use a technique which allows rapid quenching from the annealing atmosphere directly to liquid nitrogen temperatures, low temperature deformation and larger strain amplitudes during measurement. These techniques were used for the copper and nickel results. It was not possible to use these techniques with the composite resonator because of the necessity of making a joint at  $100^{\circ}\text{C}$ .

The results for the deformed aluminum are comparable with those obtained by other investigations (Routbort and Sack, 1967; Mayadas, 1966). For example, the 1% deformation which was given to the samples studied produced Bordoni peaks of maximum  $Q^{-1}$  between  $5 \times 10^{-4}$  and  $10^{-3}$ . Mayadas observed a peak height of  $2.2 \times 10^{-4}$  for 0.5% deformation while Routbort and Sack found that 2% deformation of a single crystal sample produced a peak of height  $8.9 \times 10^{-4}$ .

Mongy et al. (1963) found that there was an orientation dependence to the Bordoni peak activation energy. They observed an activation energy which varied from .042 eV for  $\langle 111 \rangle$  longitudinal propagation to 0.20 eV for  $\langle 110 \rangle$  propagation of ultrasound. The value of the activation energy for the Bordoni peak which was obtained in this work (0.18 eV) lies in the range found by Mongy. It is substantially lower than the 0.26 eV arrived at by Routbort and Sack from the analysis of many different investigations. Since the temperature of the maximum of the Bordoni peak was observed to shift quite markedly ( $\sim 10^\circ\text{K}$ ) from one sample to the other, it seems likely that the orientation dependence is having an effect. The polycrystalline samples were made up of very large grains and one or two of these near the centre of the sample would determine most of the damping. It is unlikely that both samples had the centre grains in the same orientation. Since there has been some skepticism expressed about the results of Mongy et al (Seeger, 1972) further studies of the orientation dependence of both the Bordoni and the Niblett-Wilks peak are in order.

### Conclusions

The internal friction spectra of pure aluminum samples deformed at room temperature showed no effects of prior hydrogen charging at the strain amplitudes used for the measurements.

The internal friction measurements of deformed aluminum were in agreement with previous results. This indicates that the composite resonator technique was certainly capable of internal friction measurements even at very low strain amplitudes ( $3 \times 10^{-9}$ ). The activation energies for

the Niblett-Wilks and the Bordoni peaks, determined from peak shifts with change in applied frequency, were 0.10 eV and 0.18 eV respectively. An amplitude dependence of the shape of the internal friction spectrum was also observed.

Further experiments to determine effects of hydrogen should employ more rapid quenching techniques, low temperature deformation, and higher measurement strain amplitudes to investigate dislocation break-away effects. The orientation dependence of the activation energy of both the Niblett-Wilks and the Bordoni peak should be redetermined to test the results of Mongy et al.

## APPENDIX B

### HYDROGEN ANALYSIS

Samples heated in hydrogen atmospheres should develop an equilibrium concentration of hydrogen in solution. The following hydrogen analysis work was performed in order to verify that hydrogen had indeed been quenched into the sample following charging in a hydrogen atmosphere. The method is similar to that of Berkowitz et al. (1975).

#### Apparatus

The apparatus used for the gas analysis consisted of a high vacuum system shown schematically in Figure 1. This system regularly attained a vacuum of  $10^{-8}$  torr after being baked out at  $100^{\circ}\text{C}$  for a day. The system could be divided into two systems by closing valve A. The small system could then be opened to air and evacuated with the supplementary unit.

A small quadrupole mass spectrometer (20th Century Electronics analytical ion gauge) attached to the small part of the vacuum system was used for the analysis. The mass spectrum of the gases in the system was obtained by applying a suitable ramp signal to mass spectrometer control unit and recording the gauge output signal. The ramp signal was taken from the sawtooth output of a Tectronix 585A oscilloscope.

The sample was heated by an electron beam heating unit consisting

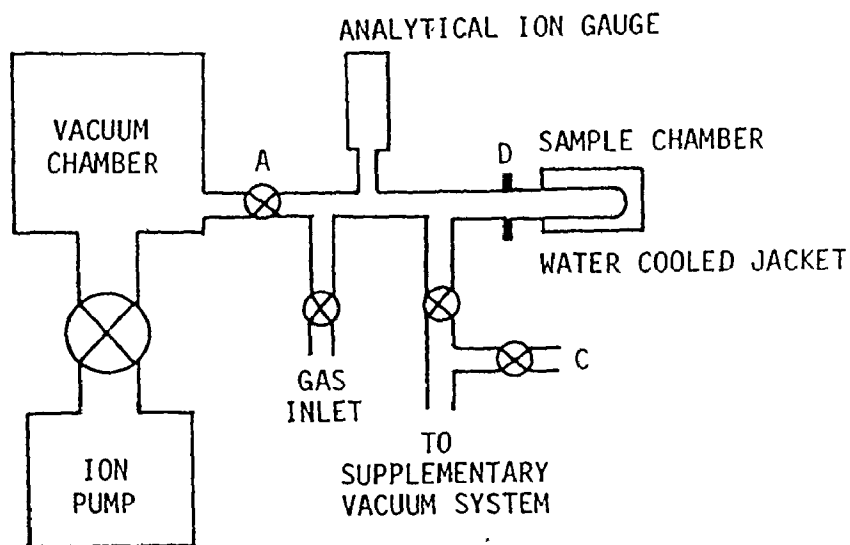


FIGURE 1

of a filament heater and high voltage source (2000 v max.). The temperature was measured with a Pt 13% Rh thermocouple the output of which could also be recorded.

The ion pump control unit provided an output proportional to the ion pump current which was also recorded.

### Technique

The following procedure was used to perform the gas analysis. In order to introduce the sample to be analysed into the vacuum system, the small system was returned to atmospheric pressure by closing valve A to the ion pump and admitting "dry" nitrogen from a cylinder through valve C. The glass envelope forming the sample chamber was removed by undoing the high vacuum flange at D. The previous sample was removed and the new sample placed onto the sample holder shown in Figure 2.

FIGURE 2

Sample holder for gas analysis showing tungsten heating filament and alumina supports



A fine platinum wire was twisted around the sample in order to hold it in place and to keep the sample pressed against the fused thermocouple-ground wire bead. Care was taken not to contaminate the sample by touching it with unshielded fingers. The glass envelope was then replaced using a new copper gasket in the flange. When the flange was sufficiently tightened, the small vacuum system was evacuated using the supplementary pumping system. The total time for which the system was exposed to the atmosphere was about ten minutes. Before opening valve A to the ion pump, the small system was baked by heating it with a propane torch. Large quantities of gas were pumped off during this procedure as verified by the rise in pressure measured on a Penning gauge in the supplementary vacuum system. When the glass envelope surrounding the sample was flamed, the sample temperature was monitored and found not to exceed 130°C. When the Penning gauge indicated a vacuum in the  $10^{-5}$  torr range, the valve to the supplementary pumping system was closed and valve A was opened. A special heater was placed around the analytical ion gauge in order to degas it. After a few hours, the outside of the system was again heated with the propane torch and allowed to cool. The heater on the analytical ion gauge was removed. When the ion pump current reached a reasonably steady value, the water jacket was put in place around the sample envelope and the sample heating was commenced. Three different single pen recorders were used to record the ion pump current, thermocouple output and mass spectrometer output.

The sample was heated within 300 seconds to 600°C with the electron beam heater. The sample chamber was open to the ion pump during the heating.



When the desired temperature was achieved, the electron accelerating voltage was turned down to that necessary to maintain the sample at 600°C. After periods of ten to twenty minutes the heating was stopped and the sample was allowed to cool to room temperature.

### Results and Discussion

Initial gas analysis attempts on a stainless steel sample, which was exposed briefly to the "dry" nitrogen from the cylinder, showed that the amount of water vapour adsorbed on the surfaces of the sample and the sample chamber was very large. When the sample was heated, this water vapour was released, which produced large signals at masses two and eighteen in the analytical ion gauge. There was a resultant signal at mass two which was so large that the possibility of using this method for hydrogen analysis of the aluminum samples seemed remote. The hydrogen evolved from the sample would have been indistinguishable from that produced by the water vapour.

It was then pointed out (P.T. Dawson, 1976) that deuterium was readily available and that charging the samples in a deuterium atmosphere at 600°C would make the gas evolved from the sample distinguishable from that produced by the water vapour.

Two different samples were used for this deuterium analysis. One was a high purity aluminum sample (6.5 g) which had previously been used for internal friction measurements and the other was an Al 0.16 at.% Mg alloy (6.5 g). The samples were charged with deuterium for 18 hours at one atmosphere pressure and 600°C in the same system used for the hydrogen

charging described in Chapter 3. The samples were quenched from the deuterium atmosphere into water at room temperature. The samples were then etched in Tucker's etch to remove any adsorbed deuterium before washing in pentane and placing them in the vacuum system.

The gas analysis results for these two specimens are shown in Figures 3 and 4.

Only the mass 3 peak height is plotted, which corresponds to HD of course. The deuterium evolved from the specimens during heating apparently exchanges very rapidly with the hydrogen of the water vapour since the mass 4 ( $D_2$ ) peak height was always significantly lower. The effect of deuterium on the mass 2 response could not be determined because of the large amount of  $H_2$  produced from the water vapour.

The results of Figures 3 and 4 are similar. As the heating is started, the ion pump current indicates a large quantity of gas evolved. The aluminum sample shows maxima in both the ion pump current and the mass three response when the sample reaches about  $350^\circ C$ . Maxima at  $600^\circ C$  are seen in the mass three responses for both samples. The ion pump current drops significantly when the electron accelerating voltage is decreased when the sample reaches  $600^\circ C$ .

The maximum at  $350^\circ C$  in the mass three response of the pure aluminum sample is thought to be due to the rapid release of deuterium trapped in surface blisters which were the result of a previous heat treatment in a hydrogen-water vapour atmosphere. These voids would be filled with deuterium at the charging temperature and would act as a source of deuterium very close to the sample surface during the analysis.

FIGURE 3

Gas analysis measurements for aluminum sample

+ temperature

○ ion pump current

▲ mass three response of analytical ion gauge

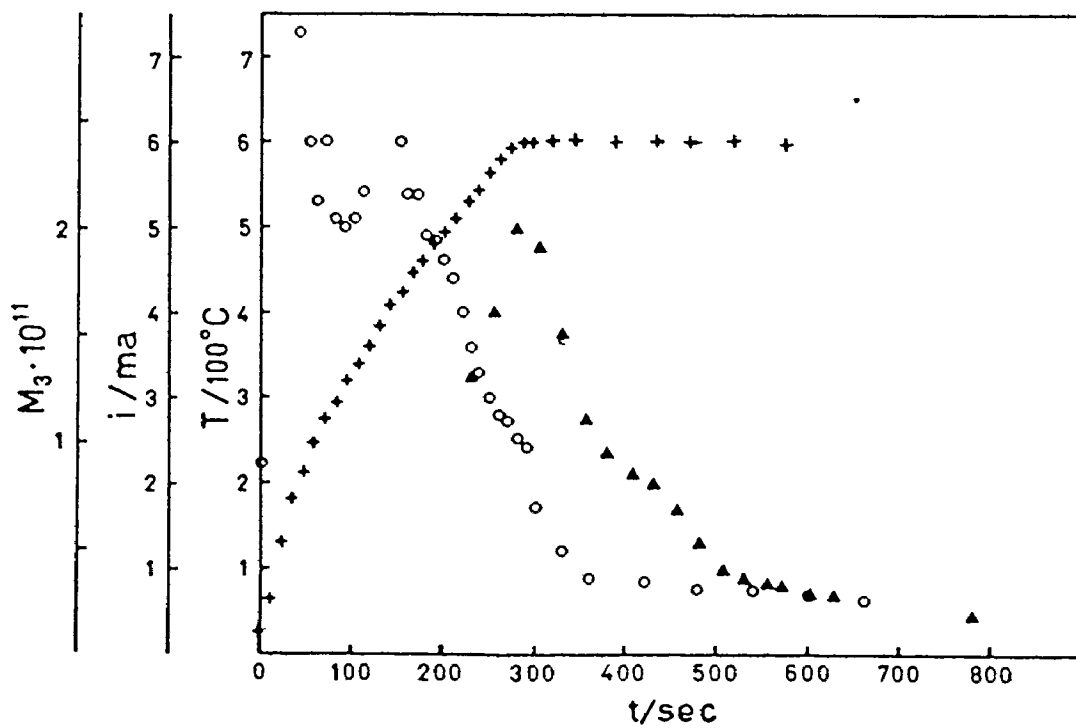
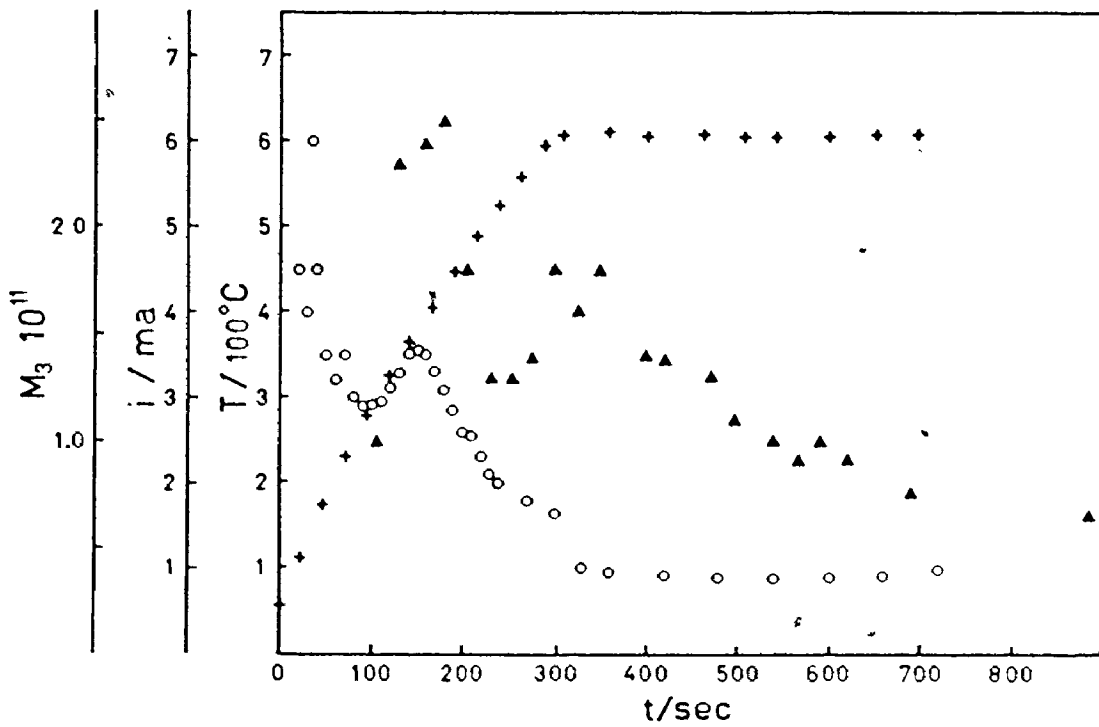
FIGURE 4

Gas analysis measurements for aluminum - magnesium alloy

+ temperature

○ ion pump current

▲ mass three response of analytical ion gauge



The determination of the actual quantity of deuterium evolved from the samples is a complex problem. The mass three peak height, at any given time, should be proportional to the amount of HD in the system. In order to determine the total quantity of deuterium evolved, the rate at which HD is removed from the system by the ion pump must be known as a function of the quantity present. This calibration was performed by admitting known quantities of hydrogen into the vacuum system and recording the ion pump current and mass two response on the mass spectrometer as a function of time. The quantity of gas admitted each time was  $5.8 \times 10^{-8}$  moles  $H_2$ . The natural logarithm of the mass two response of the mass spectrometer as a function of time is shown in Figure 5. The relation between the number of moles of gas in the system ( $N$ ) and the mass two response ( $M_2$ ), found by extrapolation to zero time, was

$$N = 4.75 (M_2) \quad (1)$$

The initial rate of removal of  $H_2$  from the system is proportional to the amount present (as shown by the straight line relationship between  $\ln M_2$  and time). This proportionality is given by

$$\frac{dN}{dt} = -2N \quad (2)$$

Therefore,

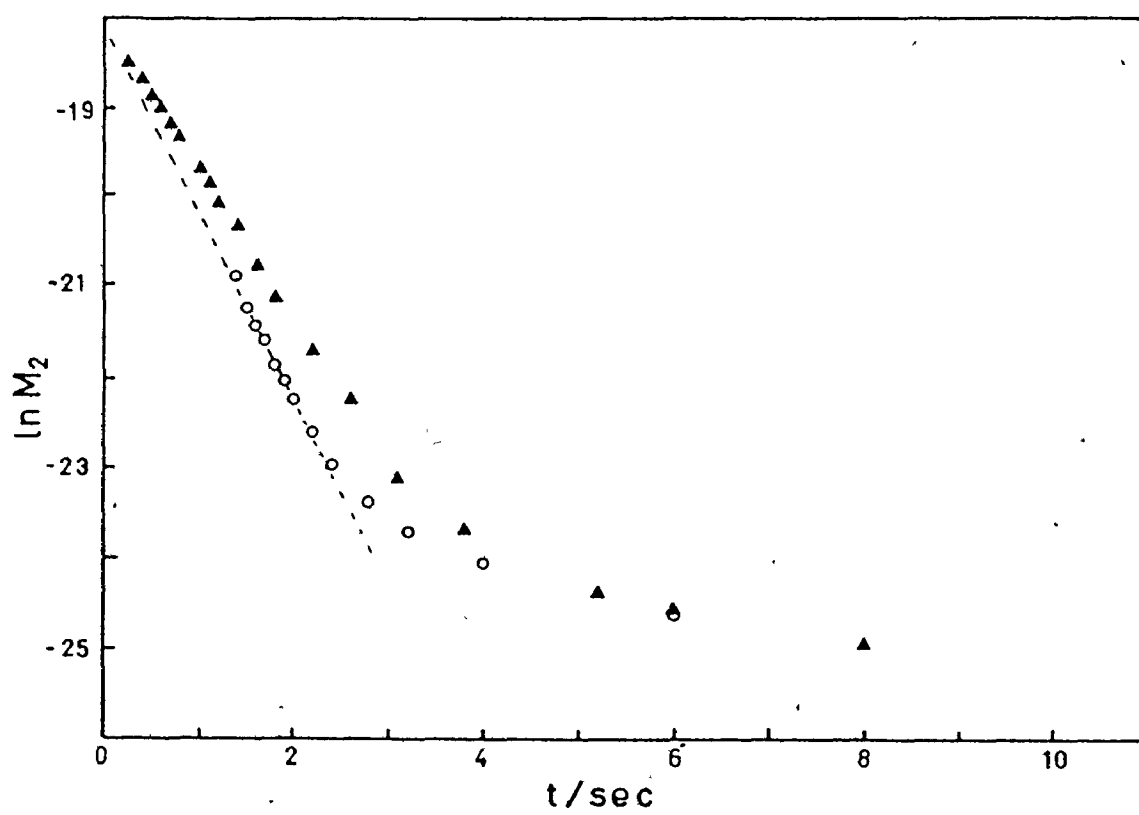
$$\frac{dN}{dt} = -9.5 M_2 \quad (3)$$

FIGURE 5

Measurements used for calibration of the response of the analytical  
ion gauge and pumping speed

○ first sample

▲ second sample



The linear relationship between  $\ln M_2$  and time does not hold over the whole range of  $M_2$ . The rate of removal becomes less than that given by equation 3 at the lower values of  $M_2$ .

The total amount of HD pumped away from the metal samples was found by determining the areas under the mass three response curves of Figures 3 and 4, using equation 3 to change the values of the mass three response to removal rate of HD. The proportionality given by equation 3 was assumed to hold for mass three. The amount of HD removed from the system was calculated to be  $4.8 \times 10^{-8}$  moles for the aluminum sample and  $3.3 \times 10^{-8}$  moles for the aluminum magnesium sample. The expected quantity of gas, using Eichenauer's (1968) solubility data, was  $9.5 \times 10^{-8}$  moles assuming that all the deuterium in the sample was converted to HD.

The discrepancy between the expected quantity of gas and that calculated with the use of equation 3 is quite large. A small part of this difference can be accounted for by the fact that not all the deuterium is removed as HD; there are also small quantities of  $D_2$  and D.

The error in the use of equation 3 could be considerable. The pumping rates determining equation 3 were obtained when hydrogen was by far the most abundant species being pumped. In the gas analysis experiments, however, water vapour was the principal constituent. Since there will be more sputtering in the ion pump due to the presence of the water vapour, the pumping rate given by equation 3 is probably too low.

The gas analysis results shown in Figure 3 perhaps provide some indication of what the pumping rate really was when the water vapour was present. The mass three maximum at  $350^\circ\text{C}$  was accompanied by a maximum in

the ion pump current. If both maxima are attributed to the same cause, release of deuterium from the sample, then another relationship between pumping speed and mass three response of the mass spectrometer can be determined. Previous calibration experiments with hydrogen have shown that the number of molecules pumped per charge in the ion pump current is 0.54. Since the additional current due to the burst of deuterium was about 1 ma. therefore, the pumping rate was about  $5.6 \times 10^{-9}$  moles/sec. The pumping rate given by equation 3 is  $2.3 \times 10^{-10}$  moles/sec. The former value is probably too high but it does indicate that the relationship given by equation 3 underestimates the pumping rate. This means that the calculated quantities of gas are too small, perhaps by a factor of ten or so.

### Conclusion

These gas analysis measurements have shown that samples charged in a deuterium atmosphere and quenched into water did contain deuterium. This implies that similar samples equilibrated with hydrogen atmospheres at 600°C and quenched into water must contain hydrogen.

In order to determine the actual quantities of gas present in the sample, the pumping rate of the ion pump for mixtures of hydrogen and water vapour must be known.

## APPENDIX C

### INTERNAL FRICTION DUE TO TEMPERATURE DEPENDENCE OF THE ELASTIC COMPLIANCE

The effects of an inhomogeneous temperature distribution in internal friction measurements have been discussed by Barrow and Szkopiak (1970). Internal friction due to heat flow caused by the inhomogeneous applied stress distribution is well known (Zener, 1948). In this appendix an expression is derived for the internal friction due to the change in elastic compliance caused by temperature changes during the period of a stress cycle.

Consider first a perfectly elastic body with a compliance,  $J$ , which is temperature dependent. If the temperature of the body is allowed to change with time, then the compliance becomes time dependent. This can produce an internal friction in the following manner.

The work done per unit volume of the body over one complete cycle of an alternating applied stress

$$\sigma = \sigma_0 \sin \omega t \quad (1)$$

is given by

$$W = \oint \sigma d\epsilon = \int_0^{2\pi/\omega} \sigma \frac{d\epsilon}{dt} dt \quad (2)$$

Now the strain is given by

$$\epsilon = J(t) \sigma_0 \sin \omega t \quad (3)$$

showing the time dependence of the compliance explicitly. If a linear time dependence of the compliance is assumed

$$J(t) = J_0 + J_t t$$

then, with appropriate substitutions into (2) the work done per unit volume per cycle is

$$W = \frac{J_t \sigma_0^2 \pi}{2\omega}$$

Since the maximum energy stored per unit volume is  $1/2 J_0 \sigma_0^2$ .

Therefore the measured internal friction is

$$Q^{-1} = \frac{J_t}{2J_0\omega} \quad (5)$$

Following essentially the same method for an anelastic body, in which the strain normally lags the stress by a phase angle  $\phi$ , i.e. with a normal internal friction  $Q^{-1} = \tan \phi$ , the total internal friction is given by

$$Q^{-1} = \frac{1}{2} \frac{J_t}{J_0 \omega} + \tan \phi \left[ 1 + \frac{J_t \pi}{J_0 \omega} \right]$$

Since  $J_t \pi / J_0 \omega \ll 1$ , the value of  $Q^{-1}$  is very nearly the sum of the normal internal friction and that contributed by equation (5).

The dependence of  $Q^{-1}$  on  $J_t$  and frequency means that it can be significant for rapid temperature changes, where the compliance has a large temperature dependence, and for low frequency measurements. Also, since this term depends upon the sign of  $J_t$ , this contribution to the total internal friction would be added or subtracted depending upon the direction of the temperature change.

The effect, for typical heating rates, for measurements in aluminum can be easily calculated using the elastic constant data of Kamm and Alers (1964). If a rate of change of temperature of  $100^\circ$  per hour at 220 K is assumed for a 1 Hz pendulum, the difference between heating and cooling on the logarithmic decrement  $\delta = \pi Q^{-1}$  would be  $7 \times 10^{-6}$ . If the total decrement is  $\delta \approx 10^{-4}$ , this is a 7% effect. For a pendulum operating at .1 Hz, the difference would be  $7 \times 10^{-5}$ . Sometimes, in order to detect mobile point defects, very large heating rates are used--eg.  $3000^\circ\text{K}/\text{hour}$ . In such a case, with the 1 Hz pendulum, the effect could amount to a decrement of  $2.1 \times 10^{-4}$ .

Although this effect is generally small, it can become appreciable for experiments in which low frequencies and fast heating rates are used to detect a supersaturation of defects before they anneal out, or for measurements near phase transitions, in which the elastic compliance is strongly temperature dependent.

## REFERENCES

- Abarenkov, I.V. and Heine, V. (1965) *Phil. Mag.* 12, 529.
- Adler, E. (1965) *Z. Metallkunde* 56, 249.
- Ascarelli, P. (1968) *Phys. Rev.* 173, 271.
- Balamuth, L. (1934) *Phys. Rev.* 45, 715.
- Barrow, D.E. and Szkopiak, Z.C. (1970) *J. Phys. D* 3, 1140.
- Baukloh, W. and Oesterlen, F. (1938) *Z. Metallkunde* 11, 386.
- Beaman, D.R., Balluffi, R.W. and Simmons, R.O. (1965) *Phys. Rev.* 137, A917.
- Beck, W., Bockris, J. O'M., McBreen, J. and Nanis, L. (1966) *Proc. Roy. Soc.* 290 A, 220.
- Berkowitz, B.J., Preece, C.M., and Strozier, J.A. (1975) *Scripta Met.* 9, 803.
- Brudnoy, D.M. (1974) *J. Phys. Chem. Solids* 35, 1491.
- Cady, W.G. (1946) *Piezoelectricity* (McGraw Hill, New York).
- Cohen, M.L., Heine, V. and Weaire, D. (1970) *Solid State Physics* 24 (Academic Press, New York).
- Combette, P., Renard, M. and Grilhe, J. (1972) *Phys. Stat. Sol. (a)* 11, 677.
- Corless, G.K. and March, N.H. (1961) *Phil. Mag.* 6, 1285.
- Dauphinee, T.M. and Preston-Thomas, H. (1954) *Rev. Sci. Instrum.* 25, 884.
- Dawson, P.T. (1976) Private Communication.
- De Batist, R. (1972) *Internal Friction of Structural Defects in Crystalline Solids* (North-Holland, Amsterdam).
- Ebisuzaki, Y., Kass, W.J. and O'Keefe, M. (1967) *J. Chem. Phys.* 46, 1378.
- Eborall, R. and Ransley, C. (1945) *J. Inst. of Met.* 71, 525.
- Eichenauer, W. (1968) *Z. Metallkunde* 59, 613.

- Eichenauer, W., Hattenbach, K., and Pebler A. (1961) Z. Metallkunde 52, 684.
- Eichenauer, W. and Pebler, A. (1957) Z. Metallkunde 48, 373.
- Eshelby, J.D. (1956) Solid State Physics 3 (Academic Press, New York).
- Fast, J.D., Meijering, J.L. and Verrijp, M.B. (1961) Métaux. Corros. Inds. 36, 112.
- Flynn, C.P. (1972) Point Defects and Diffusion (Oxford University Press, London).
- Foster, L.M., Gillespie, A.S. Jr., Jack, T.H. and Hill, W.W. (1963) Nucleonics 21 No. 4, 53.
- Gest, R.J. and Troiano, A.R. (1974) Corrosion-N.A.C.E. 30, 275.
- Gibala, R. (1967) Acta Met. 15, 428.
- Gupta, D. and Weinig, S. (1962) Acta Met. 10, 292.
- Hardy, J.R. (1968) J. Phys. Chem. Solids 29, 2009.
- Hardy, J.R. and Bullough, R. (1967) Phil. Mag. 15, 237.
- Hearmon, R.F.S. (1957) Acta Cryst. 10, 121.
- Huntington, H.B. and Johnson, R.A. (1962) Acta Met. 10, 281.
- Kamm, G.N. and Ters, G.A. (1964) J. Appl. Phys. 35, 327.
- Kandarpa, V. and Spretnak, J.W. (1969) Trans. A.I.M.E. 245, 1439.
- Kê, T.S. and Tsien, C.T. (1956) Sci. Sinica 5, 625.
- March, N.H. and Rousseau, J.S. (1971) Crystal Lattice Defects 2, 1.
- Marx, J. (1951) Rev. Sci. Instr. 22, 503.
- Mason, W.P. (1950) Piezoelectric Crystals and their Application to Ultrasonics (Van Nostrand, New York).
- Mâyadaş, A.F. (1966) NYO 2471-12.
- Mongy, M., Saïama, K. and Beckman, O. (1963) Solid State Communications 1, 234.
- Mosher, D., Dollins, C. and Wert, C. (1970) Acta Met. 18, 797.

- Murty, K.N. and Vasu, K.I. (1972) *Phil. Mag.* 20, 241.
- Noggle, T.S. (1953) *Rev. Sci. Instr.* 24, 184.
- Nowick, A.S. and Berry, B.S. (1972) Anelastic Relaxation in Crystalline Solids (Academic Press, New York).
- Nowick, A.S. and Heller, W.R. (1963) *Advan. Phys.* 12, 251.
- Opie, W. and Grant, N. (1950) *Trans. A.I.M.E.* 188, 1237.
- Pearson, W.B. (1958) A Handbook of Lattice Spacing and Structures of Metals and Alloys (Pergamon Press, London).
- Peterson, J.A., Gibala, R. and Troiano, A.R. (1969) *J. Iron and Steel Inst.* 207, 86.
- Popović, Z.D. (1974) Ph.D. Thesis, McMaster University.
- Popović, Z.D., Stott, M.J., Carbotte, J.P. and Piercy, G.R. (1976) *Phys. Rev. B* 13, 590.
- Puls, M.P. (1970) Ph.D. Thesis, McMaster University.
- Ransley, C. and Neufeld, H. (1948) *J. Inst. Met.* 74, 599.
- Ridley, N. and Stuart, H. (1970) *Met. Sci. J.* 4, 219.
- Ritchie, I.G., Rosinger, H.E. and Atrens, A. (1976) Private Communication (presented at Canadian Metal Physics Conference, Kingston, June 1976).
- Robinson, W.H. and Edgar, A. (1974) *I.E.E.E. Trans. on Sonics and Ultrasonics* SU-21, 98.
- Routbort, J.L. and Sack, H.S. (1967) *Phys. Stat. Sol.* 22, 203.
- Rutter, J.W. (1968) in Techniques of Metals Research Vol.1 pt. 2 (R.F. Bunshah, ed., Interscience Publishers, New York).
- Sagues, A.A. and Gibala, R. (1974) *Acta Met.* 22, 1423.
- Saul, R.H. and Bauer, C.L. (1967) *Rev. Sci. Instr.* 38, 1449.
- Saul, R.H. and Bauer, C.L. (1968) *J. Appl. Phys.* 39, 1469.
- Schoeck, G. (1963) *Acta Met.* 11, 617.
- Seeger, A. (1971) *J. de Physique* 32, (C2) 249.

- Shimomura, Y. and Yoshida, S. (1967) J. Phys. Soc. Jap. 22, 319.
- Simmons, R.O. and Balluffi, R.W. (1960) Phys. Rev. 117, 52.
- Singwi, K.S., Sjölander, A., Tosi, M.P. and Land, R.H. (1970) Phys. Rev. B1, 1044.
- Sokol'skaya, L.I. (1961) Gases in Light Metals (Pergamon Press, New York).
- Sørensen, K.O. and Cotterill, R.M.J. (1974) Acta Met. 22, 1331.
- Speidel, M.O. (1974) in Hydrogen in Metals, p. 249 ASM.
- Straalsund, J.L. and Bates, J.F. (1974) Metallurgical Transactions 5, 493.
- Troiano, A.R. (1974) in Hydrogen in Metals, p. 3 ASM.
- Wachtman, J.B. Jr. and Peiser, H.S. (1962) Appl. Phys. Letters 1, 20.
- Wagner, C. (1971) Acta Met. 19, 843.
- Wert, C. and Marx, J. (1953) Acta Met. 1, 113.
- Widawski, E. and Saverwald, F. (1930) Z. anorg. allgem. Chem. 192, 145.
- Zener, C. (1948) Elasticity and Anelasticity in Metals (University of Chicago Press, Chicago, Ill.)
- Ziman, J.M. (1964) Adv. in Physics 13, 89.